Exploiting Mobile Energy Storages for Overload Mitigation in Smart Grid

by

Nan Chen

A thesis
presented to the University of Waterloo
in fulfillment of the
thesis requirement for the degree of
Doctor of Philosophy
in
Electrical and Computer Engineering

Waterloo, Ontario, Canada, 2019

Examining Committee Membership

The following served on the Examining Committee for this thesis. The decision of the Examining Committee is by majority vote.

External Examiner:	Vojislav Misic Professor, Ryerson University
Supervisor(s):	Xuemin (Sherman) Shen University Professor, University of Waterloo
Internal Member:	Kankar Bhattacharya Professor, University of Waterloo
Internal Member:	Xiaodong Lin Associate Professor, University of Guelph
Internal-External Member:	Yaoliang Yu Assistant Professor, University of Waterloo

Author's Declaration

I hereby declare that I am the sole author of this thesis. This is a true copy of the thesis, including any required final revisions, as accepted by my examiners.

I understand that my thesis may be made electronically available to the public.

Abstract

The advancement of battery and electronic technologies pushes forward transportation electrification, accelerating the commercialization and prevalence of plug-in electric vehicles (PEVs). The development of PEVs is closely related to the smart grid as PEVs are considered as high power rating electric appliances that require frequent charging. As PEVs become regular transportation options, charging stations (CSs) are also extensively deployed in the smart grid to meet the PEV charging demand. During peak traffic hours, the increasing PEV charging demand could exceed the loading capacities of CS-connected transformers, causing heavy charging overload in-station. Without proper overload mitigation, the energy imbalance issues will result in severe feeder degradation and power quality issue. Therefore, solutions for CS overload mitigation are in urgent demand.

Considering the rechargeable nature of PEV batteries, PEVs can serve as potential mobile energy storages (MESs) to carry energy from power nodes with excess energy to overloaded CSs to compensate the overloads. Compared to infrastructure upgrade and installing stationary energy storages at CSs, the utilization of PEVs not only minimizes the additional upgrade/installation expenditure, but also maximizes the energy utilization in the smart grid with high flexibility. However, the PEV utilization for overload mitigation is confronted with a variety of challenges due to vehicular mobility and the fear of battery degradation. Because of vehicular mobility, the CS operation dynamics become stochastic processes, increasing the difficulty of the CS demand estimation. Without accurate demand estimation, the overload condition cannot be timely predicted and controlled. Moreover, the stochastic on-road traffic could impair the time-efficiency of the PEV overload mitigation service. Further, as the overload mitigation service demands frequent charging and discharging, the fear of battery degradation could impede PEV owners from providing the service, making the overload mitigation tasks harder to fulfill.

In this thesis, we address the above challenges to effectively utilize PEVs for overload mitigation in the smart grid. In specific, different approaches are designed according to the PEV properties at different commercialization stages. First, at the early PEV commercialization stage, power utility company purchases large battery capacity PEVs as utility-owned MESs (UMESs) whose only responsibility is fulfilling the energy compensation task. The fleet of UMESs is rather small due to the company's limited budget, and therefore UMESs priorly serve the CSs with large energy imbalance (e.g., 500-1000kWh). Thus, the stochastic CS charging demand needs to be accurately estimated and then UMESs can be scheduled to these CSs for overload mitigation. To achieve this objective, we develop a two-dimensional Markov Chain model to characterize the stochastic process in-station so that the CS charging demand can be precisely estimated. Based on the estimated CS

demand status, a two-tier energy compensation framework is designed to schedule UMESs to the heavily overloaded CSs in a timely and cost-efficient manner. Second, at the medium stage of PEV commercialization, vehicle-fleet based companies are motivated by legislation to purchase a large fleet of PEVs which can be served as potential MESs, referred to as legislation-motivated MESs (LMESs). To deliver energy to overloaded CSs using LMESs would introduce a large amount of additional traffics to the transportation network. When injecting these LMES traffics into an already busy transportation network, unexpected traffic delay could occur, delaying the overload mitigation service. To avoid the potential traffic delay incurred by LMES service, we develop an energy-capacitated transportation network model to measure the road capacity of accommodating additional LMES traffics. Based on the developed model, a loading-optimized navigation scheme is proposed to calculate the optimal navigation routes for LMES overload mitigation. To stimulate LMESs following the optimal navigation, we propose a dynamic pricing scheme that adjusts the service price to align the LMES service routes with the optimal routes to achieve a time-efficient service result. Third, when PEVs are prevalent in the automobile market and become regular transportation options for every household, on-road private-owned PEVs can be efficiently used as energy porters to deliver energy to overloaded CSs, named as private MESs (PMESs). As the primary objective of PMESs is to reach their planned destinations, the monetary incentive is demanded to stimulate them actively participating in the overload mitigation tasks. Therefore, a hierarchical decision-making process between the utility operator (UO) and PMESs is in demand. Moreover, considering PMESs have different service preferences (e.g., the fear of battery degradation, the unwillingness of long service time, etc.), individual PMES decision making process on the task should be carefully modelled. Thus, we propose to characterize the price-service interaction between the operator and PMESs as a Stackelberg game. The operator acts as the leader to post service price to PMESs while PMESs act as followers, responding to the posted price to maximize their utility functions.

In summary, the analysis and schemes proposed in this thesis can be adopted by the local power utility company to utilize PEVs for overload mitigation at overloaded power nodes. The proposed schemes are applicable during different PEV commercialization stage and present PEVs as a flexible solution to the smart grid overload issue.

Acknowledgements

I would like to express my sincere thank to my supervisor, Professor Xuemin (Sherman) Shen, for his continuous support, patient guidance, and endless help during my Ph.D. study in University of Waterloo. Starting as a novice in the research area, I receives endless and precious guidance from Professor Shen to help me develop academic skills, plan and build a better career path. His great understanding to all his students and valuable advice on both academia and life all aspire me to become a better researcher and person. I feel very fortunate and privileged to be his student.

I would like to thank Professor Xiaodong Lin, Professor YaoLiang Yu, Professor Kankar Bhattacharya for serving my defence committee. I would also like to thank Professor Vojislav Misic from Ryerson University to serve as my external examiner. Their valuable comments and insightful questions have effectively improved the presentation and quality of my work.

In the past five years, I received precious friendship, help, and support from current and former BBCR members. I would like to express my sincere thank to all BBCR members. I would like to especially thank Professor Miao Wang, Professor Ning Zhang, Professor Kuan Zhang, Professor Jianbin Ni, Professor Nan Cheng, Dr. Wenchao Xu, Mushu Li, Junling Li, Weisen Shi, Professor Shan Zhang, Dr. Peng Yang, Professor Yujie Tang, Professor Yuan Wu, Professor Ran Zhang, for their inspiring discussions and valuable insights on my research and life.

This thesis is dedicated to my parents. Their love and encouragement have been my dearest support during my Ph.D. study.

Nan Chen
June 23, 2019
Waterloo, Ontario, Canada

To my dear parents

Table of Contents

List of Tables

List of Figures

List of Abbreviations

AC	Alternating Current
CS	Charging Station
DC	Direct Current
DoD	Depth-of-Discharge
DSRC	Dedicated Short-Range Communication
GCS	Group of Charging Stations
LCS	Limited-capacity Charging Station
LMES	Legislation-motivated Mobile Energy Storage
LoS	Level of Service
LTE-V	Long-Term Evolution-Vehicle
MES	Mobile Energy Storage
OBU	On-Board Unit
PEV	Plug-in Electric Vehicle
PMES	Private-owned Mobile Energy Storage
QoE	Quality of Experience
RCS	Resourceful Charging Station
RSU	Road-Side Unit
SCADA	Supervisory Control and Data Acquisition
SoC	State-of-Charge
UMES	Utility-owned Mobile Energy Storage
UO	Utility Operator
VANET	Vehicle Ad Hoc Network
V2G	Vehicle-to-Grid

Chapter 1

Introduction

As electricity demands growing rapidly in recent years, conventional power grid demands numerous energy suppliers to achieve the energy balance in a wide geographic area. Therefore, renewable energy generations and energy storages are gradually integrated into the power grid to provide additional energy supply in a sustainable manner [1]. As the electricity generation of renewable energy is closely related to the weather conditions, the power grid operator needs to monitor and estimate the renewable generation condition to enable the system energy balance. Therefore, communication and information technologies are applied in the power grid to help monitor and communicate power data/commands among the system. Empowered with communication and information technologies, the renewable energy integrated power grid will become a green, sustainable, and autonomous smart grid [2].

Meanwhile, the advancement of battery technology and the launch of PEV purchase/lease incentives push forward the PEV commercialization [3, 4]. To meet the increasing PEV charging demands, the smart grid operator will deploy a large number of charging stations (CSs) at different loading levels in the power distribution system. As PEV commercialization proceeds, some CSs could encounter charging overload when PEV charging demand exceeds the loading capacity of the feeder transformer at peak hours [5]. Without proper energy scheduling, the charging overload would result in severe feeder transformer degradation and power quality issues in the smart grid [6]. An intuitive solution is to upgrade the aged power infrastructure. However, the infrastructure upgrade demands high expenditure and can be inflexible when the load distribution varies in the future. Instead, energy storage devices can be deployed at the overloaded CSs upon requests. While stationary energy storages are an effective solution for the overload mitigation, they face the same problem as the infrastructure upgrade: high expenditure and inflexibility. Considering the

rechargeable nature of PEV on-board batteries, PEVs can be utilized to carry energy from power nodes with excess energy to overloaded CSs [7], presenting as a mobile and flexible energy storage option.

In this chapter, we first provide an overview of the smart grid and introduce the potential power overload issue incurred by increasing PEV charging. Then, as a possible solution to the issue, PEVs as MESs are introduced with respect to their characteristics and challenges. Research motivation and contribution are then discussed, followed by the thesis outline.

1.1 An Overview of Smart Grid

Smart gird is defined as the green power system that employs communication and information technologies to improve the efficiency, reliability, flexibility, and security of the system [8]. Compared with the conventional power grid, the smart grid integrates a large number of renewable energy generations and energy storage devices, which introduces high randomness in the system operation. Therefore, communication technology is employed to transmit the power data in the smart grid while information technology is used to process and analyze the operation statuses. Next, we introduce the architecture of the smart grid to provide the system background knowledge. Then, the power overload issue incurred by the increasing PEV charging demands will be discussed.

1.1.1 Architecture of the Smart Grid

The architecture of the smart grid is shown in Fig. 1.1, which consists of three subsystems: power sub-system, communication sub-system, and information sub-system. The power sub-system is a traditional power grid integrated with renewable energy generations and energy storage devices. To fully utilize the local energy resource, the grid operator deploys bulk-size renewable energy generations at the generation side while also has renewable energy deployed at the distribution side as additional power supply. Through the distributed generations and bi-directional power infrastructure, consumers can become the electricity providers [9]. For example, during peak hours, consumers can utilize the electricities that are generated by local renewable generations to reduce electricity cost, or even provide additional electricity to the grid for monetary rewards. Moreover, energy storage devices such as PEVs, flywheels, stationary batteries are also integrated at the distribution side as the energy buffers to enable the local energy balance.

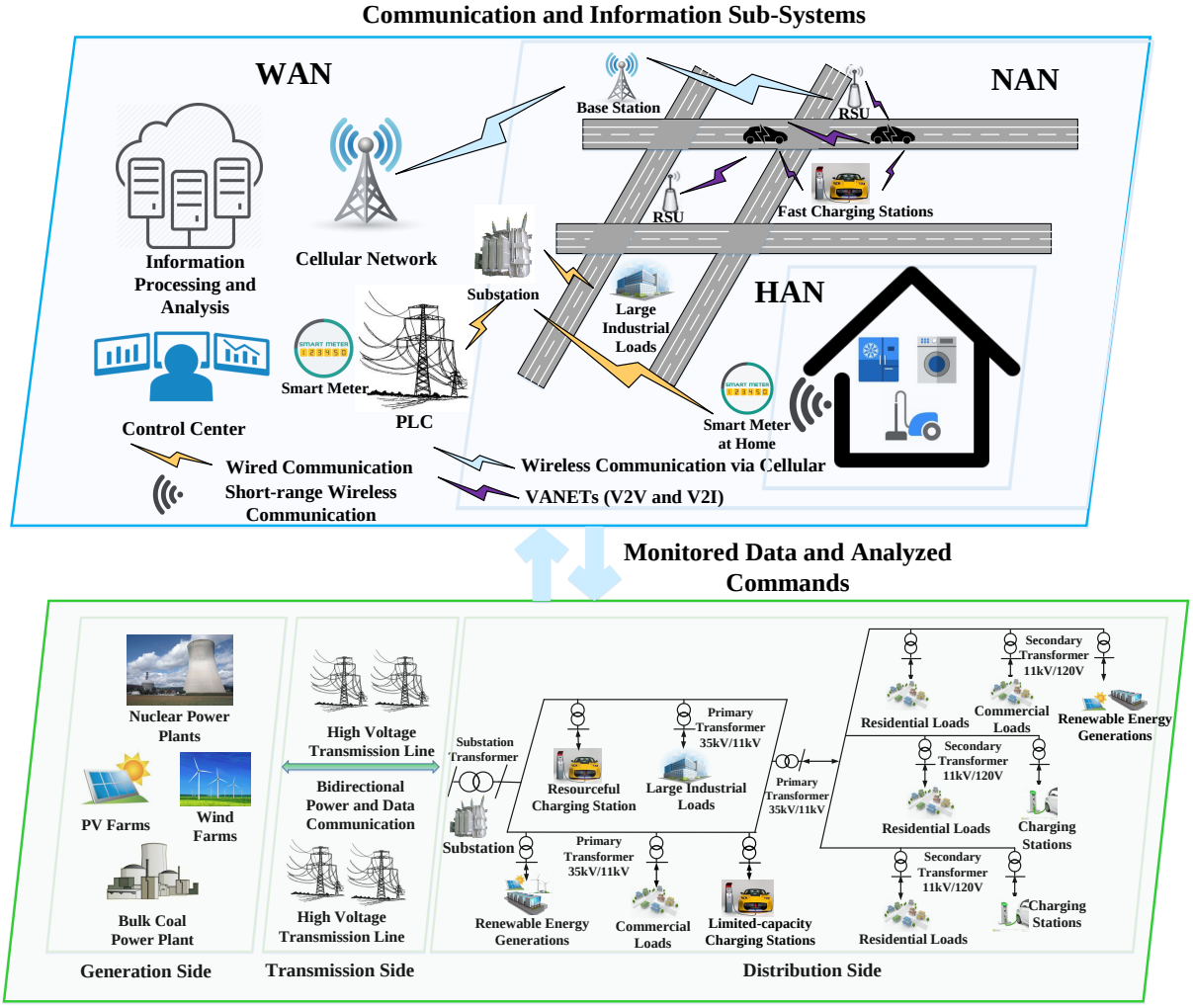

Figure 1.1: Architecture of the smart grid.

To enable a smooth system operation, essential power components (e.g., generations, feeders, PEVs etc.) are monitored and the operating data are sent to the smart grid operator with different communication technologies in the communication subsystem. The variety of power application requires a heterogeneous communication environment to satisfy different operation requirements [10, 11]. For example, for data communication from power generation side to the distribution side, long-distance communication technologies

such as power line communication, fiber optic, and cellular network are good options [12–14]. In particular, as the fifth-generation (5G) cellular network develops, the technology can be applied at the distribution side to support both stationary and mobile data communication [15]. Moreover, consider the exponentially increasing transmitted data on-road, dedicated short-range communication (DSRC) technology such as vehicle ad hoc networks (VANETs) are adopted in the smart grid for vehicle-to-vehicle and vehicle-to-infrastructure communication [16].

The transmitted data are then stored and analyzed in the information sub-system (e.g., data center, supervisory control and data acquisition (SCADA) system). In terms of operation objectives, computational intelligence is applied in the sub-system to balance between the energy supply and demand so that the efficiency, stability, and robustness of the smart grid is achieved.

1.1.2 Power Overload Issue

PEVs in Smart Grid

With transportation electrification proceeding rapidly, PEV will become an essential component in the smart grid. According to [17], PEVs are the vehicles that can be charged from an external electric source by plugs or wall sockets. Currently, manufactured PEV such as Nissan leafs has a 40kWh battery capacity with 150-mile driving range [18] while luxury PEV such as Tesla Model S can travel up to 335 miles with an 85kWh battery [19].

PEVs are communication-enabled vehicles with on-board units (OBUs) to connect with on-road vehicles and infrastructures. Bluetooth is a commonly adopted technology for intra-vehicle connection while WiFi and VANETs are good options for communicating with on-road vehicles and road-side units (RSU). GPS and satellite communication technologies enable vehicle connection in rural areas. Recently, long-term evolution-vehicle (LTE-V) built upon LTE standard is expected to achieve a high data rate up to 100Mbps under high travelling speed, which can be used by PEVs for mobility-aware charging and discharging navigation [5, 20].

Consider PEVs as high power rating electric appliances, they are integrated into the smart grid at the distribution side through interfaces such as CSs. In terms of different charging requirements, CSs are deployed at different loading levels, as shown in Fig. 1.1. Public and fast CSs are usually deployed at high-voltage, large-capacity feeders while private/home chargers are usually deployed in the residential area with low voltage. Therefore, PEV charging has normally two modes: home charging with low power rating, and public/fast charging for driving range extension, and has medium to high power rating.

To facilitate the interoperability between CSs and PEVs, charging standard has been developed globally, by categorizing PEV charging based on their plug types, power rating, voltage etc., as summarized in Table 1.1. Alternating current (AC) charging takes up to 17 hours to fully charge a PEV [21]. This charging method is usually applied at home for overnight charging. Direct current (DC) charging has a faster speed with the charging time between 22 minutes to 1.7 hours [22]. It is mainly applied to public/fast CSs to help PEVs extend driving range quickly.

Table 1.1: Charging standard

Charging Method	Charging Power Requirement	Charging Time
AC level 1	120VAC, 12A, 1-phase, 1.4-1.9kW	7-17hours
AC level 2	208-240VAC, $\leqslant$ 80A, 1/3-phase, $\leqslant$ 19.2kW	22min-3hours
SAE CCS (DC)	200-600VDC, 80-400A, $\leqslant$ 240kW	$\leqslant$ 1.2hours
CHAdeMO (DC)	417VDC, 120A, 50kW	$\leqslant$ 1.7hours
SuperCharger (DC)	450-600VDC, 200-225A, 90-120kW	$\leqslant$1 hour

Power Overload of Charging Stations

The great electricity demand and high power rating of PEVs make their charging process in the smart grid significantly different from the electricity consumption of other appliances. The automobile market foresees a high PEV penetration in the future. In 2018, about 2 million PEVs were sold globally, recording a year-over-year growth of 57.3% [23]. As predicted in the report [4], PEVs are expected to have 30% market share with an average 120kWh battery capacity by 2030. Correspondingly, charging standards are expected to have more high power-rating options to make the PEV competitive with conventional vehicles. In March 2019, Tesla announced its third generation superchargers that can provide charging power up to 250kW [24]. Last year, Porsche also connected its ultra-fast charging station to the grid with an 800-volt, up to 350kW charging rate [25].

However, the development of the smart grid does not catch up with the commercialization speed of PEVs. As the penetration rate of PEVs increases, the aged power infrastructure will face increasing PEV charging demand that would exceed the planned loading

capacity. Therefore, overload issue would incur at the limited-capacity feeder and causing severe operating issues such as voltage deviation, transformer overheating, etc. Simulation in [26] shows that when PEVs reach the market share of 30%, their integration to the residential grid can incur significant voltage deviation. Moreover, connecting a large number of PEVs to the distribution feeder increases the overhead distribution transformer ageing factor due to excessive operating temperature [27]. In addition, the power fluctuation of PEV charging is closely related to human behaviour, e.g., the charging power reaches peak value at night for home charging and during busy traffic hours for public charging [28, 29]. Thus, how does the aged power infrastructure cope with the time-variant power demand spike is of great challenges.

Ever since the PEV launch, its overload threaten to the smart grid has attracted many researcher's attention. CS planning has been a hot research topic that estimates the charging demands at CS candidate nodes and sets the CS power limit accordingly to mitigate the potential overload issue. To estimate the CS charging demand, PEV traffic pattern and CS dynamic have been extensively studied [30–35]. For example, PEV traffic pattern modelling problem has been investigated using data-based model [30, 31], synthesis model [32, 33], and simulator-based model [34, 35]. By considering the stochastic properties of PEV travelling and battery condition, the CS dynamic analysis is studied to estimate the time-variant PEV charging demand. By applying queue theory and modelling the CS operation dynamics as a first-come first-serve queueing model such as $M/M/c$ queue [36, 37] or $M/G/c/c$ queue [38, 39], the PEV charging demand in-station can be estimated. Then, the siting and sizing of CSs are determined by solving a multi-objective optimization problem which satisfies the power limit of the system, ensures reasonable utility of charging, and meets the PEV driver's charging demand [40–42].

However, CS planning has its ceiling: the power infrastructure limitation. Therefore, to expand the smart grid service capacity, the energy utilization of the system needs to be optimized. On the one hand, by proper scheduling, PEVs are either directed to charge at other available stations as in works [5, 43, 44] or temporally scheduled to be charged at other off-peak hours as in works [28, 45, 46]. On the other hand, the smart grid service capacity can be enhanced from the energy supplier perspective. An intuitive method is to upgrade the aged power infrastructure, which can be a huge and costly project. Another similar idea that has been mentioned in many works is to install stationary batteries at the overloaded power nodes [47–49]. However, the installation of stationary battery not only increases the infrastructure expenditure, but also leads to energy redundancy during off-peak charging hours. Its lack of flexibility could fail to meet the charging demand fluctuation incurred by the traffic regime evolution [50]. Therefore, a flexible and cost-efficient energy supply/storage approach is in urgent demand to help improve the smart

grid charging capacity.

We look back at the smart grid architecture, as shown in Fig. 1.1, where public CSs are categorized in terms of their loading levels: the resourceful CSs (RCSs) and the limited-capacity CSs (LCSs). RCSs are normally deployed in the urban area where the primary feeders have excess loading capacity, and LCSs are deployed at rural areas with limited power sources for PEV charging demand. To fully utilize the energy resource in the smart grid, surplus energy at power nodes with excess electricity (e.g., RCSs) can be delivered to LCSs to compensate the overloads. In this thesis, we exploit the potentials of using PEVs as MESs to provide the energy delivery service for overload compensation.

1.2 Mobile Energy Storage

With a similar nature to the stationary battery, the rechargeable battery in PEV has the potential to be the aforementioned medium for overload mitigation. The predicted PEV prevalence in the automobile market means that no excessive expenditure is required for installing batteries. Moreover, mobile PEVs present themselves as spatially flexible energy storages, and thus, can efficiently address the variant charging distribution problem (i.e., the role transitions between RCSs and LCSs) incurred by traffic regime evolution [50]. In this section, we first explore the energy storage potential of PEVs, followed by introducing the MES characteristics. Finally, the challenges of MESs will be presented.

1.2.1 Energy Storage Potential in PEVs

The large-size rechargeable batteries and electric chargers provide the on-road vehicle with an efficient and sustainable propulsion resource, electricity. As the PEV battery lifetime prolongs and bi-directional electric chargers develop, PEVs become more than electric consumers, but potential energy storages in smart grid.

The rechargeable battery technology development has been a long journey since the late 90s: from the lead-acid battery with 30-40Wh/kg energy density to the nickel metal battery with 30-80Wh/kg, and until now, the lithium-ion battery with more than 200Wh/kg energy density [51]. As the most prevalent battery in PEVs, lithium-ion battery has more than 4000 cycles that can support 100,000 mile driving or 8 years of driving equivalently [52]. Accounting for the main proportion of the PEV cost, the price of lithium-ion battery has dropped from $1,000/kWh in 2010 to $200/kWh in 2019 [53]. The significant price drop will continue in the next decade until the price reaches $73/kWh by 2030, at which time

PEVs are very cost-competitive with conventional vehicles. Besides, PEV also has a lot of potential battery options under develop. For instance, the zinc-air battery has a low price of $100/kWh while the hydrogen cell battery has a high energy density of 40,000Wh/kg, but the battery efficiency needs to be enhanced [54]. The lithium-air battery has similar features to hydrogen cell battery: high energy density but low efficiency and stability [55]. Solid lithium battery has been attracted many industrial attention (e.g., Tesla, Toyota, Nissan etc.) due to its high energy density up to 1,000Wh/L when the lithium-ion has an energy density between 250-693Wh/L [56, 57].

Another technical focus on the rechargeable battery is its lifetime and cost regarding charging/discharging cycle. The battery ageing depends on several factors: temperature, charging level, depth-of-discharging (DoD), rate of charge/discharge, and battery type. In terms of DoD condition, a moderate DoD prolongs the battery cycle life [58, 59]. For example, for a 40% DoD, the battery cycle life is between 1,000-3,000 while the battery cycle reduces to the range between 400 and 900 when DoD is 80% [58]. Recent research works present a promising future for prolong the lifetime of rechargeable battery when it is frequently charged and discharged: the works in [60, 61] explore and validate the potential of extending cycle life with proper vehicle-to-grid (V2G) scheduling while the works in thermal management can improve the energy efficiency of battery discharge [62].

For PEVs to be served as energy storages, bi-directional chargers are essential for realizing the reverse power flow. Extensive research works explore the feasibility of bi-directional charger in both DC/AC and DC/DC modes [63, 64] while the power quality improvement and thermal management for the charger are also investigated in the works [65, 66]. Foreseeing the bi-directional charger potential and PEV prevalence in the market, PEV and interface manufacturers are developing their roadmap and pilot projects for vehicle-to-grid (V2G) technology. The V2G roadmap proposed by Charging Interface Initiative e.V. (CharIN e.V.) predicts that around 2025, V2G aggregated charging will be achieved [67]. Currently, Fermata has released its 25kW bidirectional fast charger, partnered with Nissan to launch its Nissan Energy project [68]. Cisco also launched a V2G test project in the UK that can simultaneously connect 200 PEVs with 10kW bi-directional chargers [69].

With the rechargeable battery and bi-directional charger technologies advancing, PEVs can undertake the MES roles to store energy at power nodes with excess energy (e.g., RCSs) and deliver the surplus energy to overloaded CSs (i.e., LCSs).

1.2.2 Characteristic of MESs

The service process of MES consists of three steps: charging at RCSs, on-road travelling, and discharging surplus energy at LCSs. Compare with low-voltage power transmission at the distribution side, the energy efficiency of MES energy delivery is decent. The energy efficiency of MES charging and discharging can be as high as 95% when DC/DC converters of bi-directional chargers perform optimally. During the MES travelling period, the energy loss mainly depends on the PEV battery retention performance, which is at 99% efficiency. This calculation is obtained under the service regulation that MESs are guaranteed not using the stored energy, and the energy consumption of on-road travelling will be compensated monetarily. Therefore, the MES energy compensation service has an energy efficiency around 90% [70].

As PEV commercialization proceeds, on-road PEVs also evolve in terms of their battery capacity, fleet size, ownership, and mobility control. In this thesis, we categorize MESs into three types: utility-owned MESs (UMESs), legislation-motivated MESs (LMESs) and private MESs (PMESs) and introduce their characteristics, respectively.

UMES

In the early stage of PEV commercialization when PEVs are not pervasive, smart grid operator needs to have its own MESs to deliver energy in the smart grid. Inspired by the oil tank, the operator uses large battery capacity PEVs as MESs, which are referred to as UMESs. Since their primary responsibilities are overload mitigation, they are frequently charged and discharged on demand. The UMES prototype could refer to the developed electric truck by Tesla, semi [71], which has the battery capacity range between 800kWh and 1MWh. Consider the battery size and cost, the fleet size of UMESs is very limited and UMESs will be scheduled priorly to serve heavily overloaded LCSs.

LMES

To push forward the PEV commercialization, government has launched incentive legislation for PEVs worldwide. For example, in Canada, most provinces have PEV lease/purchase reward up to $8,000 [72, 73]. As such, vehicle fleet-based companies (e.g., lease/rental companies and public transportation) are motivated to purchase a large number of PEVs as LMESs. LMESs are normally medium battery capacity PEVs with a medium fleet size (hundreds of MESs). Refer to currently developed PEVs and global outlook, the battery capacities of LMESs are expected to be around 100kWh[19] for long-distance travelling.

The stochastic property in LMESs increases compared to UMESs due to their fleet size and their injection impact on the transportation network. When LMESs are travelling on-road, they account for a non-negligible portion of on-road traffic, which could incur additional travelling delays in peak traffic hours. Therefore, LMES scheduling needs to analyze their travel impacts in the transportation network [74].

PMES

As PEVs gradually dominate the automobile market and they become regular transportation option for every household, private PEVs can be stimulated by the grid operator to provide overload compensation service as PMESs for additional economic benefits. As each PMES wants to achieve its objective (e.g., arrive at destination timely, maximize service revenue etc.), it behaves independently of the operator. Therefore, the stochastic property of PMESs is the highest among all MESs and needs to be carefully scheduled considering their individual objectives. In terms of the driver's travelling pattern, PMESs can be both commuting vehicles or long-distance vehicles. Therefore, the battery capacity of PMES is within the range of 50-100kWh. The objective of PMESs is different from other MESs. UMESs and LMESs are additional vehicle fleets whose sole responsibility is overload compensation, and they travel on-road as additional traffic. On the other hand, PMESs only accept MES tasks when their planned routes pass the assigned CSs, and they have spare battery space [75]. Therefore, PMESs account for part of the regular on-road traffic and have little impact on the transportation network. The PMES scheduling is then focused on their service stimulation.

1.2.3 Challenges of MESs

While MESs present as an effective and flexible solution to the overload issue, their scheduling encounters several challenges from both technical and social perspectives. First is the stochastic property of MES service, where the randomness main comes from the following aspects:

1. **In-station Dynamic**: Since the energy delivery process consists of energy storage and supply, stochastic property arises in the energy charging/discharging time in RCSs/LCSs, which depends on the CS adopted standard and MES service capacity;
2. **Traffic Condition in Transportation Network:** The on-road traffic condition affects the MES travelling time on-road, which introduces stochastic properties to the MES service.

As the energy compensation service requires battery discharge, concerns about battery degradation arise and need to be carefully considered for MES scheduling. Moreover, some drivers may find the service time-consuming due to additional charging and discharging time. Therefore, MES stimulation is essential, especially for PMESs.

In this thesis, we try to address these challenges when scheduling MESs in terms of their characteristics during different commercialization stages.

1.3 Motivation and Contribution

Considering the high-efficiency, flexibility, and cost-efficiency of MESs, they are seen as essential smart grid components that help mitigate the CS overload issues. To our interests in this thesis, we will answer the question of how to exploit MES potential for overload mitigation considering the stochastic CS operation status and social impact of the service. As PEV commercialization proceeds, the characteristics of MESs change in terms of their battery capacity, fleet size, ownership, and mobility control, which also have a non-negligible impact on scheduling results. Therefore, the posted question will be discussed and studied under different PEV commercialization stages (i.e., from UMESs to LMESs, and finally PMESs).

1.3.1 Two-tier Energy Compensation Framework for UMESs

The rapid PEV commercialization demands an extensive deployment of CSs to meet the PEV charging demands. While some of CSs are installed at primary feeders with large transformer loading capacities, other CSs deployed at rural area where the transformers have limited loading capacities could encounter power overload during peak charging hours. Without proper power management, LCSs could encounter severe transformer degradation and power quality issues [6, 76–78]. Therefore, the smart grid demands cost-efficient and fast-response energy storages to help alleviate the potential overloading pressure while avoiding additional infrastructure upgrade. Inspired by the oil tank truck, power utility company can adopt huge battery capacity PEV to store surplus energy at RCSs and deliver the energy to LCSs as additional energy supply as UMES. In the early PEV commercialization when PEVs are not prevalent, UMESs are the efficient energy storage options whose sole responsibility is to deliver energy to LCSs for overload mitigation.

Regarding PEV discharging scheduling, there have been many research works that study the V2G scheduling for overload mitigation [79], renewable energy integration [80–82] and

frequency regulation [83, 84]. PEVs can either be scheduled to discharge energy directly back to connected vehicles as in works [85, 86], or scheduled for overload mitigation when connected in the parking lots as in works [87–90]. The above works consider discharging the energy that is originally the PEV propulsion resource, in which case, most PEVs will be reluctant to do so due to range anxiety issue. On the other hand, UMESs do not have the range anxiety concerns, as their primary functionalities are energy storages: as long as the UMES has spare battery space, it can be used to store and deliver surplus energy. In works [91–94], the concept of MESs has been utilized for demand response and renewable energy integration service. However, the stochastic properties of charging demand and traffic condition demand operation dynamic analysis of CSs. Moreover, the scheduling of UMESs needs to be designed according to time-variant charging demand and transportation condition. Therefore, to efficiently schedule UMESs, we need to address the following challenges:

a) The strong correlation between traffic condition and PEV charging demands requires modelling of CS operation dynamics considering the stochastic property of PEV traffic. Moreover, the heterogeneity of PEV state-of-charge (SoC) statuses also affects the CS operation dynamics and needs to be considered in dynamic analysis;

b) From the smart grid operator's aspect, how to balance the CS energy while minimizing MES scheduling cost and enabling a time-efficient energy delivery is of great challenges.

Overall, the UMES scheduling problem aims to answer the question of how to allocate the UMES energy distribution and transportation route to balance the system power and minimize the scheduling cost. To this end, we develop an energy compensation framework to schedule UMESs. Specifically, to characterize the charging process at RCSs and discharging process at LCSs, a two-dimensional Markov chain model is developed to analyze the CS dynamics. The energy delivering process in transportation network is characterized as a graph-based problem. To comprehensively analyze the MES and power system data, a two-tier energy compensation framework is introduced. Based on the framework, the MES scheduling is formulated as an optimization problem to minimize the scheduling cost while guaranteeing the power balance among a group of CSs (GCS).

1.3.2 Dynamic Pricing-based Navigation of LMESs

For LCSs which have predictable and long-term charging overload issues, UMESs can deliver a large amount of energy by prior scheduling. As a further step from the long-term

scheduling, it is also significant to investigate the GCS power balancing problem considering the short-term stochastic vehicle mobility. For example, some LCSs deployed at traffic-intensive area have predictable power shortages up to 2MWh frequently, in which case UMESs can be scheduled priorly to prevent power overload [7]. Other LCSs at rural regions only need 500kWh during 2 p.m.to 5 p.m., in which case, UMESs are not cost-efficient candidates to fulfill the energy compensation task. As PEV commercialization proceeds and incentive legislation launches globally, the increasing number of PEVs belonged to vehicle-fleet based companies become potential LMES candidates. Unlike UMESs, the large fleet-size and moderate battery capacities of LMESs make them flexible MESs suitable for dynamic energy compensation tasks.

The works in [7, 70, 92–95] study the MES scheduling problem to balance the power supply and demand efficiently, mainly focusing on the energy perspective. However, to use LMESs for compensation service means that a large number of additional traffic will inject in the transportation network. In busy traffic hours, additional traffic delay and energy compensation service delay could incur, and therefore, the injected LMES impact on the transportation network should be considered during scheduling. Regarding the PEV navigation in the transportation network, there have been some works study the PEV charging impact on the transportation network [96, 97] and conclude that without proper navigation, PEV charging could interfere with the transportation network operation. Therefore, in the works [98–102], the coupled operation of smart grid and transportation network have been extensively studied for PEV charging navigation. Compared to the above navigation works, LMES analysis focuses on the injected MES traffic analysis, rather than overall system analysis, and thus the potential delay incurred by LMES traffic is the main concern. Moreover, as LMESs do not have the complete information of on-road conditions and injected traffic, the navigation is provided by the smart grid operator to achieve the optimal travelling results. To stimulate LMESs following the provided navigation requires additional motivation (e.g., monetary rewards). Although pricing has been used in several works by analyzing Wardrop equilibrium, the convergence of Wardrop Equilibrium requires iterated simulation between the utility operator and LMESs. However, consider the importance of time-efficiency for LMES energy delivery, a more time-efficient scheduling scheme is required. To efficiently schedule LMESs at both smart grid and transportation network level, the following questions should be answered:

Q(1) How to navigate LMESs in the transportation network to avoid potential traffic delay and congestion incurred by LMESs;

Q(2) As LMESs tend to maximize their service revenue, how to stimulate LMESs accomplishing the assigned tasks under the navigated routes while the utility operator minimizes the scheduling cost.

To answer the above questions, a dynamic pricing-based scheduling scheme is proposed to adjust the service price to encourage LMESs delivering assigned energy following the navigated route. An energy-capacitated graph model is introduced to calculated the available traffic capacity on each route to enable a stable on-road travelling condition. A loading-optimized scheduling scheme is proposed to calculate the LMES travelling routes while optimizing the loading pressure at RCSs. Then, a dynamic pricing scheme is proposed to stimulate LMESs following the navigated route while minimizing the utility scheduling cost.

1.3.3 Energy Scheduling of On-road PMESs: a Stackelberg Approach

As the technology advances and PEV commercialization proceeds, PEVs are expected to have 30% market share with an average 120kWh battery capacity by 2030 [4]. As PEV becomes prevalent, the large fleet size of private PEVs makes them potential on-road PMESs with high flexibility [75]. Therefore, PMES can be a good candidate to mitigate short-term power overload issue at LCSs. Different from LMESs, scheduling on-road PMESs does not need to consider the additional traffic impact issues on the transportation network, as PMESs are originally part of the on-road traffic. The smart grid operator schedules PMESs to CSs that are along their planned routes as travelling to destined place is PMES's primary objective. Therefore, energy compensation tasks become the secondary objective for on-road PMESs. When PEVs are prevalent in the automobile market, and there are a large number of PMES candidates on-road, the overload compensation can be accomplished by on-road resource efficiently.

In literature, the centralized pricing scheme has been applied for PEV charging shift as in works [98, 103]. Hierarchical pricing decision making process has been studied in works [104–106] consider the heterogeneity of PEV preferences and objectives. Besides, game theory can be used to precisely characterize the interaction between the smart grid operator and PEVs. Specifically, the grid operator first posts the service price to stimulate PMESs and then, PMESs decide their service capacities according to the posted price. Therefore, a sequential game model such as Stackelberg game can be applied for on-road PMES scheduling. Stackelberg game model has been applied in both PEV charging and discharging schedule as in works [107–110]. However, consider MES service process, the Stackelberg game needs to consider multiple aspects. For PMESs to accomplish energy compensation tasks, both charging and discharging at CSs should be stimulated. Rewards for additional battery degradation and service time are required. Therefore, to efficiently schedule on-road PMESs, the following questions should be answered:

Q(1) How to stimulate PMESs which have different objectives and preferences to fulfill the assigned energy compensation tasks;

Q(2) How to adjust the stimulation price so that the energy balance among a GCS is achieved in a cost-efficient manner.

To answer these questions, we propose a price-incentive scheme to stimulate PMESs by maximizing their service revenues. Meanwhile, the scheme guarantees that overload issues among a GCS are effectively mitigated. Based on the scheme, a Stackelberg game is formulated to characterize the stimulation process between grid operator and PMESs where grid operator acts as the leader to post service price while PMESs act as followers, responding to the posted price.

1.4 Thesis Outline

The remainder of this thesis is organized as follows: Chapter 2 presents a comprehensive overview of related works in V2G scheduling, PEV navigation, and pricing strategies. Chapter 3 introduces a two-tier energy compensation framework that uses UMESs to balance GCS energy supply and demand. In Chapter 4, a pricing-based navigation scheme is proposed to schedule LMES energy compensation service along the optimal navigated routes. Chapter 5 proposes to use the Stackelberg game model to characterize the price-service interaction between the smart grid operator and on-road PMESs to mitigate the overload issues among a GCS. Finally, Chapter 6 concludes the thesis and presents future works.

Chapter 2

Literature Review

In this chapter, we aim to provide a comprehensive review of strategy design of MES scheduling, including PEV discharging scheduling, MES navigation scheme, and incentive strategy design.

2.1 PEV Discharging Strategy for Overload Mitigation

An essential technology that supports MES is the V2G technology where PEVs send their battery energy back to the smart grid. Existing works on V2G can be classified into three types: renewable energy integration, regulation service provision, and peak load mitigation. The stochastic energy output of renewable energy can be smoothly integrated to the smart grid using PEVs as energy buffers to flatten the violent generation fluctuation [80–82]. V2G can also be used in regulation service to fine-tune the frequency and voltage of generation through balancing between power demand and supply [80]. Due to the randomness in PEVs and regulation service, the V2G regulation service capacity estimation has been studied in works [38, 112]. Works in [83, 84] thoroughly study the scheduling schemes to maximize the PEV profit in the regulation market.

Extending the connected PEV functionality to energy storage, vehicle-to-vehicle (V2V) discharging and V2G technologies can be used to mitigate the peak power loads. The related works are summarized in Table 2.1. V2V technology considers directly using the PEV discharged energy to charge other PEVs with charging demands. Using PEV aggregators (e.g., parking lot, CSs, etc.) as V2V energy exchange interface, the works in

Table 2.1: Comparison of related works on overload mitigation

Application Scenario	Scheduling Objective	Solution/Technique
Stationary V2V	Peak load shaving + charging cost reduction [85]	Fuzzy logical controller
	QoE + grid reliability enhancement [86]	Matching theory
Stationary V2G	Minimize peak load [87]	Cooperative game
	Evaluate V2G service potential [88]	Quadratic programming
	Flatten microgrid power profile [89]	Optimal power flow
	Multi-objective power dispatch [90]	Mixed-inter linear programming
Mobile V2G	Minimize charging cost [79]	Convex optimization
	Minimize transmission loss [70]	Minimal cost-flow
	Demand balance [93, 94]	Dynamic network simplex
	Optimize PEV charging/discharging policy [111]	Markov decision process

[85, 86] schedule the PEVs connected in parking lots for V2V service to mitigate the PEV charging impact on the smart grid. The work in [85] uses a fuzzy logical controller to adjust the charging/discharging rates of connected PEVs to mitigate their charging impact on smart grid and reduce the PEV charging costs. Similarly, the work in [86] schedules connected PEVs in the parking lot using matching theory to improve their quality of experience (QoE) while enhancing the smart grid reliability. PEVs can also participate in V2G service by discharging their energy back to the power grid. The potential benefits of V2G technology on the smart grid have been investigated in works [87, 88]. The work in [87] proposes a distributed demand response algorithm to adjust PEV charging/discharging to minimize the peak load. The work in [88] concludes that with V2G, the PEV charging capacity of the existing infrastructure can be significantly enhanced. The reliability enhancement for V2G application in the microgrid is also assessed and validated in works [89, 90]. Interregional V2G is considered in the work [89] to balance the power supply and demand among multiple micro-grids while in work [90], PEVs are considered as stationary energy storages for power dispatch. However, most of the above works consider V2G in the stationary PEV mode, in which PEVs are considered as large battery capacity energy storages. For the smart grid to further improve the system loading capacity based on its existing infrastructure, PEVs can be used as MESs to maximize energy utilization.

Several works have exploited the potentials of mobile PEVs under the V2G scenario

[70, 79, 93, 94, 111]. The V2V charging is investigated in the work [79] by encouraging on-road PEVs discharging their excess energy to relieve the overload issue of PEV charging via price control and advanced communication architecture. However, the mobile V2V method has a high risk of power imbalance due to its limited energy capacity. Consequently, the energy network concept of using PEVs as energy porters to deliver energy from renewable energy sources to CSs is proposed in the work [70]. The impact of mobile V2G network on the smart grid stability and reliability has been studied in works [93, 94] using dynamic network simplex methods. In the work [111], to optimize the MES performance in micro-grid, a Markov decision process problem is formulated to obtain the optimal policies of MES charging and discharging. However, most of the reviewed works have not considered the scenario where only the storage space of PEV battery is used for overload compensation. This scenario considers two unique features: first is to use PEV battery space rather than existing energy in PEVs due to range anxiety issue; second is to use MESs delivering energy among a GCS to maximize the energy source utilization in the system and mitigate the overload issues at LCSs. Due to the randomness of both charging demands and local traffic condition, operation dynamics of RCSs and LCSs are require to be modelled and analyzed. Moreover, an efficient framework is demanded to schedule MESs based on station dynamics and current transportation condition to minimize the scheduling cost and enable energy transmission time-efficiency.

2.2 MES Navigation Scheme Design

To promote PEVs in the automobile market, legislation (e.g., PEV lease/purchase incentive) has been launch worldwide [4]. Vehicle fleet-based companies will therefore become the main proportion of PEV owners with a large fleet of PEVs that have the potential to be LMESs. To study the MES potentials of PEVs, many works investigate the MES energy delivery scheduling for power balance [70, 93, 94, 111]. In our work on scheduling UMESs [7], the CS dynamics are modelled as two-dimensional Markov Chains to predict the CS energy surplus/demand and a convex optimization problem is formulated to schedule UMESs among a GCS. While the energy scheduling of MESs has been studied, the impact of MES fleet on the transportation network has yet to be discussed. When LMESs participate in energy compensation tasks, a large number of additional traffics will then inject in the transportation network. Without proper traffic navigation, additional traffic delay and service delay could incur in busy traffic hours.

Consider the primary objective of PEV integration to the smart grid is charging for travel range extension, PEV charging navigation and its impact on the smart grid and transportation network have been extensively studied, as summarized in Table 2.2. The

Table 2.2: Comparison of related works on PEV navigation

Application Scenario	Scheduling Objective	Solution/Technique
System impact evaluation	Vehicular mobility-based modelling [96]	Monte-Carlo simulation
	Charging facility-based modelling[97]	Activity-based simulation
Coupled system operation	Cost-minimized charge and travel [98]	Wardrop principle
	Robust energy dispatch [99]	Convex optimization
	Elapsed time minimization [100]	Non-linear program
	Travel + CS waiting +charging time minimization [101]	Dynamic programming
	Route energy minimization [102]	Convex relaxation

charging activity of a large fleet of PEVs can couple the operation of smart grid and transportation network. The reliability of both systems has been investigated in work [96] using a quasi sequential Monte-Carlo simulation to sample the EV travelling on the transportation network. It is concluded that the proposed PEV charging/discharging control can improve the smart grid reliability but has a reverse impact on the transportation network. In addition to modelling vehicular traffic patterns, another crucial factor in the coupled system is the "tie points": CSs [97]. The work in [97] uses an activity-based model to co-simulate the smart grid and transportation network to understand the multi-role of EV CSs. To study the coupled system, the work in [98] characterizes the PEV charging process as part of the operation of the transportation network by considering PEV charging as virtual arcs in the transportation graph model. An optimal pricing scheme is used to schedule PEVs on the coupled system, and by obtaining second Wardrop equilibriums, the social optimum of smart grid economic dispatch and traffic assignment is achieved. In the work [99], the traffic assignment and power analysis are formulated together as an optimal traffic-power flow convex optimization problem to enable a robust energy dispatch in smart grid considering traffic demand uncertainty. In the work [100], a similar energy virtual-arc graph is adopted to analyze both user-centric and system-centric PEV charging navigation for minimizing the total elapsed time of travel and recharge. Consider the time-dependent congestion conditions on-road and in-CS, the work in [101] proposes to minimize the travel time when having the context of other PEVs' intention of charging. In addition to minimizing elapsed time during operation, some PEVs are concerned about their energy consumption in-travel and therefore, in the work [102], a minimum energy route search problem is formulated to help PEVs find their minimum energy-consumed

routes considering the random effects of on-road traffic condition.

While extensive research on PEV charging navigation has been conducted, the scheduling of LMESs has its unique feature from the following perspectives. First, LMESs are additional injected traffic that has the stochastic property related to time-dependent charging demand. Thus, rather than minimizing the overall travelling time, the potential delay incurred by the LMES traffic is the primary concern. Second, consider the ownership of LMESs, it is essential to maximize their revenues, which can also be the motivation for them to follow the operator's navigation by price-incentive. Although Wardrop equilibrium has been proposed in some works to achieve social optimum, the convergence of Wardrop equilibrium requires iterated interaction between grid operator and LMESs, while a more time-efficient scheduling scheme is required for overload mitigation. Therefore, we propose a dynamic pricing-based scheme to navigate LMESs following the scheduled route to mitigate their potential impact on the transportation network. The proposed scheme enables minimal LMES impact on the transportation network while guaranteeing a time-efficient energy compensation service.

2.3 Incentive Strategy Design for MESs

Table 2.3: Comparison of related works on incentive strategy

Application Scenario	Scheduling Objective	Pricing Scheme
Centralized pricing	Minimize generation + travel cost [98]	Wardrop principle
	Unify PEV charging demand distribution [103]	Iterated rule-based model
Hierarchical pricing	UO: max revenue + PEVs: max utilities [104]	Home/roaming pricing
	UO: max social welfare + PEVs: max utilities [105]	Menu-based pricing
	Peak load flatten [106]	Linear programming
	CS: max revenue + PEVs: max charging benefits [107]	Stackelberg game
	CSs: max revenue + PEVs: min overall service costs [108]	
	UO: max energy utilization + PEVs: min service costs [109]	
	CS: max revenue + PEVs: max revenue and satisfaction [110]	

When PEVs dominate the automobile market, PMESs will be the popular MES options for overload mitigation. As PMESs have different objectives and service preferences,

a proper incentive should be provided to ensure the service task accomplishment. In literature, there have been extensive works that use the monetary incentive for PEV charging/discharging control, as summarized in Table 2.3. For PEV charging that couples the operation between smart grid and transportation network, a toll is posed to selfish drivers to align their behaviours with social optimum that minimizes generation cost and traffic time cost [98]. Specifically, a marginal congestion pricing scheme is proposed according to Wardrop principle to achieve the user equilibrium. In the work [103], temporal PEV charging shifting is considered to reduce the overlaps between residential and CS load during peak evening hours. The reaction of PEV charging profile in response to the price can be effectively characterized as an iterated rule-based pricing model.

In most works, PEVs are assumed to have similar objectives, such as minimize charging costs/maximizing V2G service revenue. However, consider the heterogeneity in PEV charging/discharging preferences and goals, the PEV decision making process should also be studied. Therefore, the interaction between smart grid operator, CSs, and PEVs become a hierarchical decision marking process. In the work [104], to balance the energy supply and demand within each micro-grid, home-pricing and roam-pricing policies are adopted by the micro-grid utility operator (UO) to optimize its revenue. Based on the posted price, PEVs then make their charging/discharging decisions to maximize their utilities. A discrete pricing scheme is proposed in the work [105], where PEVs select their service in the menu provided by UO to maximize their utilities. The UO-PEV scheduling via pricing can also be conducted decentralized as in the work [106], where PEVs determine their charging/discharging processes based on the real-time price and demand-supply curve under a decentralized cloud computing architecture.

As a mature mathematical model, game theory can precisely characterize the interaction between the UO and PEVs in a hierarchical architecture. The UO first posts its electricity price/service price, and then PEVs make their service decisions in response. The interaction can be characterized as a sequential game model such as the Stackelberg game. Stackelberg game model has been applied to both PEV charging and V2G scheduling [107–110]. The CS operator is considered as the game leader in the work [107] to maximize its charging revenue while PEVs act as followers to maximize their charging energy fairly. Multiple-leader multi-follower game can be applied when CSs compete with each other to maximize their own revenue in terms of their waiting time, travel distance and so on, as in the work [108]. The Stackelberg game can also be used in a multi-layer architecture where the smart grid operator is the first layer leader that is in control of multiple CSs among a GCS to maximize the overall energy utilization and revenue as in the work [109]. When scheduling both PEV charging and discharging, the work in [110] proposes a game model that maximizes the service revenue and charging satisfaction of PEVs and EV aggregator's

profit using the real-time electricity trading price.

While the incentive strategy design has been extensively explored in the above works, two key factors of PMES scheduling have not been considered collaboratively: hierarchical pricing and MES service process. While PEV charging and discharging schedule has been discussed before, the main focus is on PEV in-station scheduling. However, when schedule PMESs, the service process consists of three stages, including MES charging, discharging, and on-road travelling. Moreover, to stimulate PMES providing service, rewards for additional battery degradation and service time should be considered. For the smart grid operator, how to mitigate the LCS overload issues using on-road MES source in a cost-efficient manner is its main concern. Therefore, our objective in the PMES scheduling scenario is to design an effectively pricing-incentive strategy to stimulate on-road PMESs participating in the service by considering the heterogeneity in their objectives and preferences.

2.4 Summary

In this chapter, we have provided a comprehensive review of the existing works about PEV discharging and MES scheduling in smart grid and transportation network, and the incentive strategy design for PMESs. From the literature review, we can conclude that while the PEV discharging scheduling has been extensively studied, challenges of multi-stage MES scheduling have not been solidly resolved yet. In the following chapters, we will introduce our proposed schemes to address the challenging issues during different development stages of MESs and ultimately reach the research objectives of this thesis.

Chapter 3

Two-Tier Energy Compensation Framework for UMESs

3.1 Introduction

As PEV gradually dominates the automobile market, CSs will be deployed extensively in the smart grid to provide charging service. However, the implementation of this project requires necessary upgrade on the aged power infrastructure. Specifically, some CSs are expected to be deployed at primary feeders that have excess energy, guaranteed with sufficient loading capacities at MWh level [6]. On the other hand, to complement the charging demand where these primary feeders cannot reach, some CSs are deployed at feeders whose transformers have limited loading capacities. Adjacent CSs with different loading capacities are clustered together as a GCS.

Due to the temporal-spatial variation of PEV charging distribution in smart grid [5], overload concerns arise for the CSs with limited capacities. Without proper scheduling for energy balance at these CSs, the overloaded feeders could encounter severe transformer and power quality degradation [113, 114]. To address this potential issue without spending excessive expenditure on the infrastructure upgrade, cost-efficient and fast-response energy storages are in urgent demand. This requirement can be abstracted as how to allocate the energy resources to a group of service nodes within the area beyond their inherent limits corresponding to real-time energy demand distribution.

A possible solution is to utilize mobile electric storages as resource porters to carry energy from RCSs to the overloaded LCSs. Instead of deploying brand new mobile electric storages, we could use what we already have: the soon to be prevalent PEVs, and rethink

their energy storage features. The rechargeable batteries in PEVs not only store energy for vehicular mechanical propulsion, but also can be a potential flexible energy storage device. Therefore, in this chapter, we utilize the PEV as a flexible energy storage device to compensate for the lacking energy and mitigate the overload issue at LCSs. These PEVs that deliver surplus energy from RCSs to LCSs are referred to as MESs. Inspired by the oil tank trucks, local power utility company adopts large battery capacity PEVs as UMESs to mitigate the heavy overload issues at LCSs. Since PEV charging demands are strongly correlated to on-road traffic condition which varies temporally and spatially, the stochastic properties of PEV traffics need to be considered. From the UO perspective, UMESs should accomplish energy compensation tasks in a cost-efficient manner. Therefore, the UMES scheduling aims to minimize the scheduling cost while enabling the energy balance among a GCS.

To efficiently allocates UMES energy distribution, we introduce a two-tier energy compensation framework. Although PEV discharging scheduling has been extensively studied in works [70, 79, 85–90, 93, 94, 111], few research works have utilized MESs as utility-scaled energy storages to address the CS overload issue. The main contribution of the work are threefold. First, in terms of the stochastic on-road PEV traffic, MES charging, and discharging processes at RCSs/LCSs are characterized as Markov chain to normalize the operation dynamics. Second, consider the heterogeneity of input data (e.g., CS loading status, MES status, on-road traffic, etc.), a two-tier energy compensation framework is introduced to schedule UMESs among a GCS. Finally, to minimize the scheduling cost while guaranteeing power balance, a cost-minimized optimization problem is formulated and solved for MES scheduling.

The remainder of the chapter is organized as follows. The system model is developed in Section 3.2 to characterize station operations. Energy compensation framework is introduced in Section 3.3. Based on the framework, the optimization problem is formulated and solved in Section 3.4. Section 3.5 presents the performance evaluation of the proposed scheme, and Section 3.6 summarizes this chapter.

3.2 System Model

In this section, we analyze the CS dynamics and transportation network. Operation dynamics of RCSs/LCSs are characterized as Markov Chains to analyze the CS energy status. Then, a directed graph is used to abstract the transportation network to plan UMES travel routes. A summary of useful notations in this chapter is shown in Table 3.1.

As shown in Fig. 3.1, we consider a group of PEV charging stations S that are deployed

Table 3.1: Notations for Chapter 3

Symbols	Description
$\lambda_{\mathrm{PEV,h}}$	The on-road PEV traffic flow at time h, vehicles/hour
$\lambda_{\mathrm{s,h}}$	The PEV arrival rate at CS s at time h, vehicles/hour
$\lambda_{\mathrm{sM,h}}$	The average UMES arrival rate at CS s at time h, vehicles/hour
μ_{s}	The service rate of CS s, vehicles/hour
π	The steady-state probability of Markov Chain
$\alpha_{\mathrm{r_e},1/2/3}$	Energy charging price parameters
β	Transportation price, $\$/km/kWh$
$\Delta E_{\mathrm{av.}}$	The average UMES discharging capacity, kWh
$\rho_{\mathrm{s,h}}$	The percentage of arriving PEVs at CS s at time h, %
a	The overall number of PEVs being served in the CS, vehicles
b	The number of PEVs being served by UMESs, vehicles
$C_{\mathrm{charge,h}}$	The cost of charging UMESs at RCS at time h, \$
$C_{\mathrm{charge,r_e,h}}$	Charging price at RCS r_{e} at time h, $\$/kWh$
C_{h}	Overall scheduling cost at time h, \$
$E_{\mathrm{Mq_f,h}}$	The energy supplied by UMESs at LCS q_{f}, kWh
$E_{\mathrm{Mr_e,h}}$	The allocated UMES energy be charged at RCS r_{e} at time h, kWh
C_{sL}	The energy supplied by local feeder at CS s, kWh
$C_{\mathrm{trans,h}}$	The transportation cost of UMESs at time h, \$
$D_{\mathrm{z_n z_m}}$	The distance between road intersections z_{n} and z_{m}, km
$E_{\mathrm{q_f,k,h}}$	The energy discharged by the kth UMES at LCS q_{f} at time h, kWh
$E_{\mathrm{r_e,q_f,h}}$	The energy transmitted from RCS r_{e} to LCS q_{f} at time h, kWh
$G(V, Ed)$	The directed transportation graph
$g_{\mathrm{s,h}}$	The MES energy supply rate at CS s at time h, vehicles
$L_{\mathrm{av.}}$	The average PEV charging demand, kWh
M	The transition matrix of Markov Chain
$N_{\mathrm{q_f M,h}}$	The number of PEVs charged by UMESs at LCS q_{f} at time h, vehicles
N_{sL}	The number of PEVs charged by local feeder at CS s, vehicles
$P_{\mathrm{s,L}}$	The power capacity of local feeder connected to CS s, kW
h	Index of time
R/Q	The set of RCS/LCS
S	The set of GCS
Z	The set of road intersections

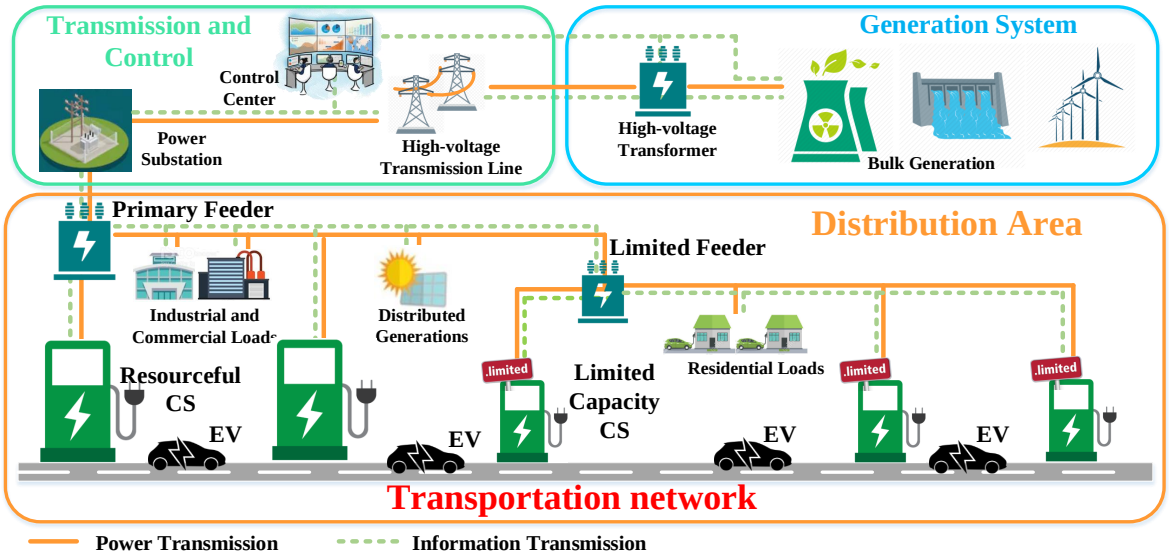

Figure 3.1: System overview of the GCS.

at different levels in the power distribution system, while the UO controls the scheduling activities. In terms of energy capacity, CSs S can be categorized into two classes: R and Q. The first one is RCSs, whose set is denoted by $R = \{r_1, r_2 \dots r_e\}$. They are connected to primary feeders with stable and sufficient power supplement from the bulk generations. On the other hand, LCSs, whose set is denoted by $Q = \{q_1, q_2 \dots q_f\}$ are connected to limited-capacity feeders in the remote areas. With sufficient power supply, RCSs potentially have excess energy supply capacity to satisfy PEV charging even in peak traffic hours. Moreover, their excess charging energy can be reallocated to LCSs with UMESs to mitigate their potential overload issues.

3.2.1 Station Energy Capacity Characterization

CS can be supplied by two sources: either by generation system through local feeders, or by additional energy storages such as UMESs. The energy can be supplied through local feeders, depends on the loading capacities of the distribution transformer, which is denoted as C_{sL}. It is further characterized as the number of PEV charging services N_{sL} that the local feeder can provide simultaneously in an hour considering incoming PEVs have the average charging demand $L_{\mathrm{av.}}$. In our work, the average charging demand is set to 15kWh,

which is 50% battery capacity of the PEV model Nissan Leaf. Considering that the station connected feeder has a power capacity of $P_{\mathrm{s,L}}$, the number of PEVs charged by the local feeder denoted as N_{sL} satisfies the following equation:

$$C_{\mathrm{sL}} = \int_{h} P_{\mathrm{s,L}} dt = N_{\mathrm{sL}} \cdot L_{\mathrm{av.}}. \tag{3.1}$$

In terms of the hourly on-road traffic flows, PEV charging demands at station s, denoted as $R_{\mathrm{s,h}}$ is time-variant. Regarding the relation between C_{sL} and $R_{\mathrm{r_e,h}}$, CSs with different capacities response differently. Enabled with sufficient power supply, RCS r_{e} can easily fulfill incoming PEV charging demands $C_{\mathrm{r_eL}}$, which is denoted as:

$$C_{\mathrm{r_eL}} \geq R_{\mathrm{r_e,h}}. \tag{3.2}$$

On the other hand, LCS q_{f} may encounter power imbalance at peak traffic hours, which is denoted as:

$$C_{\mathrm{q_fL}} \leq R_{\mathrm{q_f,h}}. \tag{3.3}$$

To address the overload issues in LCSs, the allocated UMES energy $E_{\mathrm{Mq_f,h}}$ at LCS q_{f} should compensate the energy gap between energy supplied through local feeders and PEV charging demands, denoted as:

$$E_{\mathrm{Mq_f,h}} + C_{\mathrm{q_fL}} = R_{\mathrm{q_f,h}} \tag{3.4}$$

the UMES allocated energy is the summation of all the UMES discharging energy at the station during hour h. Similar to the local feeder capacity, it is also characterized by the number of PEV charging service $N_{\mathrm{q_fM,h}}$ that can be provided simultaneously in an hour, as:

$$E_{\mathrm{Mq_f,h}} = \sum_{k} E_{\mathrm{q_f,k,h}} = N_{\mathrm{q_fM,h}} \cdot L_{\mathrm{av.}}, \tag{3.5}$$

where $E_{\mathrm{q_f,k,h}}$ denotes the energy discharged by the kth UMES coming to LCS q_{f} during time h. On the other hand, RCSs need to undertake the UMES charging tasks besides charging PEVs. The UMES charged energy at RCS r_{e}, denoted as $E_{\mathrm{Mr_e,h}}$, needs to satisfy the following equation:

$$C_{\mathrm{reL}} \geq E_{\mathrm{Mre,h}} + R_{\mathrm{re,h}}, \tag{3.6}$$

to ensure the RCS feeder capacity can fully supply the in-station PEV charging and UMES energy reallocation.

3.2.2 Station Dynamic Model

By introducing UMESs as energy porters in the smart grid and considering the temporal-spatial variant traffic distribution, dynamics of CSs need detail analysis. The station dynamics are analyzed hourly to estimate their energy status during h-th hour, where $h \in [0, 1, 2...22, 23]$. The station dynamic is characterized as a continuous-time Markov Chain. In terms of the station property, the modellings of LCSs and RCSs will be introduced respectively.

Limited-Capacity Charging Station

In the LCS, charging-demand PEVs and energy supplier UMESs both arrive at the station randomly. The PEV behaviour can be characterized as a stochastic process based on the following assumptions.

Assumption 1 *PEVs arrive at the CS s following a Poisson process with an average arrival rate of $\lambda_{\mathrm{s,h}}$ at time h.*

As validated in [115], the arrival distribution of vehicles at CSs follows a Poisson process since each vehicle arrives at stations independently and memoryless. Hence, in our model, PEVs are considered to follow the Poisson process. The average arrival rate $\lambda_{\mathrm{s,h}}$ depends on the on-road PEV traffic flow $\lambda_{\mathrm{PEV,h}}$, the time h of a day, and the arriving percentage of PEVs at the CS $\rho_{\mathrm{s,h}}$ among the overall on-road PEV traffics as

$$\lambda_{\mathrm{s,h}} = \lambda_{\mathrm{PEV,h}} \cdot \rho_{\mathrm{s,h}}. \tag{3.7}$$

UMESs are another independent set of vehicles functioning sorely as energy storage devices. Upon receiving the energy compensation tasks, UMESs randomly arrive at RCSs to store surplus energy and depart. Depends on the on-road stochastic traffic condition, UMESs can be considered travel on-road independently and memoryless. Therefore, UMES arrival distribution at LCSs is considered as a Poisson process.

Assumption 2 *UMESs arrive at the charging station s following a Poisson process with an average arrival rate of* $\lambda_{\mathrm{sM,h}}$ *at hour h.*

The UMES energy supply rate $g_{\mathrm{s,h}}$ at LCS s is characterized as the number of PEVs that UMESs can charge simultaneously in an hour. The rate depends on the UMES arrival rate $\lambda_{\mathrm{sM,h}}$, the average UMES energy-storing capacity $\Delta E_{\mathrm{av.}}$, and average PEV charging demand $L_{\mathrm{av.}}$. It can also be characterized as the summation of incoming UMES energy $E_{\mathrm{Mqf,h}}$ divided by the average PEV charging demand:

$$g_{\mathrm{s,h}} = \frac{\lambda_{\mathrm{sM,h}} \cdot \Delta E_{\mathrm{av.}}}{L_{\mathrm{av.}}} = \frac{E_{\mathrm{Mqf,h}}}{L_{\mathrm{av.}}}. \tag{3.8}$$

LCS manages the energy coming from UMESs and local feeder together, and then distributes to each charger following the same charging standard.

Assumption 3 *The service rate of station s follows an exponential distribution with an average service rate of* μ_{s}.

As each station provides charging services to different types of PEVs with different SoC conditions, the PEV charging service is also a stochastic process. The service time can be modelled as a lognormal distribution based on 2009 NHTS data [116]. To make the service process analytically tractable, we consider that station operators adopt the developed smart charging mechanism in the work [38] to make the service process an exponential distribution. The service rate μ_{s} is related to the adopted charging standard $P_{\mathrm{C,s}}$ and PEV charging demand $L_{\mathrm{av.}}$ and denoted as:

$$\mu_{\mathrm{s}} = \frac{P_{\mathrm{C,s}}}{L_{\mathrm{av.}}}. \tag{3.9}$$

Based on the above modelling, station dynamics in the LCS is characterized as a two-dimensional continuous-time Markov Chain as shown in Fig. 3.2.

Each state in the Markov Chain has two parameters. a denotes the overall number of PEVs being served by local feeders and UMESs. b represents the number of PEVs being charged by the energy supplied by UMESs. Therefore, the number of PEVs being served by the local feeder is $a - b$.

First, looking at the Markov Chain by the row, as the state proceeds horizontally, a increases gradually, denoting that the number of PEVs being served in the station increases.

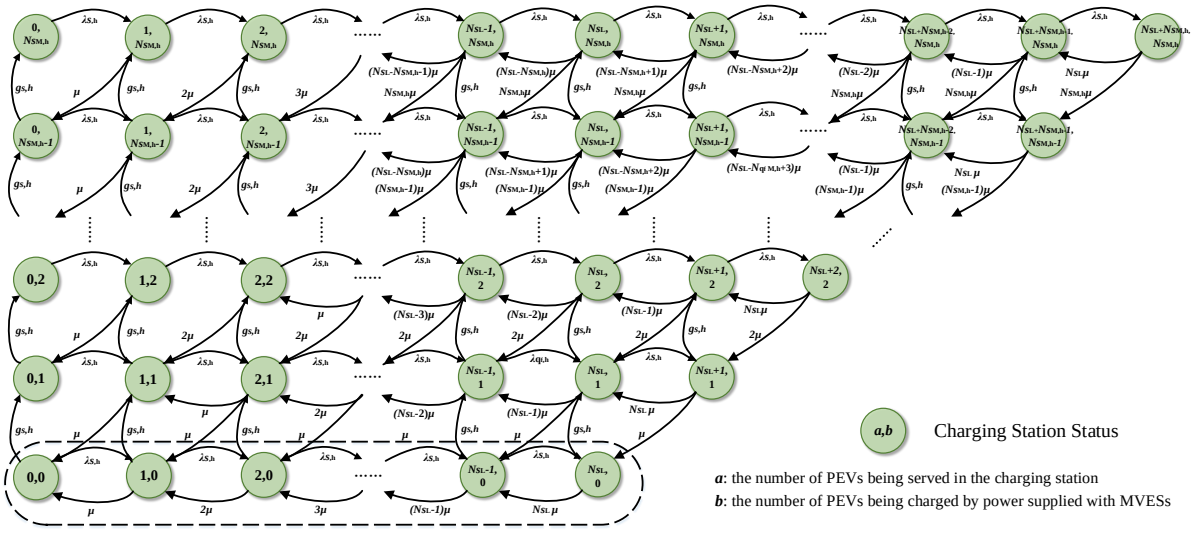

Figure 3.2: Hourly Markov Chain with two dimensional state space.

When the state reaches to the right end, it means that local feeder and all the incoming UMESs energy has been used up, and the next incoming PEVs cannot be served. On the other hand, as the state moves vertically, b increases, i.e., the incoming reallocated UMES energy increases. As the incoming UMESs increase, the state proceeds vertically and the right-end state in each row denotes a fully occupied station with an increasing allocated UMES energy. Hence, the summation of the very right states on each row denotes the probability that incoming PEVs will leave without being served at time h, which is considered as the probability of arriving at a congested station. Complementally, the station availability denotes the probability that incoming PEVs can be charged immediately upon arriving at the station without additional waiting. The station availability is considered as an essential index of the station power balance condition, which directly affects the station operation performance.

To evaluate the station performance, the steady-state station congestion probability can be calculated by analysis of the Markov Chain. The transition matrix of the Markov Chain M is given as in Equation (3.10), where the element at i^{th} row and j^{th} column is denoted as $m_{\mathrm{i,j}}$. M satisfies $m_{\mathrm{ij}} \geq 0$ (for $i \neq j$) and $m_{\mathrm{ij}} = -\sum_{i=1}^{h} m_{\mathrm{ij}}$ (for $i = j$). l denotes the total number of elements in the Markov Chain, as calculated in equation (3.11).

$$M = \tag{3.10}$$
$$\begin{pmatrix} -(\lambda_{\mathrm{s,h}}+g_{\mathrm{s,h}}) & \lambda_{\mathrm{s,h}} & ... & g_{\mathrm{s,h}} & ... & 0 \\ \mu_{\mathrm{s}} & -(\lambda_{\mathrm{s,h}}+\mu_{\mathrm{s}}+g_{\mathrm{s,h}}) & ... & 0... & 0 & \\ 0 & 2\mu_{\mathrm{s}} & ... & 0 & ... & 0 \\ \vdots & \vdots & \ddots & \vdots & \vdots & \vdots \\ 0 & 0 & ... & -(\lambda_{\mathrm{s,h}}+g_{\mathrm{s,h}}) & ... & 0 \\ \mu_{\mathrm{s}} & 0 & ... & 0 & ... & 0 \\ \vdots & \vdots & \ddots & \vdots & \vdots & \vdots \\ 0 & 0 & ... & 0 & ... & -(N_{\mathrm{s,L}}+N_{\mathrm{sM,h}})\mu_{\mathrm{s}} \end{pmatrix}.$$

$$l = \sum_{i=1}^{N_{\mathrm{sM,h}}+1} (N_{\mathrm{sL}}+i). \tag{3.11}$$

Proposition 1 *The Markov Chain is positive recurrent.*

Proof 1 *The Markov Chain is irreducible and has finite states, Hence, all states are recurrent. For a finite-state Markov Chain, all recurrent states are positive recurrent [117].*

Proposition 2 *The Markov Chain has a unique solution for the steady-state probabilities* π*.*

Proof 2 *As a positive recurrent chain, its aperiodic states are ergodic. For an irreducible ergodic Markov Chain in states* $i = 0, 1, 2..., h$*, steady-state probabilities* π *exists [117].*

In the Markov Chain, π is a $1 \times l$ vector. Let e be an all-one vector of length of l. Through the calculation of balance equations:

$$\begin{cases} \pi \cdot M = 0, \\ \pi \cdot e = 1, \end{cases} \tag{3.12}$$

the steady-state probabilities of Markov can be obtained. Hence, the station congestion probability can be obtained as:

$$p_{\text{congestion,s,h}} = \sum_{i=0}^{N_{\text{sM,h}}} \pi_{(N_{\text{sL}}+i,i)}, \tag{3.13}$$

where $\pi_{(N_{\text{sL}}+i,i)}$ denotes the right end state on each row. By contrast, the station availability that is complemental to the station congestion probability, is denoted as:

$$p_{\text{availability,s,h}} = 1 - p_{\text{congestion,s,h}}. \tag{3.14}$$

Once the station availability requirement is determined, the allocated UMES energy $E_{\text{Mqf,h}}$ at LCSs can be calculated using Equations (3.7)-(3.14).

Resourceful Charging Station

On the RCS side, its operation dynamic needs to be analyzed so that its surplus energy for UMESs can be estimated. Similar to LCSs, PEVs are considered arriving at the station according to assumption 1 and the station charging service process follows assumption 3.

Supplied with sufficient energy, RCSs are assumed to only be UMES energy supplier and no UMESs will be discharged in RCSs. Thus, $g_{\text{s,h}} = 0$ and $N_{\text{sM,h}} = 0$, making the station dynamic a $\text{M/M/}N_{\text{sL}}$ queue as dash-lined in Fig. 3.2.

In the queue, as the state proceeds horizontally, a increases gradually, denoting that the number of PEVs being served in the station increases. When the state reaches the right end, it means that all power sources are utilized. Through the calculation of Equations (3.10)-(3.14), the steady states of the RCS queue can be obtained. Then, the expected PEV charging demands $R_{\text{s,h}}$ in station s at time h can be calculated as:

$$R_{\text{s,h}} = \sum_{a=0}^{a=N_{\text{sL}}} \pi_{(\text{a},0)} \cdot m_{(\text{a},0)} \cdot L_{\text{av.}}. \tag{3.15}$$

Then, the surplus energy of RCS r_{e} that can be stored by UMESs is the energy gap between the station overall energy capacity and PEV charging demands, as:

$$E_{\text{Mre,h}} = N_{\text{sL}} \cdot L_{\text{av.}} - R_{\text{s,h}}. \tag{3.16}$$

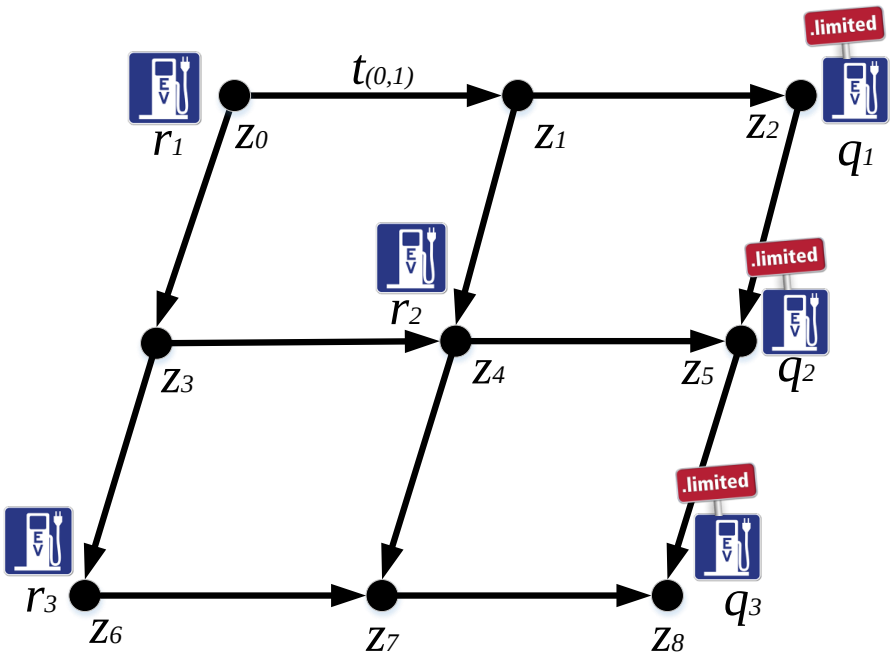

Figure 3.3: Transportation network topology of the GCS.

3.2.3 Transportation Network Model

The abstracted transportation network model, as shown in Fig. 3.3, consists of road intersections z_{g}, where $\{z_1, z_2 \ldots z_{\mathrm{g}}\} \in Z$ and edges $S_{\mathrm{m,n}}$ from intersections z_{m} to z_{n}. CSs aredeployed at intersections. In terms of time variations, traffic velocities fluctuate along routes. The traffic velocities are defined as hourly-average variables between intersections (e.g. $v_{(0,1)}$ denotes the velocity of edge $S_{0,1}$). The distance between two intersection is denoted as $D_{(0,1)}$. Then, the traffic time from intersections z_0 to z_1 is:

$$t_{(0,1)} = \frac{D_{(0,1)}}{v_{(0,1)}}. \tag{3.17}$$

A directed graph $G(V, Ed)$ is used to model the transportation network in Fig. 3.3. V stands for road intersections as vertexes, and Ed represent traffic routes as the graph edges. The edge weight is the traffic time of the edge. Suppose UMESs are charged at RCS

r_1 and are directed to transport the surplus energy to LCS q_2, the energy delivery route can be $S_{(0,1)}$-$S_{(1,4)}$-$S_{(4,5)}$. Considering the hourly on-road traffic variation, to enable a time-efficient UMES energy transmission on-road, the fastest transmission route is required. For example, when congestion happens on the edge $S_{(0,1)}$, resulting in longer transmission time (larger weight), another transmission route needs to be found. If Routes $S_{(0,3)}$-$S_{(3,4)}$-$S_{(4,5)}$ has the minimal transmission time between stations r_1 and q_2, UMESs will be directed to travel along these routes.

3.3 Two-Tier Energy Compensation Framework

To efficiently utilize UMESs, we introduce a two-tier energy compensation framework, as shown in Fig.3.2. The framework has the central controller (i.e., UO) on the upper tier in charge of controlling GCS and UMESs, and CSs on the lower tier for data monitor and operation. Considering the time-variant on-road traffic, the framework is conducted hourly to provide analysis and guidance for the next-hour operation.

3.3.1 Upper Tier Operation

The central controller on the upper tier starts to perform the hourly operation scheme at time T_{clock} by requesting the energy information of each station (e.g., demanded UMES energy at LCS and available energy for UMESs at RCS). Once the central controller receives the energy demand information from all stations via either wired communication (e.g., power line communication or fiber optics) or wireless communication (e.g., cellular network), the central controller starts to schedule UMESs charging and discharging, which consists of two stages:

- ▷ **Stage 1: UMES Transportation Route Planning**: In terms of collected on-road traffic condition, a route scheduling scheme is conducted to decide the fastest routes between each RCS-LCS pair so that the time-efficiency of UMES energy delivery can be guaranteed.
- ▷ **Stage 2: UMES Energy Scheduling**: Based on the collected energy information from RCSs and LCSs, an optimization problem is formulated and solved to arrange the charging and discharging stations for UMESs. The energy scheduling aims to minimize the overall scheduling costs while enabling the power balance among a GCS.

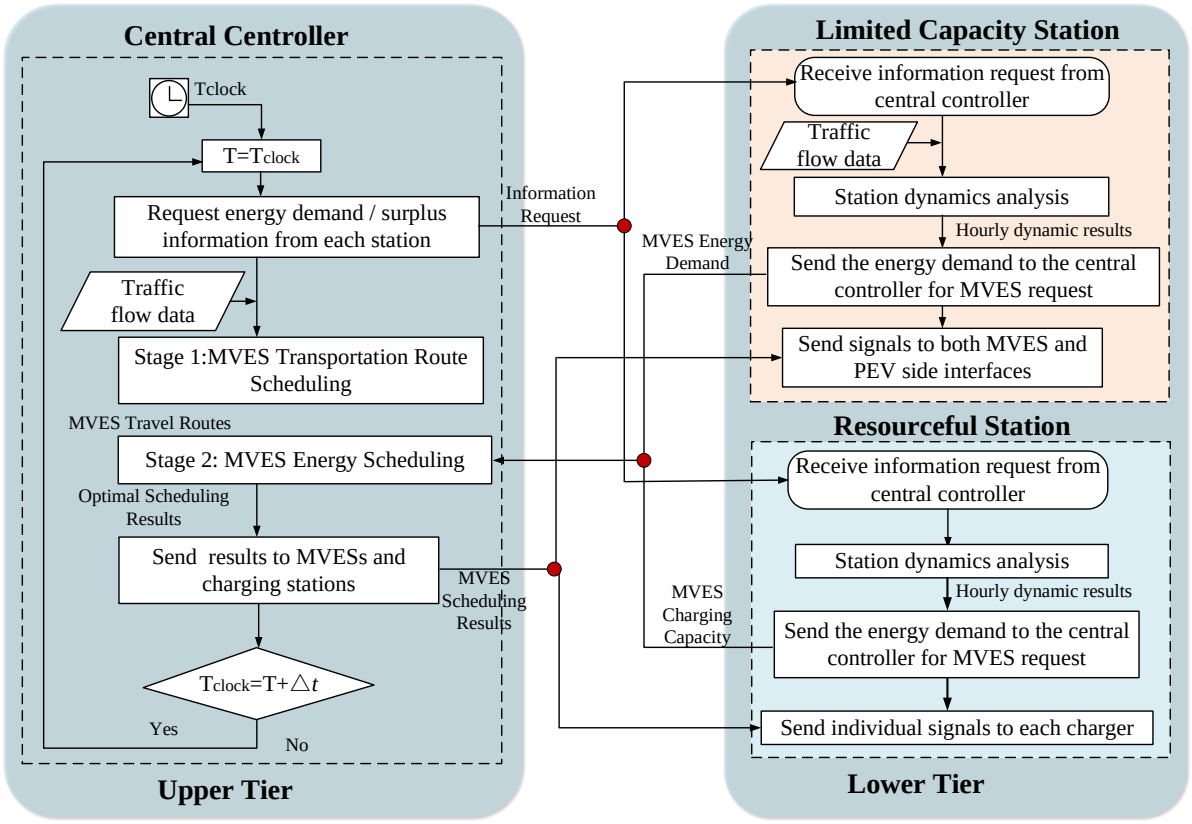

Figure 3.4: Flow chart of the two-tier energy compensation framework.

The scheduling results are then distributed to both RCSs and LCSs on the lower tier and UMESs. The whole process repeats after the time duration of Δt.

3.3.2 Lower Tier Operation

At time h, RCSs and LCSs at the lower tier estimate their energy status and communicate with the central controller upon request. Next, we introduce their operations based on their CS properties:

- ▷ **LCS** q_{f} - Once LCS q_{f} receives the information request from the upper tier, the station dynamics will be analyzed with the predicted traffic data input at time h+1. Through the two dimensional Markov Chain analysis, the next-hour energy demand forecast

will be obtained and sent to the upper tier. Then, upon receiving the scheduling results from the upper tier, the station q_{f} will operate accordingly and reserve the UMES discharging spots.

- ▷ **RCS** r_{e} - Upon receiving the information request from the central controller, RCS r_{e} analyzes the station dynamics and sends its UMES charging capacity to the upper tier as part of the input data for UMES energy scheduling. After receiving the controller scheduling results, the station r_{e} will then prepare to charge the surplus energy to UMESs.

3.4 Problem Formulation

Based on the introduced framework, the UMES scheduling problem can be formulated stage by stage. First, the UMES transportation routing in stage one is formulated as a fastest route search problem to calculate the energy delivery route of each RCS-LCS pair. Then, the UMES energy scheduling is formulated as a cost-minimized convex optimization problem and can be solved efficiently.

3.4.1 UMES Transportation Routing

As the framework is operated on an hourly basis, it is essential to enable that the allocated energy can be delivered to LCSs in time. Looking at the UMES energy delivery process, both charging and discharging processes at CSs are stochastic processes, while the on-road energy delivery process depends on the on-road stochastic traffic. Thus, the fastest path scheduling scheme is proposed to determine the fastest paths between RCS-LCS pair in terms of hourly-variant traffic conditions.

Based on the Floyd-Warshall algorithm which finds the fastest travel path between all nodes, we propose the fastest path search scheme as described in Algorithm 1. We first initialize the graph G(V,Ed) with two sets of edge weights: ***time*** as an array of UMES transmission time and ***dist*** as an array of UMES travelling distance. Meanwhile, the hopping nodes ***next*** are initialized as original nodes. Then, the algorithm iteratively chooses one node as hopping node between the origin and destination to find the shortest path. Notably, when the hopping node finds a path that has the same weight as the former recorded shortest path, the algorithm will then choose the path that has shorter transportation distance to enable the cost-efficiency of route scheduling. Further, to output the optimal path results, a path reconstruction scheme is presented in the third loop.

Algorithm 1: Fastest Path search for UMES Energy Transmission

```
Let time be a V × V array of minimum distance initialized to ∞ ;
Let dist be a V × V array of minimum distance initialized to ∞ ;
Let next be a V × V array of vertex indices initialized to null ;
Initialization;
for each edge (u,v) do
    time[u][v] ← t_(u,v) ;
    dist[u][v] ← D_(u,v) ;
    next[u][v] ← v ;
for k from 1 to V do
    for i from 1 to V do
        for j from 1 to V do
            if time[i][j] < time[i][k]+time[k][j] then
                time[i][j] ← time[i][k]+time[k][j] ;
                next[i][j] ← next[i][k] ;
            else if time[i][j] = time[i][k]+time[k][j] then
                if dist[i][j] < dist[i][k]+dist[k][j] then
                    time[i][j] ← time[i][k]+time[k][j] ;
                    next[i][j] ← next[i][k] ;
for all edges (u,v) do
    if u = r_e and v = q_f then
        if next[i][j]=null then
            return [] ;
        path=[u] ;
        while u ≠ v do
            u ← next[i][j] ;
            path.append(u) ;
        return path ;
```

3.4.2 UMES Energy Scheduling

The UMES scheduling is operated by local UO on an hourly basis with the hourly-averaged UMES scheduling result. Based on the received RCS/LCS energy estimation, the UO schedules UMESs aiming at minimizing the overall scheduling costs C_{h} while guaranteeing the power balance among a GCS. The problem is formulated as follow:

$$\min_{E_{\mathrm{r_e},\mathrm{q_f}}} \quad C_{\mathrm{h}} = C_{\mathrm{charge,h}} + C_{\mathrm{trans.,h}} \tag{3.18}$$

$$\text{s.t.} \quad p_{\mathrm{availbility,s,h}} \geq p_{\mathrm{QoS,s}}, \forall s \in S \tag{3.18. a}$$

$$0 \leq E_{\mathrm{r_e},\mathrm{q_f},\mathrm{h}} \leq E_{\mathrm{Mr_e,h}}, \forall r_{\mathrm{e}} \in R, \forall q_{\mathrm{f}} \in Q \tag{3.18. b}$$

$$\sum_{q_{\mathrm{f}} \in Q} E_{\mathrm{r_e},\mathrm{q_f},\mathrm{h}} \leq E_{\mathrm{Mr_e,h}}, \forall r_{\mathrm{e}} \in R \tag{3.18. c}$$

$$\sum_{r_{\mathrm{e}} \in R} E_{\mathrm{r_e},\mathrm{q_f},\mathrm{h}} = E_{\mathrm{Mq_f,h}}, \forall q_{\mathrm{f}} \in Q \tag{3.18. d}$$

The scheduling costs C_{h} consists of two parts: the costs $C_{\mathrm{charge,h}}$ of charging UMESs at RCSs and the transportation costs $C_{\mathrm{trans.,h}}$ of UMESs during energy compensation service. The charging costs are the summation of UMES charging costs at RCSs, depending on the charging price $C_{\mathrm{charge,r_e,h}}(E_{\mathrm{r_e},\mathrm{q_f}})$ at RCS r_{e} and the allocated UMES energy $E_{\mathrm{r_e},\mathrm{q_f}}$ at the RCS:

$$C_{\mathrm{charge,h}} = \sum_{r_{\mathrm{e}} \in R} \sum_{q_{\mathrm{f}} \in Q} C_{\mathrm{charge,r_e,h}}(E_{\mathrm{r_e},\mathrm{q_f}}) \cdot E_{\mathrm{r_e},\mathrm{q_f}}. \tag{3.19}$$

Since the energy that is used to charge UMESs should be originally used for incoming charging-demand PEVs, the more energy UMESs charge, the less charging energy is reserved for charging-demand PEVs. Therefore, the UMES charging price increases as the allocated UMES energy increases at RCSs. The UMES charging price is formulated as a quadratic function:

$$C_{\mathrm{charge,r_e,h}}(E_{\mathrm{r_e},\mathrm{q_f}}) = \alpha_{\mathrm{r_e},1} \cdot E^2_{\mathrm{r_e},\mathrm{q_f}} + \alpha_{\mathrm{r_e},2} \cdot E_{\mathrm{r_e},\mathrm{q_f}} + \alpha_{\mathrm{r_e},3}, \tag{3.20}$$

where $\alpha_{\mathrm{r_e},1}, \alpha_{\mathrm{r_e},2}, \alpha_{\mathrm{r_e},3} > 0$. The first differential of the function as shown in Equation (3.21), reflects the price deviation relation with the allocated UMES energy:

$$\frac{\mathrm{d}}{\mathrm{d}E_{\mathrm{r_e,q_f}}}\left(C_{\mathrm{charge,r_e,h}}(E_{\mathrm{r_e,q_f}})\right) = 2\alpha_{\mathrm{r_e},1}\cdot E_{\mathrm{r_e,q_f}} + \alpha_{\mathrm{r_e},2}, \tag{3.21}$$

where $\alpha_{\mathrm{r_e},2}$ denotes the primary price-setting without energy fluctuation and $\alpha_{\mathrm{r_e},1}$ represents the price fluctuation causing by the demanding energy deviation from the primary price setting.

In addition to the charging costs, UMES transportation process also incurs electricity and time consumption, which is considered as part of scheduling costs. The transportation costs are the product of travelling distance $D_{\mathrm{r_eq_f}}$ between RCS r_{e} - LCS q_{f} pair, the transportation price β per transmission distance per kWh and the transmitted energy $E_{\mathrm{r_e,q_f}}$ along the route $S_{\mathrm{r_eq_f}}$, denotes as:

$$C_{\mathrm{trans.,h}} = \sum_{r_{\mathrm{e}}}\sum_{q_{\mathrm{f}}} E_{\mathrm{r_e,q_f}}\cdot\beta\cdot D_{\mathrm{r_eq_f}}. \tag{3.22}$$

While minimizing scheduling costs, every station needs to maintain its power balance and maintain its operation performance by fulfilling most of the arriving PEV charging demands. As shown in constraint (3.18.a), every CS needs to guarantee a pre-defined station availability $p_{\mathrm{QoS,s}}$ to maintain the customer satisfaction.

From energy balance perspective, the UME charging energy $E_{\mathrm{r_eq_f}}$ that is supplied by RCS r_{e} and sent to LCS q_{f} should be within the energy capacity $E_{\mathrm{Mr_e}}$ of the RCS r_{e}, as in constraint (3.18.b). Moreover, the overall UMES stored energy at RCS r_{e} should also be within the station energy capacity, as in constraint (3.18.c). On the UMES energy supply side, the summation of arriving UMES energy at station q_{f} should equal to the LCS demanding energy $E_{\mathrm{Mq_f,h}}$, as denoted in constraint (3.18.d).

3.4.3 Solution

The formulated UMES energy scheduling problem is convex with a convex set that can be efficiently solved through Disciplined Convex Programming (DCP) of CVX [118]. Through the DCP ruleset examination, the convexity of the formulated problem can be validated. Then, the continuous functions as our formulated ones can be solved through simple convex programming implementation using atom library (regulated convex or concave functions).

The whole process of the energy compensation framework is described as Algorithm 2. After hourly traffic data input and initialization, the LCS energy demand and RCS available energy estimation are conducted by analyzing Markov Chain and queue model,

respectively. On the upper tier, UMES energy transmission routes are planned by the fastest path search scheme of Algorithm 1 using predicted on-road traffic. Then, DCP is conducted to minimize scheduling costs provided the transmission routes, energy demands, and requests, and the UMES energy compensation results can be obtained.

Algorithm 2: UMES Energy Compensation Procedure

Input: Hourly traffic flow;
Hourly transportation time of each route ;
Initialization
Let h=0 ;
Let $E_{\mathrm{Ms,h}}$=0, $R_{\mathrm{s,h}}$=0 ;
for *h=0 to 23* **do**
Markov Chain Analysis:
Calculate the demanding energy of LCSs ;
Calculate UMES charging capacity at RCSs ;
Do *Algorithm 1: fastest path search scheme* for UMES energy transportation ;
Output: Fastest transportation routes between stations ;
DCP for cost-minimized UMES energy scheduling:
DCP ruleset examination;
DCP simple implementation ;
Output: UMES energy allocation results to all stations ;
Energy allocation and transportation path to all UMESs.

3.5 Performance Evaluation

In this section, the effectiveness of the introduced framework is evaluated based on the real traffic data on California highway collected by the California department of transportation. The framework effectiveness is mainly demonstrated from the station operation, GCS overload mitigation, and cost-efficiency perspective. Further, the impacts of station availability and transportation cost on the framework results are discussed.

3.5.1 Simulation Setup

To evaluate the performance of the introduced framework, simulation is conducted based on the California highway data collected by the California department of transportation

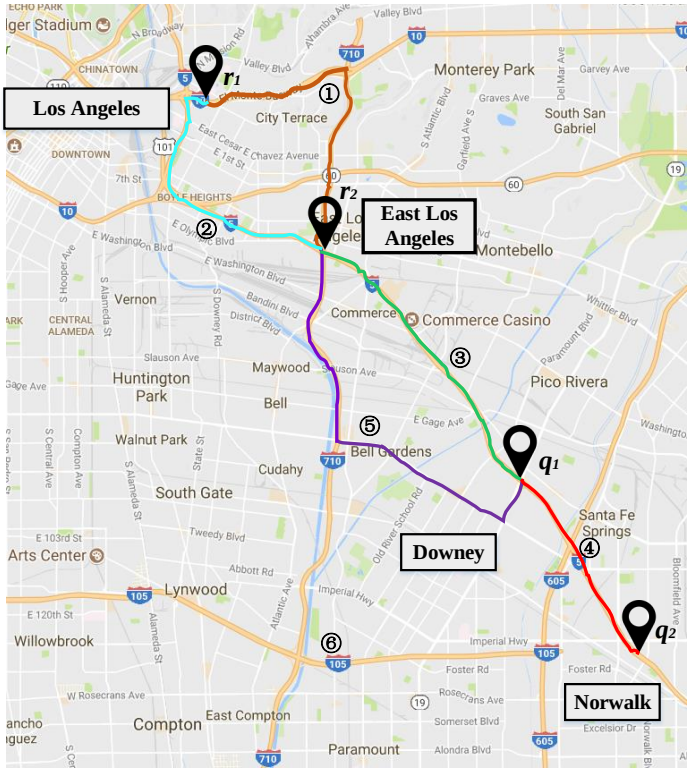

Figure 3.5: CS deployment in South California.

PeSM [119]. As shown in Fig. 3.5, the UMES travelling area covers from downtown Los Angeles (L.A.) to Norwalk, with four CSs deployed along unidirectional highway I-5S. RCSs r_1 and r_2 are deployed near downtown L.A. and East L.A. respectively. To satisfy the huge electricity demand in the urban area, large-capacity feeders and bulk generations are accessible to these two stations. LCSs q_1 and q_2 are located at Downey and Norwalk respectively. In terms of transportation conditions, we select five major travel routes connecting stations, with details shown in Table 3.2.

PEV Settings

A 10% PEV market share in the vehicle market is considered. Therefore, we consider that 10% of on-road traffics will be PEVs. For RCSs, 10% of the on-road PEVs enter their stations for recharging. 5% on-road PEVs are recharged at the LCSs. Hence, the PEV

Table 3.2: Route information

Departure	*Destination*	*Travel Highway*	*Route #*	*Mileage* (km)	*Color*
L. A. DT	East L. A.	I-10E, I-710S	1	10.6	Brown
L. A. DT	East L. A.	I-5S	2	8.1	Blue
East L. A.	Downey	I-5S	3	8	Green
Downey	Norwalk	I-5S	4	8	Red
East L. A.	Downey	I-710S, Local	5	16	Purple

arrival rate at each station in a day is shown in Fig. 3.6.

Connecting to primary feeders, RCSs have large loading capacities with fast charging speed. Station r_1 has a power capacity C_{r_1} of 2.4MWh while r_2 can provide energy C_{r_2} up to 1.8MWh [120]. For the LCSs that are connected to limited-capacity feeders in rural areas, power supply capacities reduce to hundred-kW level with a lower voltage level [120]. In this case, we consider that station q_1 can provide a maximum energy $C_{\mathrm{q}_1\mathrm{L}}$ at 480kWh and station q_2 has a feeder capacity $C_{\mathrm{q}_2\mathrm{L}}$ of 300kWh. CSs adopt different charging standards to fit the local conditions. For example, RCSs use the SAE CCS level 3 standard [21] to charge PEVs at 120kW while LCSs adopt the SAE CCS level 2 at 90kW [21]. The station availability of RCSs is set to 95% to ensure that RCSs have a great service quality before conducting the energy compensation tasks. On the other hand, LCSs should be able to meet the availability probability of 90% with UMES energy discharging. The coefficients of RCS charging price function $\alpha_{\mathrm{r_e},1}, \alpha_{\mathrm{r_e},2}$ are set as in Table 3.3 to map with the current electricity rate plan of Pacific Gas and Electric (PGE) company in California [121]. The coefficient of transportation cost β is set to 0.004 [122]. The parameter settings are also summarized in Table 3.3.

Route Choice

First, the fastest routes are calculated by the proposed fastest path search algorithm for UMES energy transmission, as shown below. The algorithm inputs data of routes travelling time are extracted from google map [123] on an hourly basis, as summarized in Table 3.4.

▷ **L.A. - Downey**:

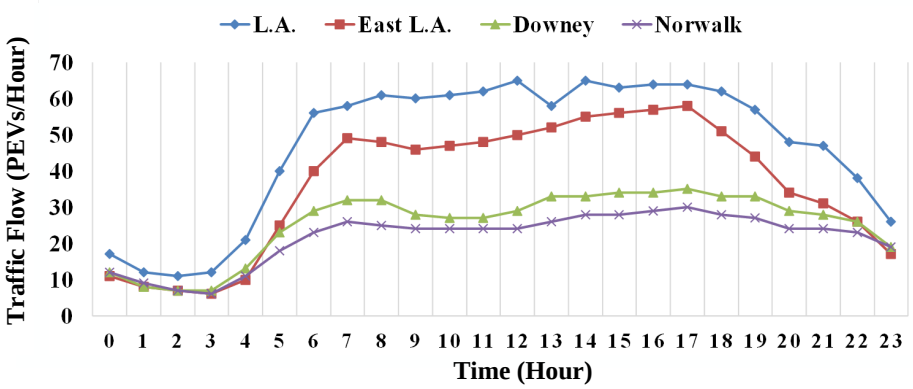

Figure 3.6: PEV hourly arrival rate at each station.

Table 3.3: Simulation parameters

Para.	Value	Para.	Value
C_{r_1}	2.4MWh	C_{r_2}	1.8MWh
$C_{\mathrm{q}_1\mathrm{L}}$	480kWh	$C_{\mathrm{q}_2\mathrm{L}}$	300kWh
$\mu_{\mathrm{r}_\mathrm{e}}$	120kW	$\mu_{\mathrm{q}_\mathrm{f}}$	90kW
$P_{\mathrm{C},\mathrm{r}_\mathrm{e}}$	120kW	$P_{\mathrm{C},\mathrm{q}_\mathrm{f}}$	90kW
$\rho_{\mathrm{r}_\mathrm{e},\mathrm{h}}$	1%	$\rho_{\mathrm{q}_\mathrm{f},\mathrm{h}}$	0.5%
$\alpha_{\mathrm{r}_1,1}$	0.000167	$\alpha_{\mathrm{r}_1,2}$	0.0332
$\alpha_{\mathrm{r}_2,1}$	0.00025	$\alpha_{\mathrm{r}_2,2}$	0
β	0.004		

Table 3.4: Average travel time of routes

Time	0	1	2	3	4	5	6	7	8	9	10	11	12	13	14	15	16	17	18	19	20	21	22	23
Route 1 (min)	10	10	12	12	10	10	9	10	11	11	11	11	12	12	16	16	16	16	14	10	10	10	12	10
Route 2 (min)	7	7	7	7	8	7	8	9	10	10	10	9	10	12	16	22	24	22	18	10	8	9	8	8
Route 3 (min)	7	8	8	8	8	8	8	8	9	8	8	9	10	12	14	20	22	24	22	16	12	10	8	7
Route 4 (min)	5	5	5	5	5	5	7	6	7	7	7	7	7	8	9	10	12	12	12	10	10	7	6	5
Route 5 (min)	14	14	14	14	14	14	16	18	20	18	18	20	18	22	25	30	35	40	40	30	18	17	16	14

  - *12a.m.-14p.m. and 19p.m.-23p.m.*: Route 1 - Route 3;
  - *15p.m.-18p.m.*: Route 2 - Route 3;

▷ **L.A. - Norwalk**:

  - *12a.m.-14p.m. and 19p.m.-23p.m.*: Route 2 - Route 3 - Route 4;
  - *15p.m.-18p.m.*: Route 1 - Route 3 - Route 4;

▷ **East L.A. - Downey**: Route 3 All day;

▷ **East L.A. - Norwalk**: Route 3 - Route 4 All day;

3.5.2 Simulation Results

Solving the optimization problem by Algorithms 1 and 2 on MATLAB platform, we can obtain the optimal UMES scheduling results. First, the improvement of station availability is presented to show that UMESs have been effectively assigned among a GCS to maintain the CS operation performance and enable energy balance. As the objective of the introduced framework is to mitigate the overload issues of GCS with minimal costs, the overload mitigation performance is then illustrated through the result comparison of demanding energy from local feeder with and without UMES participation. The cost comparison results between the introduced framework and randomly-assigned case are presented. Further, the impact of UMES transportation on the scheduling results have been carefully analyzed.

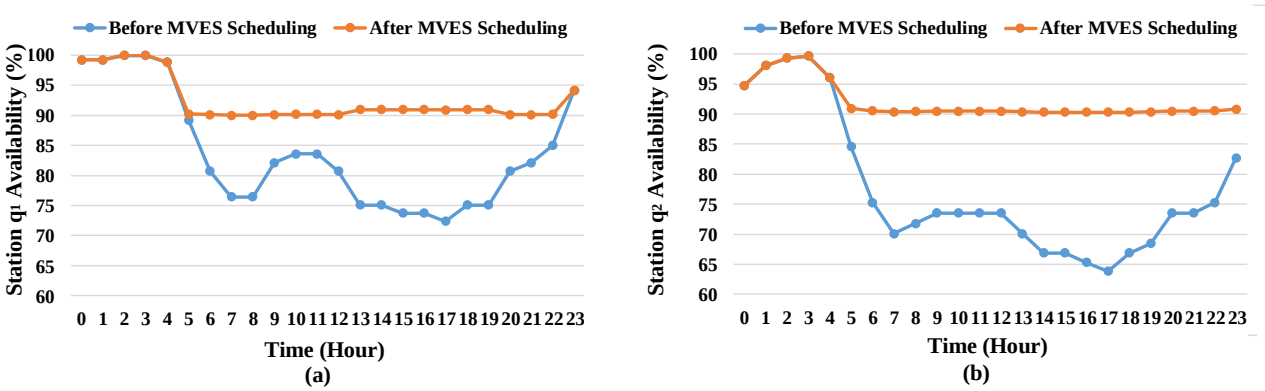

Figure 3.7: Station availability comparison.

Station Availability

Comparisons of station availabilities before and after UMES scheduling are shown in Fig. 3.7. As shown in Fig.3.7(a), without UMES scheduling, the availability of station q_1 at Downey encounters enormous drop during the daytime from 6a.m.to 11p.m.. That is, depending solely on the local power supplement, the station encounters service congestion (i.e., PEVs have more than 10% probability to leave the station without being charged) when more than 20 PEVs come to the station. During the daytime, traffic flow near Downey fluctuates between 23 to 35 PEVs/hour as shown in Fig.3.6, causing the station consistently occupied and many PEVs will leave without being charged. The situation changes when UMESs participate in energy compensation tasks. LCSs now estimate their demanding delivered energy for the LCSs to achieve a 90% station availability, and as seen in Fig.3.7(a), after UMESs being scheduled to the station, the availability of the station remains stably around 90%. Therefore, the effectiveness of UMES energy compensation on station operation performance can be validated.

Similarly, in Fig.3.7(b), the availability of station q_2 at Norwalk has effective improvement during the daytime between 6 a.m. to 11 p.m.. As UMESs are scheduled to station q_2 corresponding to the station required charging demand, the station availability remains stably around 90%.

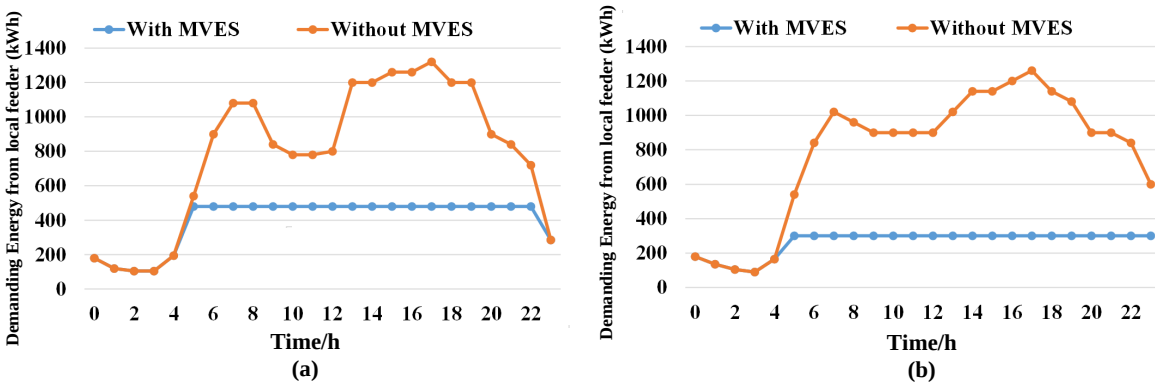

Figure 3.8: Demanding energy of local feeder.

Overload Mitigation

The overload mitigation result through UMES energy scheduling is presented in Fig.3.8. The results are compared between the cases of LCS operation with and without UMES scheduling to verify the significance of UMES participation. Without UMES scheduling, the demanding energy from the local feeder at LCS q_1, as shown in Fig.3.8(a), starts to dramatically increase at 5 a.m. due to the increasing PEV charging demand. Without UMES scheduling and proper infrastructure upgrade, the demanding energy exceeds the limit of local feeder capacity during the daytime, which can severely overload the feeder. On the other hand, with the help of UMESs, local feeder only needs to provide energy up to its capacity limit (480 kWh). Hence, with UMES participation, the potential overload issue is effectively mitigated at station q_1.

Similar to LCS q_1, station q_2 also encounters severe power overload during daytime. As shown in Fig.3.8(b), starting from 5 a.m., demanding energy from local feeder can peak up to 1200kWh without UMES scheduling. With only 300 kWh feeder capacity, the peak hour PEV charging demand can easily crash the normal power operation and cause severe transformer degradation. On the other hand, with UMES participation, local feeder only needs to provide its feeder capacity value during the daytime to effectively avoid the potential overload.

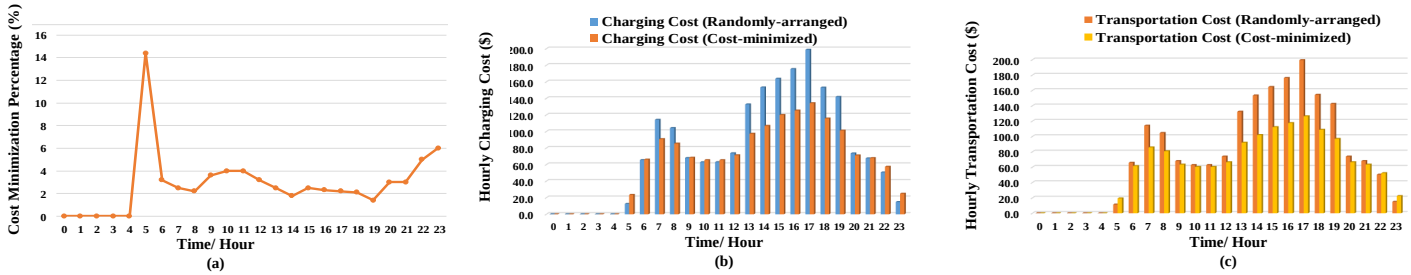

Figure 3.9: UMES scheduling cost performance comparison.

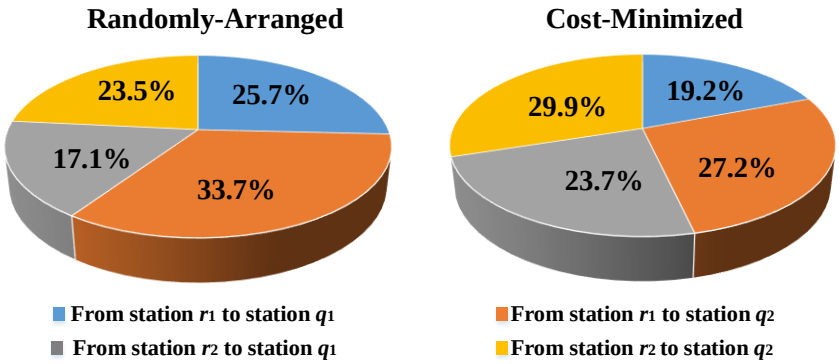

Figure 3.10: UMES charging task allocation comparison.

UMES Scheduling Costs

A randomly-arranged UMES scenario is presented as the baseline case to compare with the proposed scheme. The scheduling cost comparison is shown in Fig.3.9(a). It can be seen that through the proposed cost-minimized scheduling scheme, the scheduling cost can be effectively minimized from 6 a.m. to 11 p.m.. As part of the scheduling costs, charging cost has been effectively reduced in most of the time other than time periods of 10-11 a.m. and 9-11 p.m.. This situation occurs as transportation cost outweighs charging cost when RCSs have sufficient energy to cope with UMES charging tasks. Compared with station r_1 that has lower charging price but longer transportation distance, station r_2 will be assigned with more charging tasks. The transportation cost is also minimized as shown in Fig.3.9(c), by flexibly arranging the UMES energy tasks among RCSs.

The hourly-averaged charging task allocation results among a GCS of both cost-minimized

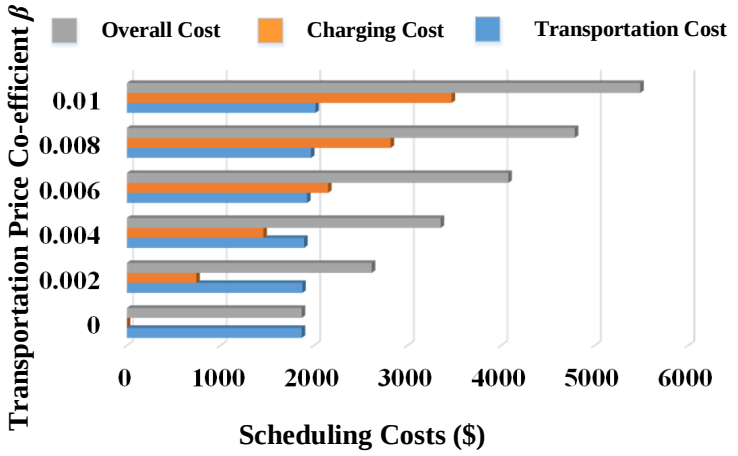

Figure 3.11: UMES scheduling costs with transportation price co-efficient.

case and randomly-arranged case are shown in Fig. 3.10. Randomly-arranged case assigns more charging tasks to station r_1 considering its large charging capacity. However, when transportation cost is included in the cost-minimized case, UMES charging tasks are allocated more to station r_2 to minimize UMES transportation distance, which is in accordance with the practical concerns of minimizing transportation cost. The comparison of the two cases validates the optimality of the cost-minimized scheme.

Influence of UMES Transportation Cost

As the electric battery technology advances, charging and discharging price of UMESs will decrease correspondingly, leading to a decrease of UMES transportation price. The fluctuation of UMES transportation price has the potential to affect UMES energy scheduling decisions. In this subsection, the transportation price co-efficient β is used as the indicator of battery technology evolution to illustrate the transportation cost influence on scheduling results.

It can be seen in Fig.3.11 that as β increases, the overall scheduling cost increases. The increment of β, leading to the transportation cost increase, accounts for a large proportion of the whole cost. Although the UMES charging demand is irrelevant to transportation routes, the transportation price coefficient does affect the UMES charging task allocation, which leads to a slightly increasing charging cost.

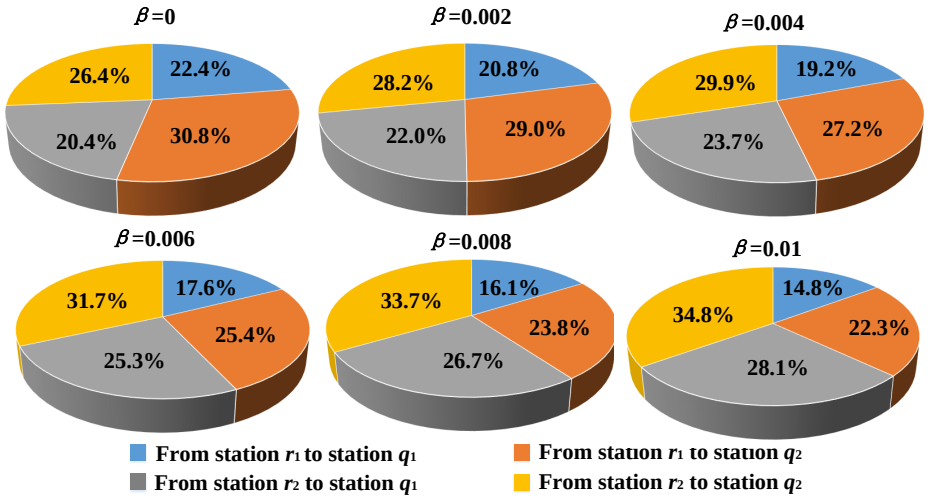

Figure 3.12: UMES charging task allocation with transportation price co-efficient.

To illustrate the influence of β on UMES charging allocation, the UMES task allocation variation with β is shown in Fig. 3.12. It can be seen that transportation price increment results in the decrease of UMES charging tasks in station r_1 as this RCS is the farther one to both LCSs. Particularly, UMESs that go to station q_1 tend to be charged at station r_2 due to a shorter transportation distance. Although RCS r_2 is closer to both LCSs, its higher charging cost and limited charging capacity require station r_1 to share some charging responsibility to ensure that enough UMESs will arrive at LCSs on time.

Station Availability v.s. UMES Scheduling Costs

In LCSs, the requirement of station availability has non-negligible impacts on UMES scheduling costs and charging task allocations among RCSs. Daily UMES scheduling cost variations with limited capacity station availability are shown in Fig.3.13. With higher station availability requirement, the overall scheduling cost increases rapidly. To maintain a higher station availability, more energy is demanded to be transferred by UMESs. Thus, charging tasks increase in RCSs, leading to higher charging cost overall. On the other hand, maintaining a higher station availability also results in an increment of UMES transportation cost. The detailed UMES charging allocations with increasing station availability are illustrated in Fig. 3.14. It can be seen that higher the station availability, more UMES charging tasks are assigned to station r_1. Considering a smaller charging capacity in

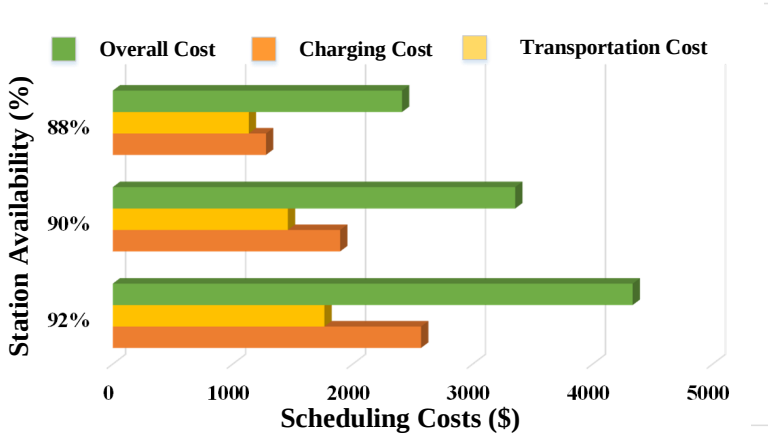

Figure 3.13: UMES scheduling costs with station availability.

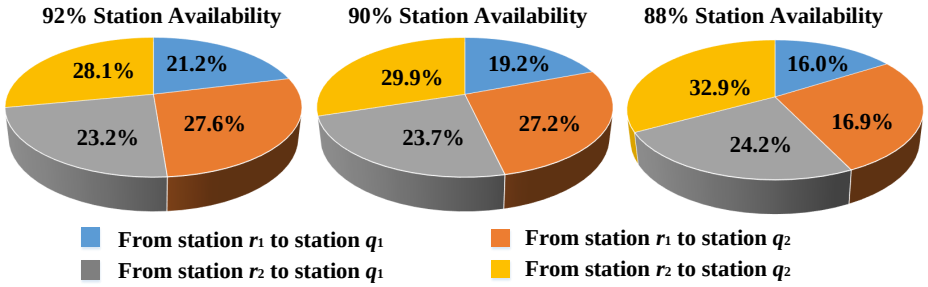

Figure 3.14: UMES charging task allocation with station availability.

station r_2 between the two RCSs, fulfilling the increasing charging tasks means allocating more UMES charging to station r_1.

3.6 Summary

In this chapter, a two-tier energy compensation framework has been introduced to use UMESs as energy porters at peak hours effectively. A convex optimization problem has been formulated aiming to minimize the scheduling. Through the simulation, the effectiveness of the introduced framework and the optimality of the formulated problem have been validated. Moreover, the influence of scheduling factors on the framework results have been illustrated. It is concluded that as battery technology develops, the increasing UMES

energy transmission efficiency can lead to wider transmission coverage and more flexible scheduling. Further, strict station availability requirement can result in a drastic increment of scheduling cost, leading to a trade-off between the station availability and scheduling costs. Based on the introduced energy compensation framework, the cost-efficient UMES scheduling scheme can be applied to the local power utility company to address the overload issues without excessive facility upgrade expenditure.

Chapter 4

Dynamic Pricing-based Navigation of LMESs

4.1 Introduction

In the previous chapter, we refer to on-road PEVs that can transmit supplementary energy among a GCS as MES. By introducing an energy compensation framework, the feasibility of using huge-capacity UMESs to mitigate overload issues is validated. The huge energy-storing capacities of UMESs make them great candidates as long-term predictable energy storages for CSs that frequently encounter energy imbalance. As a further step from the long-term scheduling, it is also significant to investigate the GCS load balancing problem considering the short-term stochastic vehicle mobility. For example, some LCSs deployed at traffic-intensive areas have predictable power shortages up to 2MWh frequently, in which case UMESs can be scheduled priorly to prevent power overload [124]. Other LCSs at rural regions only need 200kWh from 2 p.m.to 5 p.m., in which case, UMESs are not cost-efficient candidates to conduct the load balance task. As PEV commercialization proceeds and promotion legislation launches globally, PEVs that are belonged to vehicle-fleet based companies can be potential LMES candidates. Different from UMESs, LMESs are large-fleet size, medium battery-capacity PEVs that are suitable for dynamic energy compensation tasks.

The LMES realization is supported by the rapid development of battery technologies and discharging facilities. The latest development in lithium batteries promises a higher energy density and safety rechargeable battery in the future [2, 3]. Moreover, extensive studies on bi-directional chargers enhance the controllability and feasibility of PEV charging/discharging [125, 126]. Enabled by the technical support, many works investigate the

MES energy compensation scheduling to balance the power supply and demand effectively [70, 79, 93, 94, 111]. However, most works only study the scheduling problem from the energy balance perspective, while the transportation network navigation should also be considered when LMESs are participating in the service. LMESs are preferred by LCSs with time-variant energy demand owing to their relatively large fleet size and high flexibilities. To compensate the overload in these LCSs with LMESs means that a large amount of additional traffic will inject in the transportation network, incurring unexpected traffic congestion and service delay. Therefore, the impact of injected LMESs on the transportation network should be studied.

The PEV charging navigation and its potential to couple the operation of smart grid and transportation network have been studied and validated in works [96, 97]. Therefore, when a large number of PEVs that are directed by the power signals travelling on the road, their scheduling should be studied together in the coupled system. Regarding PEV charging, there have been many works exploring the interacted PEV charging scheduling of smart grid and transportation network [98–102]. However, the scheduling of LMESs has its unique features. First, LMESs are additional injected traffics that have stochastic properties related to smart grid energy status. Instead of scheduling PEVs at the system-level to minimize the overall travelling time, the main concern in LMES scheduling is to mitigate the potential delay incurred by the additional injected traffic. Second, the profit-oriented LMESs can be effectively scheduled using proper monetary incentive. Although Wardrop equilibrium has been used in many works to encourage PEVs converging to social optimum, the convergence of Wardrop equilibrium needs iterated simulation while more time-efficient scheduling scheme is required for dynamic energy compensation scheduling.

In this chapter, we propose a pricing-based scheduling scheme that dynamically uses the monetary incentive to encourage LMESs following the navigated route to accomplish energy compensation tasks. The scheduling scheme has two objectives: first is to mitigate the impact of injected LMES traffic on the transportation network, and second is to achieve the GCS energy balance using LMESs. Thus, the on-road traffic conditions should be carefully modelled and analyzed in the pricing-based scheduling. The main contributions of the work are threefold. First, an energy-capacitated directed graph model is developed to characterize the LMES traffic capacity in the transportation network. Second, consider LMESs as energy flow along the road, a loading optimized scheduling scheme is proposed to navigate the energy flow in a time-efficient manner. The scheme also guarantees the GCS energy balance and optimization of the loading pressure at RCSs. Finally, a dynamic pricing scheme is proposed to minimize the LMES scheduling cost and guarantee a well-tracked LMES navigation profile.

The remainder of the chapter is organized as follows. The energy-capacitated trans-

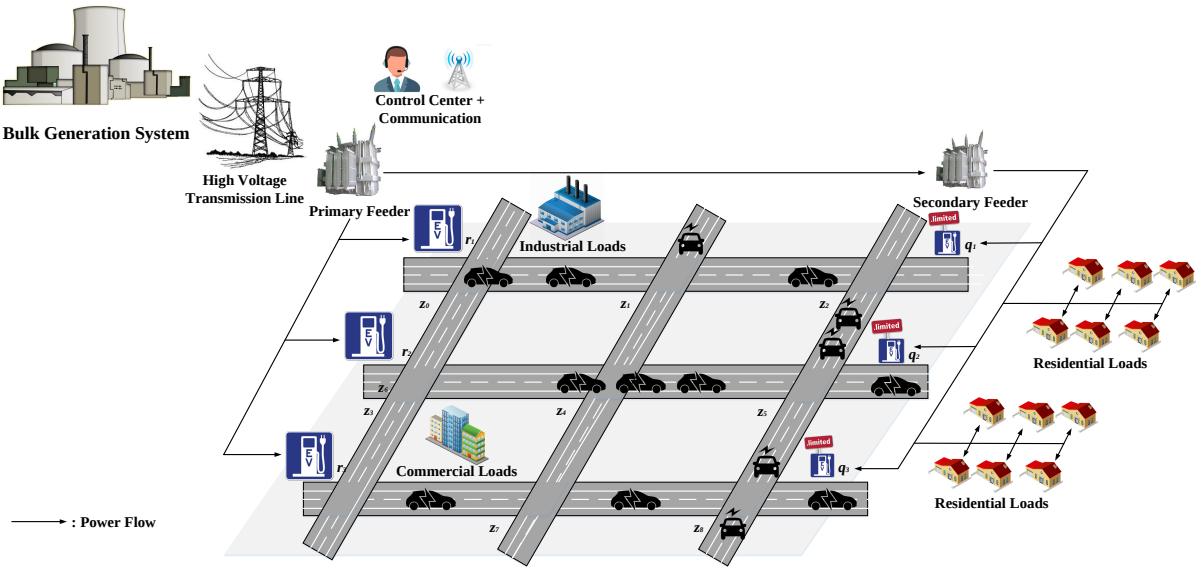

Figure 4.1: System overview of a GCS.

portation network model is developed in Section II. Section III presents the proposed pricing-based scheduling scheme, based on which, a minimum-cost flow problem and a cost-minimized convex optimization problem are formulated and solved in Section IV. Performance evaluation is provided in Section V, and Section VI summarizes this chapter.

4.2 System Model

In this section, we first briefly introduce the CS dynamics characterization model. Then, an energy-capacitated unidirectional graph is used to characterize the transportation network where the available on-road travelling capacity for LMESs is modelled as weighted LMES energy bandwidth. Based on the model, LMESs can then be navigated optimally to deliver energy compensation tasks while avoiding incurring unexpected traffic congestion. To capture the time-variant CS dynamics, the UO analyzes the system model during h time slots with the equal interval of Δt throughout a day. The time slot set is denoted by $\mathcal{H} = \{1, 2, \dots \mathrm{h}\}$, where system analysis and scheme operation are conducted during each Δt. A summary of notations that are used in this chapter is shown in Table 4.1.

The deployment of a GCS, as shown in Fig. 4.1 , are mostly in the power distribution system at different feeder levels corresponding to local charging demands. UO schedules

Table 4.1: Notations for Chapter 4

Symbol	Description
(k, l)	A directed edge from vertexes k to l
$\alpha_{\mathrm{i,j},\tau}$	The weight of LMES travelling along the τth route from RCS R_{i} to LCS Q_{j}
$\Delta E_{\mathrm{av.}}$	The average LMES discharging capacity, kWh
$\mathcal{G}(\mathcal{V}, \mathcal{E})$	The unidirectional graph
$\mathcal{H}$	The time slot set
$\mathcal{Q}$	The set of LCSs
$\mathcal{R}$	The set of RCSs
Ξ	The optimal energy flow link set
$a_{\mathrm{i}}/b_{\mathrm{i}}$	Parameters of the loading pressure function of station R_{i}
$B_{\mathrm{k,l,h}}$	The energy bandwidth of link $L_{\mathrm{k,l}}$ at time h, kWh
$C^D_{\mathrm{j,h}}$	The overall demanding energy at LCS Q_{j}, kWh
C^L_{j}	The energy capacity of station Q_{j} provided by local feeder, kWh
$C^M_{\mathrm{i,h}}$	The LMES charging capacity at station R_{i} at time h, kWh
$C^M_{\mathrm{j,h}}$	The LMES discharging capacity at station Q_{j} at time h, kWh
$C_{\mathrm{j,h}}$	The overall service capacity of LCS Q_{j} at time h, kWh
$C_{\mathrm{k,l}}$	The link capacity along the link $L_{\mathrm{k,l}}$, vehicles/hour
$E^M_{\mathrm{i,h}}$	The assigned LMES charging tasks at station R_{i} at time h, kWh
$E^M_{\mathrm{j,h}}$	The demanding LMES energy at station Q_{j} at time h, kWh
$E^P_{\mathrm{i,h}}$	PEV charging demand at station R_{i} at time h, kWh
$e_{\mathrm{k,l,h}}$	LMES energy flow along link $L_{\mathrm{k,l}}$ at time h, kWh
$L_{\mathrm{av.}}$	The average PEV charging demand, kWh
$L_{\mathrm{k,l}}$	The link between road intersections V_{k} and V_{l}
N^L_{j}	The number of PEVs charged by local feeder at station Q_{j}, vehicles
$N^M_{\mathrm{j,h}}$	The number of PEVs charged by LMESs at station Q_{j} at time h, vehicles
P^C_{j}	The adopted charging standard at station Q_{j}, kW
P^L_{j}	The local feeder power rate of station Q_{j}, kW
$t^0_{\mathrm{k,l}}$	The free-flow travel time along the link $L_{\mathrm{k,l}}$, hour
$t^A_{\mathrm{k,l}}$	The average travel time along the link $L_{\mathrm{k,l}}$, hour
$t^L_{\mathrm{k,l,h}}/t^U_{\mathrm{k,l,h}}$	The lower/upper bound of travelling time along link $L_{\mathrm{k,l}}$ at time h, hour
$u_{(\mathrm{i,j},\tau)}$	The τth optimal route from RCS R_{i} to LCS Q_{j}
$x^M_{\mathrm{k,l,h}}$	The LMES traffic flow of link $L_{\mathrm{k,l}}$ at time h, vehicles/hour
$x^R_{\mathrm{k,l,h}}$	The regular traffic flow of link $L_{\mathrm{k,l}}$ at time h, vehicles/hour
$x_{\mathrm{k,l,h}}$	The overall traffic flow of link $L_{\mathrm{k,l}}$ at time h, vehicles/hour
$x^U_{\mathrm{k,l,h}}$	The upper bound of traffic flow along link $L_{\mathrm{k,l}}$ at time h, vehicles/hour

on-road LMESs delivering energy compensation services with price-incentive. In terms of the feeder capacities and energy supply, CSs are categorized into two types: RCSs $\mathcal{R}$ and LCSs $\mathcal{Q}$. A set of RCSs, denoted as $\mathcal{R} = \{R_1, R_2 \dots R_{\mathrm{i}}\}$, are deployed at urban areas with stable and sufficient power supplement from bulk generations. Another set of CSs, LCSs, denoted as $\mathcal{Q} = \{Q_1, Q_2 \dots Q_{\mathrm{j}}\}$, are normally deployed at power feeders with limited power supply. Therefore, power overload issue can be a potential hazard at these stations. To address the overload issues, LMESs are scheduled to store surplus energy at nearby RCSs, and then transmit the energy to LCSs as additional energy supply.

4.2.1 CS Capacity Characterization

In terms of different CS properties, the CS operation capacity (i.e., can serve how many PEVs) is characterized in this section, respectively.

Limited-capacity Charging Station

The overall service capacity $C_{\mathrm{j,h}}$ of LCS Q_{j} at time h consists of two parts: the local feeder capacity C_{j}^{L} and LMES energy supply $E_{\mathrm{j,h}}^{M}$ at time h, which are denoted as:

$$\begin{cases} C_{\mathrm{j,h}} = C_{\mathrm{j}}^{L} + E_{\mathrm{j,h}}^{M}, \\ C_{\mathrm{j}}^{L} = P_{\mathrm{j}}^{L} \cdot \Delta t = N_{\mathrm{j}}^{L} \cdot L_{\mathrm{av.}}, \\ E_{\mathrm{j,h}}^{M} = N_{\mathrm{j,h}}^{M} \cdot L_{\mathrm{av.}}. \end{cases} \tag{4.1}$$

The local feeder capacity C_{j}^{L} is the product of its connected feeder power rating P_{j}^{L} and the power supply time interval Δt. In a more straightforward way, consider that incoming PEV on average has a charging demand of $L_{\mathrm{av.}}$, C_{j}^{L} can be characterized as the number of PEV charging services N_{j}^{L} that the feeder can provide simultaneously times the average charging demand $L_{\mathrm{av.}}$. Another part of energy supply is the LMES delivered energy $E_{\mathrm{j,h}}^{M}$, which can also be characterized as the number of PEV charging service $N_{\mathrm{j,h}}^{M}$ that LMESs can provide during Δt.

Without any infrastructure upgrade, the local feeder capacity C_{j}^{L} is a constant that can be easily obtained. On the other hand, the demanding LMES delivered energy $E_{\mathrm{j,h}}^{M}$ is a stochastic variable in nature as it depends on the real-time PEV charging demand at LCS Q_{j}. In this work, we consider that under a pre-determined station availability (e.g., PEVs have a probability of 90% to be charged immediately upon arriving at the station), the LCS overall demanding energy $C_{\mathrm{j,h}}$ can be obtained either by referring to historical

data or stochastic analysis. The detailed capacity analysis is out of the scope of this work. Hence, the demanding LMES energy supply can be obtained according to Equation (4.1).

Resourceful Charging Station

The RCS service capacity C_{i}^{L} is closely related to its connected feeder power rating P_{i}^{L}. Similar to the LCS case, the PEV charging demand $E_{\mathrm{i,h}}^{P}$ at RCS R_{i} is time-variant and can be obtained by historical data or stochastic analysis. Since the RCS's prior operation objective is to charge incoming charging-demand PEVs, the available energy to be delivered by LMESs is calculated as the energy gap between the station overall energy capacity and PEV charging demands, as:

$$C_{\mathrm{i,h}}^{M} = C_{\mathrm{i}}^{L} - E_{\mathrm{i,h}}^{P}. \tag{4.2}$$

As RCSs are guaranteed with sufficient electricity supply, they have excess energy to be delivered to LCS for overload compensation.

4.2.2 Energy-Capacitated Transportation Network Model

While delivering energy with small-fleet, large battery capacity UMESs has little impact on the transportation network that has thousands of vehicles on-road, LMES energy compensation is a different case. The relation between LMES energy scheduling and transportation network is shown in Fig.4.2. In the busy traffic hours, on-road PEV traffic increases in proportion to the overall on-road traffic, leading to an increasing PEV charging demands at CSs. For LCSs to satisfy the increasing PEV charging demands that exceed their local feeder capacities, more surplus energy is required to be delivered. Therefore, more LMESs will travel from RCSs to LCSs to help LCS achieve energy balance during peak traffic hours. Consider the large fleet size of LMESs (e.g., hundreds of vehicles), without proper LMES navigation, the LMES injection in the transportation network could incur travelling delay or severe traffic congestion when the on-road traffic is already dense. The incurred delay not only affects the regular traffics, but also reduces the time-efficiency of energy compensation tasks, further resulting in energy imbalance at LCSs. Thus, the LMES travelling in the transportation network should be carefully studied to mitigate their impacts.

The transportation network is modelled as a unidirectional graph $\mathcal{G}(\mathcal{V}, \mathcal{E})$, as shown in Fig.4.3. Mapping the road intersections to graph vertex set $\mathcal{V} = \{V_1, V_2 \cdots\}$ while the graph edge set $\mathcal{E}$ denotes the road link between intersections. Edge *(k,l)* $\in \mathcal{E}$ denotes a

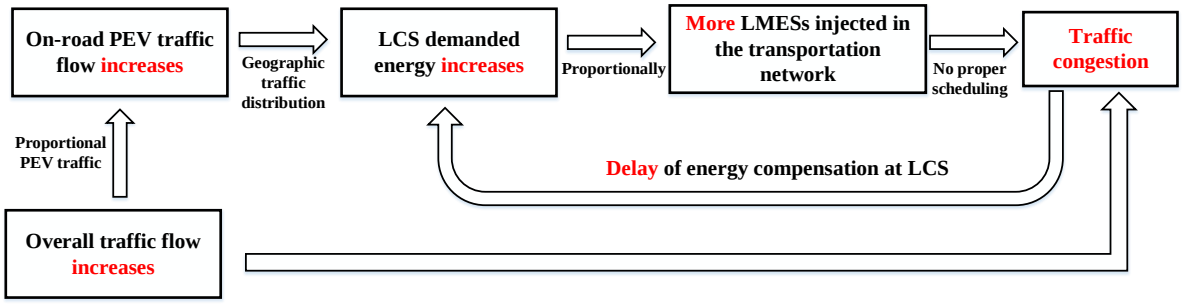

Figure 4.2: LMES impact on the transportation network.

directed edge from k to l. Therefore, a traffic link is mapped as an edge where LMESs travel from intersections k to l, denoted as $L_{\mathrm{k,l}}$. In the remainder of system modelling, traffic link is used as the basic unit for parameter setting and analysis.

For simplicity, we consider LMESs mainly travelling on the freeway to accelerate their energy delivery on-road. As shown in Table 4.2 [127], level of service (LoS) is the basic freeway status evaluation parameter that qualitatively describes the on-road speed, delay, traffic volume, and so on. LoS level A to level F indicate the traffic conditions from free-flow to congestion, along with a quantified range of speeds and traffic volumes of each level. Refer to Table 4.2, we can have a better understanding of the traffic volume and speed range of the desired LoS level.

The on-road traffic flow $x_{\mathrm{k,l,h}}$ of link $L_{\mathrm{k,l}}$ at time h consists of regular vehicle flow $x^{R}_{\mathrm{k,l,h}}$ and LMES traffic flow $x^{M}_{\mathrm{k,l,h}}$. According to the Bureau of Public Roads (BPR) [99], the travelling time function $t_{\mathrm{k,l,h}}(x_{\mathrm{k,l,h}})$ of link $L_{\mathrm{k,l}}$ at time h is closely related to traffic flow $x_{\mathrm{k,l,h}}$, as denoted as:

$$t_{\mathrm{k,l,h}}(x_{\mathrm{k,l,h}}) = t^{0}_{\mathrm{k,l}} \cdot [1 + 0.15 \cdot (\frac{x_{\mathrm{k,l,h}}}{C_{\mathrm{k,l}}})^{4}]. \tag{4.3}$$

$t^{0}_{\mathrm{k,l}}$ denotes the free-flow time along the link, which can be calculated as the link distance over the link speed limit. $C_{\mathrm{k,l}}$ denotes the traffic capacity of the link, which is usually empirically observed from freeway. To enable a time-efficient LMES energy delivery, the link travelling time $t_{\mathrm{k,l,h}}$ at time h should be within the range of $(t^{L}_{\mathrm{k,l,h}}, t^{U}_{\mathrm{k,l,h}})$. The lower bound $t^{L}_{\mathrm{k,l,h}}$ is the travelling time of regular vehicle traffic (i.e.,$t_{\mathrm{k,l,h}}(x^{R}_{\mathrm{k,l,h}})$). The upper bound is regulated by the UO (e.g., $1.25 \cdot t^{0}_{\mathrm{k,l}}$) in terms of the desired on-road traffic condition. When the upper bound is decided, the maximum allowed traffic flow $x^{U}_{\mathrm{k,l,h}}$ can be calculated using equation (4.3).

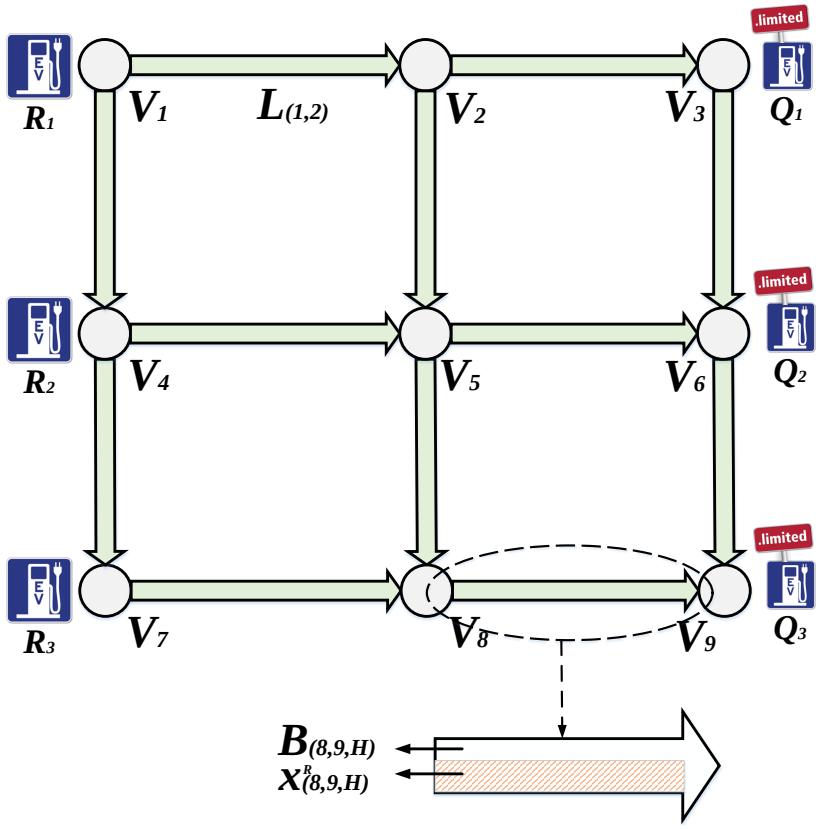

Figure 4.3: Transportation network topology of the GCS.

Consider that on-road LMES flows are mobile energy flows, their on-road energy flow can be characterized as a product of the average LMES stored energy $\Delta E_{\text{av.}}$ and the LMES traffic flow $x^{M}_{\text{k,l,h}}$ along the link $L_{\text{k,l}}$ at time h:

$$e_{\text{k,l,h}} = \Delta E_{\text{av.}} \cdot x^{M}_{\text{k,l,h}}. \tag{4.4}$$

Correspondingly, the road link capacity for LMES injection can also be characterized as link energy bandwidth $B_{\text{k,l,h}}$, which can be calculated as the capacity difference between the maximal traffic flow $x^{U}_{\text{k,l,h}}$ and the regulate traffic flow $x^{R}_{\text{k,l,h}}$ along the link $L_{\text{k,l}}$, multiplying by the average LMES stored energy, denoted as:

Table 4.2: LoS criteria for 70mph freeway.

LoS	Speed	Volume/Capacity	Description
A	≥ 70.0	0.318/0.304	Free-flow condition with unimpeded manoeuvrability
B	≥ 70.0	0.509/0.487	Reasonably unimpeded operation with slightly restricted manoeuvrability
C	≥ 68.50	0.747/0.715	Stable operation with more restriction
D	≥ 63.0	0.916/0.876	Approaching unstable operation with small delay increase
E	$\geq 60.0/58.0$	1.00	Operation with significant intersection approach delays
F	variable	variable	Low speeds incurred by intersection congestion

$$B_{\mathrm{k,l,h}} = \Delta E_{\mathrm{av.}} \cdot (x^{U}_{\mathrm{k,l,h}} - x^{R}_{\mathrm{k,l,h}}). \tag{4.5}$$

For each link, its injected LMES flow should not exceed the link energy bandwidth so that a smooth link travelling can be enabled. Consider the LMES energy flow from the GCS energy balance perspective, the summation of LMES energy at LCS $Q_{\mathrm{j,h}}$ should equal to the LCS demanding energy $E^{M}_{\mathrm{j,h}}$, denoted as:

$$\Delta E_{\mathrm{av.}} \cdot (\sum_{k} x^{M}_{\mathrm{k,j,h}} - \sum_{l} x^{M}_{\mathrm{j,l,h}}) = E^{M}_{\mathrm{j,h}}, \quad \forall Q_{\mathrm{j}} \in \mathcal{Q}, \tag{4.6}$$

To develop a precise transportation network model during each time period, the UO regularly receives the regular on-road vehicle flow $x^{R}_{\mathrm{k,l,h}}$ and determines the upper bound travel time for each link. Then, the link energy bandwidth can be calculated using equations (4.3)-(4.6). Based on the energy-capacitated transportation network model, the LMES energy delivery route between each RCS-LCS pair can be selected while mitigating the LMES traffic impact on the transportation network. For example, if LMESs need to deliver 500kWh from RCS R_1 to LCS Q_2, without the introduced model, all LMESs will choose the shortest route (i.e., $L_{1,2}$-$L_{2,3}$-$L_{3,6}$). However, in peak traffic hours when $L_{2,3}$ is

congested with $B_{2,3,\mathrm{h}} = 200\mathrm{kWh}$, 500kWh energy flow injection in the route exceeds the bandwidth. If the energy bandwidth regulation is determined under LoS level E, excessive traffic injection will let the on-road traffic enter LoS level F, which is road congestion. In this case, instead of injecting all LMESs into one single route, another longer distance but with more energy bandwidth route (e.g., $L_{1,2}$-$L_{2,5}$-$L_{5,6}$) will be chosen to accommodate part of the energy flow (e.g., 300kWh). As such, both time-efficiency of LMES energy compensation tasks and an uncongested transportation operation can be achieved.

4.3 Pricing-based LMES Scheduling Scheme

Based on the introduced system model, the UO needs to schedule LMESs from two perspectives: first, allocate LMESs energy delivering among a GCS to mitigate the overload issues at LCSs; second, navigate LMESs in the transportation network to avoid incurring additional traffic delay. Moreover, the ownership of LMESs requires sufficient monetary incentive for them to follow the scheduling direction offered by the UO. Therefore, in this section, we propose a pricing-based scheduling scheme that dynamically uses monetary incentive (i.e., service price) to guide LMESs accomplish assigned energy compensation tasks along the navigated routes.

The flowchart of the proposed scheme is shown in Fig.4.4. The scheme is performed on a Δt time interval based: at time h, the scheduling results for the next time slots $h+1$ will be calculated. The UO uses the historical traffic data as the input to analyze the station dynamic analysis in either statistic or stochastic forms to obtain the GCS energy status. Then, in terms of the LMES energy scheduling objectives, navigation and price-incentive schemes are conducted step by step:

- ▷ **Step 1-LMES Navigation**: Inputting the on-road traffic flow data and the GCS energy status, a loading-optimized navigation scheme is conducted to calculate the recommended traffic route and corresponding LMES flow between each RCS-LCS pair. Moreover, by allocating the LMES charging station, the proposed scheme also optimizes the loading pressure at RCSs;
- ▷ **Step 2-Real-time Pricing:** Based on the navigation scheme results, LMES response functions and price incentive function, a real-time pricing scheme is proposed to determine the service price of LMESs to motivate them following the navigation routes while minimizing the overall scheduling cost.

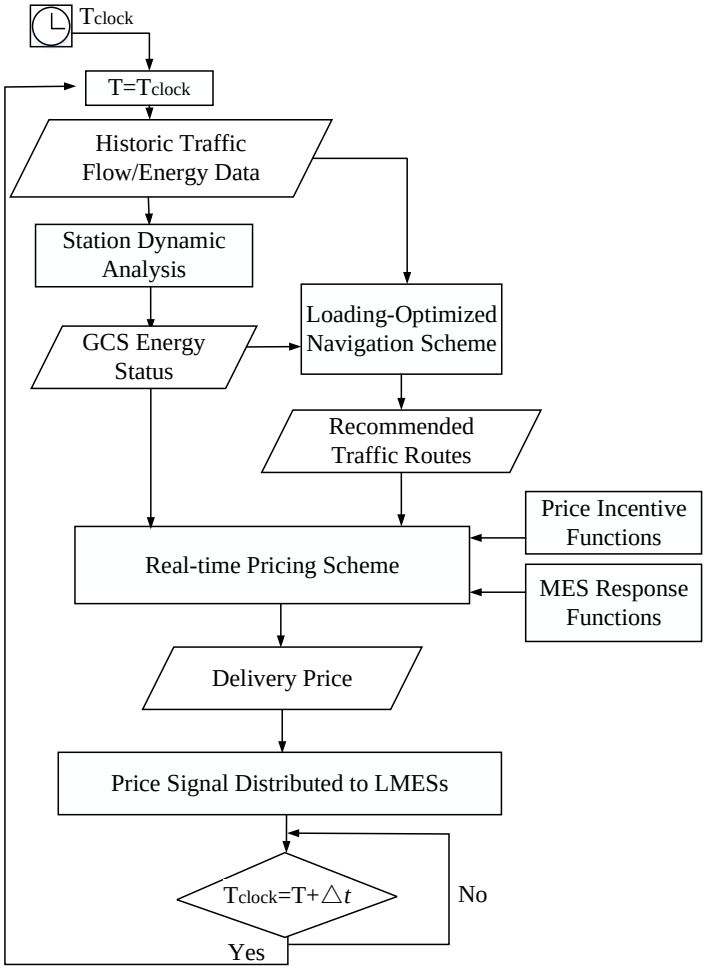

Figure 4.4: Structure of pricing-based scheduling scheme.

The two-step results are then distributed to LMESs through wireless communication technologies (e.g., cellular networks, VANETs, or WiFi), and LMESs conduct the tasks in response to the posted price and navigation routes.

4.4 Problem Formulation

Based on the proposed scheme, the LMES energy scheduling problem can be solved in two steps. First, to plan the navigation routes for LMESs, a minimum-cost flow problem is formulated based on the energy-capacitated transportation network. Then, the price incentive function and LMES response function to the price are introduced to characterize the pricing interaction between LMESs and UO. The dynamic pricing scheduling is then formulated as a convex optimization problem to minimize the scheduling costs while enabling that most LMESs following the navigation routes. Finally, solutions to both problems are presented at the end of the section.

4.4.1 Loading-Optimized Navigation Scheme

During each time slot h, the UO receives the demanding energy $E^M_{\mathrm{j,h}}$ from LCSs and available energy charging capacity $C^M_{\mathrm{i,h}}$ from RCSs, and allocate LMESs to RCSs for energy storage. Although RCSs are connected to power feeders with sufficient power supply, heavy loadings at feeders can still pose great pressures on the feeder transformers, shortening their life cycles. Hence, when allocating LMESs to RCSs, the RCS loading pressure needs to be optimized. First, the loading ratio of RCS R_{i} at time h is denoted as:

$$\gamma_{\mathrm{i,h}} = \frac{E^P_{\mathrm{i,h}} + E^M_{\mathrm{i,h}}}{C^L_{\mathrm{i}}}, \tag{4.7}$$

where the loading ratio is calculated as the summation of PEV charging energy $E^P_{\mathrm{i,h}}$ and MES charging energy $E^M_{\mathrm{i,h}}$ over the feeder capacity C^L_{i} [128]. When the loading ratio approaches 1, meaning the feeder loading is almost at its full capacity, the feeder pressure would increase dramatically as now the feeder will be more likely overloaded and overheated. On the contrary, when the loading ratio is low, the feeder pressure decreases fast and becomes almost negligible. Therefore, the loading pressure function $\Gamma(\gamma_{\mathrm{i,h}})$ is defined as an exponential function:

$$\Gamma(\gamma_{\mathrm{i,h}}) = a_{\mathrm{i}} \cdot e^{b_{\mathrm{i}} \cdot \gamma_{\mathrm{i,h}}}, \tag{4.8}$$

where a_{i} is the weight parameter of RCS R_{i} and b_{i} denotes the incline degree of the exponential function. The navigation scheme aims to minimize RCS loading pressures while enabling enough LMES energy is delivered to LCSs for overload mitigation, which is formulated as an optimization problem:

$$\min_{\gamma_{\mathrm{i,h}}} \quad \sum_{R_{\mathrm{i}}} \Gamma(\gamma_{\mathrm{i,h}}) \tag{4.9}$$

$$\text{s.t.} \quad 0 \leq \gamma_{\mathrm{i,h}} \leq 1, \forall R_{\mathrm{i}} \in \mathcal{R} \tag{4.9. a}$$

$$\sum_{\mathrm{R_i} \in \mathcal{R}} E^{M}_{\mathrm{i,h}} = \sum_{\mathrm{Q_j} \in \mathcal{Q}} E^{M}_{\mathrm{j,h}}. \tag{4.9. b}$$

The objective is to minimize the summation of RCS loading pressure while constraints enable the energy balance among a GCS. Constraint (4.9.a) guarantees that the LMES charging tasks do not overload the RCS feeders. Constraint (4.9.b) enables that all stored energy in LMESs is delivered to LCSs by the energy storage and supplement equality. By solving the optimization problem, LMES allocated energy $E^{M}_{\mathrm{i,h}}$ at station R_{i} can be obtained.

Based on the LMES energy allocation results among a GCS, the operator now can calculate the LMES navigation route. As the navigation is conducted during each time slot, the notation h is omitted. Consider LMESs as energy flow travelling within a energy-capacitated transportation network, the UO aims to find the fastest routes from RCSs to LCSs. The route search problem can be formulated as a minimum-cost flow problem to find the fastest routes to send the LMES energy flow between RCS-LCS pairs under the energy bandwidth limit. The minimum-cost flow problem is formulated as follow:

$$\min_{e_{\mathrm{k,l}}} \quad t_{\mathrm{overall}} = \sum_{(k,l) \in \mathcal{E}} t^{A}_{\mathrm{k,l}} \cdot e_{\mathrm{k,l}} \tag{4.10}$$

$$\text{s.t.} \quad \sum_{k \in \mathcal{V}} e_{\mathrm{k,l}} - \sum_{l \in \mathcal{V}} e_{\mathrm{k,l}} = 0 \quad \forall k, l \neq \{\mathcal{R} \bigcup \mathcal{Q}\} \tag{4.10. a}$$

$$\sum_{l \in \mathcal{V}} e_{\mathrm{i,l}} - \sum_{k \in \mathcal{V}} e_{\mathrm{k,i}} = E^{M}_{\mathrm{i}} \quad \forall R_{\mathrm{i}} \in \mathcal{R} \tag{4.10. b}$$

$$\sum_{k \in \mathcal{V}} e_{\mathrm{k,j}} - \sum_{l \in \mathcal{V}} e_{\mathrm{j,l}} = E^{M}_{\mathrm{j}} \quad \forall Q_{\mathrm{j}} \in \mathcal{Q} \tag{4.10. c}$$

$$\sum_{R_{\mathrm{i}} \in \mathcal{R}} E^{M}_{\mathrm{i}} = \sum_{Q_{\mathrm{j}} \in \mathcal{Q}} E^{M}_{\mathrm{j}} \tag{4.10. d}$$

$$0 \leq e_{\mathrm{k,l}} \leq B_{\mathrm{k,l}}, \quad \forall (k,l) \in \mathcal{E}. \tag{4.10. e}$$

The objective is to minimize the summation of energy delivery time along each link. The energy delivery time of a link is a product of the link average travel time $t^{A}_{\mathrm{k,l}}$ and the energy

flow $e_{\mathrm{k,l}}$ along the link. Link average travel time $t^{A}_{\mathrm{k,l}}$ is the average value of $t^{L}_{\mathrm{k,l}}$ and $t^{U}_{\mathrm{k,l}}$. For the passing nodes on-road (i.e., the intersections that CSs are not deployed at), all the incoming flow is equal to the output flow, as shown in constraint (4.10.a). Energy conservation at RCSs and LCSs are shown in constraints (4.10.b) and (4.10.c). Constraint (4.10.d) enables that all the energy stored from RCSs is delivered to LCSs. The energy bandwidth constraint to enable uncongested traffic is denoted in constraint (4.10.e). By solving the minimum-cost flow problem, the UO obtains the optimal traffic flow $e^{*}_{\mathrm{k,l}}$ along each link and the delivery time cost.

The optimal flow link results $e^{*}_{\mathrm{k,l}}$, constitute a vector Ξ as $e^{*}_{\mathrm{k,l}} \in \Xi \in R^{m\times 1}$. Denote the τth optimal flow route from R_{i} to Q_{j} as $u_{\mathrm{i,j},\tau}$, belongs to a vector $\mathcal{U}^{*} \in R^{n\times 1}$. The relation between the optimal link and optimal route can be characterized by the matrix $M^{I} \in R^{m\times n}$ as follows:

$$\Xi = M^{I} \cdot \mathcal{U}^{*}, \tag{4.11}$$

where each element $M^{I}_{(\mathrm{m,n})} \in M^{I}$ is an indicator function that denotes whether the mth optimal link is included in the nth optimal route, denoted as:

$$M^{I}_{(\mathrm{m,n})} = \begin{cases} 1 & \Xi_{\mathrm{m}} \in \mathcal{U}^{*}_{\mathrm{n}} \\ 0 & Otherwise. \end{cases} \tag{4.12}$$

Since the link number m is always larger than the route number n. M^{I} always has a left inverse as $((M^{I})^{T}M^{I})^{-1}(M^{I})^{T} \cdot M^{I} = I_{\mathrm{n}}$. Hence, the optimal route results $\mathcal{U}^{*}$ can be calculated as:

$$\mathcal{U}^{*} = M^{\dagger} \cdot \Xi. \tag{4.13}$$

Therefore, the travelling time $t^{*}_{\mathrm{u_{i,j},\tau}}$ along the τth route from R_{i} to Q_{j} can be calculate using indicator function as:

$$t^{*}_{\mathrm{u_{i,j},\tau}} = \sum_{(k,l)\in\mathcal{E}} I_{(\mathrm{u_{i,j},\tau})}(e_{\mathrm{k,j}}) \cdot t^{A}_{\mathrm{k,l}}, \quad \forall u_{\mathrm{i,j},\tau} \in \mathcal{U}^{*}, \tag{4.14}$$

where the indicator function $I_{(\mathrm{u_{i,j},\tau})}(e_{\mathrm{k,j}})$ equals one when the link $e_{\mathrm{k,l}}$ is included in the route $u_{\mathrm{i,j},\tau}$ as:

$$I_{(\mathrm{u_{i,j,\tau}})}(e_{\mathrm{k,j}}) = \begin{cases} 1 & e_{\mathrm{k,l}} \in u_{\mathrm{i,j,\tau}} \\ 0 & Otherwise. \end{cases} \tag{4.15}$$

The optimal route $\mathcal{U}^*$ and travelling time $t^*_{\mathrm{u_{i,j,\tau}}}$ are then input in the dynamic pricing scheme for price-incentive.

4.4.2 Dynamic Pricing Scheme

The optimal navigation route calculated by the UO would direct LMESs to a longer travelling distance, and potential range anxiety issue could incur. Therefore, LMESs need monetary incentive (e.g., economic rewards) to be motivated to follow the navigation. In this section, we first characterize the price incentive function for LMESs at the UO side and LMES response function to the price. Then, a dynamic pricing scheme is proposed to adjust the LMES service rewards through pricing.

Price Incentive Function Characterization

During each time slot h, the UO determines the energy delivery price $p_{\mathrm{N}}(\alpha_{\mathrm{i,j,\tau}})$ per energy unit, along the route $u_{\mathrm{i,j,\tau}}$ denoted as:

$$p_{\mathrm{N}}(\alpha_{\mathrm{i,j,\tau}}) = \alpha_{\mathrm{i,j,\tau}} t^*_{\mathrm{i,j,\tau}} + p^B_{\mathrm{N}}, \tag{4.16}$$

where $\alpha_{\mathrm{i,j,\tau}}$ is pricing weight of LMES travelling along the τth optimal route $u_{\mathrm{i,j,\tau}}$ along the route from RCS R_{i} to LCS Q_{j}. p^B_{N} is the base price for energy delivery. The price reflects that LMESs need more incentive to follow the navigation when longer travelling time is required to follow the directed route.

To characterize LMES response to the energy delivery price, a linear function $f(p_{\mathrm{N}}(\alpha_{\mathrm{i,j,\tau}}))$ is formulated as:

$$f(p_{\mathrm{N}}(\alpha_{\mathrm{i,j,\tau}})) = \frac{p_{\mathrm{N}}(\alpha_{\mathrm{i,j,\tau}}) - p^L_{\mathrm{N}}}{p^H_{\mathrm{N}} - p^L_{\mathrm{N}}}. \tag{4.17}$$

$f(p_{\mathrm{N}}(\alpha_{\mathrm{i,j,\tau}}))$ is the percentage of MESs following the route $u_{\mathrm{i,j,\tau}}$, while p^L_{N} and p^H_{N} denote the lower and upper bound of the incentive price for energy delivery respectively.

Problem Formulation

Based on the function characterization, a dynamic pricing scheme is formulated as a weighted-sum optimization problem to achieve two objectives: minimizing the scheduling costs and maximizing the LMESs that follow the optimal navigation route, which is denoted as:

$$\min_{\alpha_{\mathrm{i,j},\tau}} \quad \kappa_1 C_{\mathrm{Navi.}}(\alpha_{\mathrm{i,j},\tau}) + \kappa_2 \sum_{u_{\mathrm{i,j},\tau} \in \mathcal{U}^*} |f(p_{\mathrm{N}}(\alpha_{\mathrm{i,j},\tau})) - f^e_{\mathrm{i,j},\tau}|^2 \tag{4.18}$$

$$\text{s.t.} \sum_{\tau} f(p_{\mathrm{N}}(\alpha_{\mathrm{i,j},\tau})) N_{\mathrm{M.}} \Delta E_{\mathrm{av.}} = E^M_{\mathrm{i}}, \forall R_{\mathrm{i}} \in \mathcal{R} \tag{4.18. a}$$

$$\sum_{\tau} f(p_{\mathrm{N}}(\alpha_{\mathrm{i,j},\tau})) N_{\mathrm{M.}} \Delta E_{\mathrm{av.}} = E^M_{\mathrm{j}}, \forall Q_{\mathrm{j}} \in \mathcal{Q} \tag{4.18. b}$$

$$0 \leq f(p_{\mathrm{N}}(\alpha_{\mathrm{i,j},\tau})) \leq 1, \forall u_{\mathrm{i,j},\tau} \in \mathcal{U}^*. \tag{4.18. c}$$

The first part of the objective is the scheduling cost $C_{\mathrm{navi.}}(\alpha_{\mathrm{i,j},\tau})$ that is used to encourage LMESs following the optimal navigation routes.

$$C_{\mathrm{navi.}}(\alpha_{\mathrm{i,j},\tau}) = \sum_{u_{\mathrm{i,j},\tau}} p_{\mathrm{N}}(\alpha_{\mathrm{i,j},\tau}) N_{\mathrm{M.}} f(p_{\mathrm{N}}(\alpha_{\mathrm{i,j},\tau})) \Delta E_{\mathrm{av.}}. \tag{4.19}$$

The scheduling cost is calculated as the summation of the incentive price $p_{\mathrm{N}}(\alpha_{\mathrm{i,j},\tau})$ per kWh along the route $u_{\mathrm{i,j},\tau}$ multiplying with the energy delivered along that route. $N_{\mathrm{M.}}$ denotes the total number of on-road LMESs. The product of $N_{\mathrm{M.}}$, the percentage of LMES $f(p_{\mathrm{N}}(\alpha_{\mathrm{i,j},\tau}))$ along the route and the average LMES delivered energy $\Delta E_{\mathrm{av.}}$ is the energy delivered along the route $u_{\mathrm{i,j},\tau}$. On the other hand, to ensure that most on-road LMESs follow the optimal routes, the norm form of percentage difference between the real-life percentage of LMESs $f(p_{\mathrm{N}}(\alpha_{\mathrm{i,j},\tau}))$ following the optimal route and the expected LMES percentage $f^e_{\mathrm{i,j},\tau}$ needs to be minimized, which forms the second part of the objective. The expected percentage is calculated as:

$$f^e_{\mathrm{i,j},\tau} = \begin{cases} 0 & u_{\mathrm{i,j},\tau} \notin \mathcal{U}^* \\ \frac{u_{\mathrm{i,j},\tau}}{\sum_{\tau} u_{\mathrm{i,j},\tau}} & u_{(\mathrm{i,j},\tau} \in \mathcal{U}^*. \end{cases} \tag{4.20}$$

For the routes that are not optimal according to the navigation results, the expected probability is zero. For the routes that are optimal, the expected percentage is proportional to

its assigned LMES flow over the overall LMES flow between the RCS-LCS pair. κ_1 and κ_2 are the coefficients for scheduling costs and navigation route follow percentage respectively. The κ_1/κ_2 ratio denotes the objective tendency towards scheduling cost minimization or optimal navigation following maximization. For problem (4.18), constraint (4.18.a) ensures that the overall energy transmitted by LMESs equal to the energy stored at RCSs. Constraint (4.18.b) ensures that the overall stored energy is delivered to LCSs. Constraint (4.18.c) provides the mathematical constraint for the price response function.

4.4.3 Solution

In this section, we provide the solutions and algorithms to the navigation scheduling and the pricing-based scheduling, respectively.

Loading-Optimized Navigation Scheme

The navigation scheme is performed every Δt, as shown in Algorithm 3, by first inputting the historical traffic/energy data for station dynamic analysis, and output the predicted RCS/LCS energy status at the next time slot. Then, input the CS energy status to problem (4.9). As problem (4.9) is convex in a convex set, the problem can be efficiently solved using interior point method in the CVX toolbox with Mosek 8 [118]. The CVX optimization outputs the allocated LMES energy tasks at RCSs, which is the input to the navigation scheme.

The LMES navigation in the energy-capacitated network is formulated as a minimum-cost flow problem where RCSs behave as supply nodes and LCSs as demand nodes. The other road intersections are mapped as pass nodes. To enable an initial feasible solution, a dummy node v is introduced to create an auxiliary network, as shown in Algorithm 3.

In this paper, a network simplex algorithm is adopted to solve the minimum-cost flow problem efficiently in polynomial time. To use the network simplex algorithm, the solution set is represented in the form of spanning tree $\mathcal{F} = (F, J, K)$. Originally, the edge set $\mathcal{E}$ is divided into three subsets:

1. F: the edges in the spanning tree;
2. J: the non-tree edges whose flows are restricted to zero;
3. K: the non-tree edges whose flows are restricted to their edge capacities.

Algorithm 3: Loading-Optimized Navigation Scheme

Input: Historic traffic/energy data ;
Initialization
Let h=0
for *h=0 to 23* **do**
  Markov Chain Analysis:
  Calculate LCS demanded energy $E^M_{\mathrm{j,h}}$ and RCS available capacity $C^M_{\mathrm{i,h}}$;
  DCP: Loading Pressure Optimization
  Output: LMES allocated energy $E^M_{\mathrm{i,h}}$ at RCSs;
  Energy-capacitated network simplex:
  Phase I - Initial feasible solution
  Create an auxiliary network:
  for *all nodes* **do**
    if *node i is demand node* **then**
      add virtual arc from v to i: flow$(v,i) = -E^M_{\mathrm{i,h}}$;
    else
      add virtual arc from i to v: flow$(i,v) = E^M_{\mathrm{i,h}}$

  Assign arc cost +1 to all virtual arcs and cost 0 to all original arcs ;
  Primal-simplex Algorithm
  Initialize (F, J, K) with auxiliary network ;
  Calculate all node potential $\varpi(i)$;
  while *nontree arc violates the optimal condition* **do**
    Select an entering arc c that violate the optimal condition ;
    Add arc c to F, forming cycle W ;
    Augment the maximal possible flow δ in W and find a leaving arc p that reaches its bottleneck ;
    Update flow, (F, J, K) and ϖ;
  if *total cost* $\geq$ *0* **then**
    Return no feasible solution;
    break ;
  else
    proceed to Phase II
  Phase II- Solving the original problem
  Assign the original arc costs to original arcs ;
  for *all arcs* **do**
    if $(k,l) \notin F$ *and* $v \in (k,l)$ **then**
      Delete the arc ;
    else
      flow(k,l)=0 ;
      cost(k,l)=0
  Start from the basic solution in **Phase-I**, solve the problem with the **Primal-Simplex** algorithm ;
  Output: PMES navigation link and volume.

Using the spanning tree structure, the optimal solution of the formulated minimum-cost flow problem is denoted as $\mathcal{F}^*$.

Theorem 1 *$\mathcal{F}^*$ is the optimal solution to the minimum-cost flow problem if and only if satisfies:*

$$\begin{cases} r_k - r_l = t^A_{k,l}, & (k,l) \in F \\ r_k - r_l \leq t^A_{k,l}, & (k,l) \in J \\ r_k - r_l \geq t^A_{k,l}, & (k,l) \in K \end{cases} \tag{4.21}$$

Proof 3 *Define $r \in R^n$, $w \in R^m$ as the dual variables for problem (4.10), $A \in R^{n \times n}$ as the adjacency matrix of the introduced network, $s \in R^m$ as the slack variables that represent the flow difference between assigned flow along the link and the link capacity. The introduction of dummy nodes enables an initial feasible solution. Then, the complementary slackness conditions are:*

$$(\begin{bmatrix} (t^A)^T & 0^T \end{bmatrix} - \begin{bmatrix} r^T & w^T \end{bmatrix} \cdot \begin{bmatrix} A & 0 \\ I & I \end{bmatrix}) \cdot \begin{bmatrix} e \\ s \end{bmatrix} = 0. \tag{4.22}$$

To satisfy the above conditions for optimality qualify [129], each edge should satisfy the following conditions:

$$\begin{cases} (t^A_{k,l} - r_k + r_l - w_{k,l}) e_{k,l} = 0, \\ w_{k,l} s_{k,l} = 0. \end{cases} \tag{4.23}$$

For $(k,l) \in F$, since $e_{\mathrm{k,l}} \neq 0$ and $s_{\mathrm{k,l}} \neq 0$, equation (4.23) is simplified as:

$$t^A_{k,l} - r_k + r_l = 0, (k,l) \in F. \tag{4.24}$$

For $(k,l) \in J$, since $e_{\mathrm{k,l}} = 0$ and $s_{\mathrm{k,l}} \neq 0$, to satisfy equation (4.23), we must have $w_{\mathrm{k,l}}$ and

$$r_k - r_l \leq t^A_{k,l}, (k,l) \in J. \tag{4.25}$$

For $(k,l) \in K$, since $e_{\mathrm{k,l}} \neq 0$, from equation (4.23), we have

$$t_{k,l}^{A} - u_k + u_l = w_{\mathrm{k,l}}, (k,l) \in K. \tag{4.26}$$

Since the dual of equation (4.10) regulates that $w_{\mathrm{k,l}} \leq 0$, we have

$$r_k - r_l \geq t_{k,l}^{A}, (k,l) \in K. \tag{4.27}$$

To enable that an optimal solution of the original problem is found, dummy node-connected edges should be excluded from the final solution. Based on the optimal condition, a primal-simplex algorithm is then conducted, as shown in Algorithm 3. First, the initialized spanning tree with a dummy node is checked for the optimality violation. If any arc violates the optimality, it is selected as an entering arc to augment the maximal flow in the formed fundamental cycle. During the augment, the arc that reaches its minimal/maximal flow is selected as a leaving arc. The whole process is conducted until no arc violates the optimal conditions. If the output contains virtual nodes, then there is no feasible solution. Otherwise, an initial feasible solution is obtained. In phase II, a primal-simplex algorithm is applied by starting with the initial feasible solution to obtain the optimal LMES navigation link results. Through the calculation of Equations (4.11)-(4.15), the optimal PMES navigation route and time can be obtained and input to the dynamic pricing scheme.

Dynamic Pricing Scheme

With the input of the optimal navigation results, the dynamic pricing problem can calculate the incentive price by dynamically adjusting the price coefficient in problem (4.18), which is a quadratic programming problem in the form of:

$$\min_{x} \quad x^T P x + Q^T x + s \tag{4.28}$$

$$\text{s.t.} \quad Ax \leq b, \tag{4.28. a}$$

where P is shown in equation (4.29).

Since $x^T P x \geq 0$, P is positive definite, and problem (4.28) is convex. Therefore, problem (4.18) is convex in nature and can be solved efficiently using the interior point method. In this paper, SDPT3 in CVX is used to solve the quadratic programming problem in polynomial time [118]. The calculated incentive price is then distributed to LMESs on-road through wireless communication to encourage them following the operator's navigation routes.

$$P = \tag{4.29}$$
$$\begin{pmatrix} \frac{(\alpha_1 N_{\mathrm{M.}} \Delta E_{\mathrm{av.}})(p_{\mathrm{N}}^H - p_{\mathrm{N}}^L) t_{\mathrm{u}_1}^3 + \alpha_2 t_{\mathrm{u}_1}^2}{(p_{\mathrm{N}}^H - p_{\mathrm{N}}^L)^2} & 0 & \cdots & 0 \\ 0 & \frac{(\alpha_1 N_{\mathrm{M.}} \Delta E_{\mathrm{av.}})(p_{\mathrm{N}}^H - p_{\mathrm{N}}^L) t_{\mathrm{u}_2}^3 + \alpha_2 t_{\mathrm{u}_2}^2}{(p_{\mathrm{N}}^H - p_{\mathrm{N}}^L)^2} & \cdots & 0 \\ \vdots & \vdots & \ddots & \vdots \\ 0 & 0 & \cdots & \frac{(\alpha_1 N_{\mathrm{M.}} \Delta E_{\mathrm{av.}})(p_{\mathrm{N}}^H - p_{\mathrm{N}}^L) t_{\mathrm{u}_\mathrm{i}}^3 + \alpha_2 t_{\mathrm{u}_\mathrm{i}}^2}{(p_{\mathrm{N}}^H - p_{\mathrm{N}}^L)^2} \end{pmatrix}.$$

4.5 Performance Evaluation

In this section, we validate the effectiveness of the proposed pricing-based scheduling scheme based on the real traffic data on California freeway collected by the California department of transportation [119]. The impact of objective weights and the resulting trade-off of the scheme are also discussed.

4.5.1 Simulation Setup

We choose an urban/rural intersected area within Los Angeles (L.A.) region, as shown in Fig. 4.5, with RCSs deployed at L.A. and East L.A. respectively, LCSs at Hollydale Park and Norwalk respectively, and another two passing points at West Athems and Santa Fe Springs. Based on the data collected by the California department of transportation PeSM [119], information of each link is shown in Table 4.3. The link capacity information is obtained by observing the traffic flow when LoS=E for 100% traffics [127]. All the links have regulated speed limits of 112km/h, based on which, the link free-flow time can be obtained according to equations (4.3). The historical regular traffic flow on each link is obtained based on [119]. According to [127], vehicles travelling on the 112km/h freeway is within the time range of $(1.05t^0, 1.15t^0)$, as shown in Table 4.4.

We consider a 30% PEV penetration rate in the automobile market according to the prediction in [1]. Among these PEVs, 30% of them are in the SoC range of 15%-50%, which needs to be recharged. For these charging-demand PEVs, 10% of them arrive at RCSs for charging while 20% of PEVs recharge at LCSs due to their range anxieties in the rural area with fewer LCSs. On the other hand, 20% of on-road PEVs are in the state-of-charge (SoC) range of 50%-75%, which are considered as LMESs candidates. Based on the above consideration, PEV arriving rate at RCS R_{i} at time h - $\rho_{\mathrm{i,h}}$ and PEV arriving rate at LCS

Table 4.3: Link information

Departure	*Destination*	*Hwy*	*Cap.* (veh./h)	*Mile.* (km)	*Color*
L. A.	East L. A.	I-10E	5360	11.65	Orange
East L. A.	Santa Fe Spring	I-5S	4700	8.22	Light blue
L. A.	West Athems	I-110S	4850	10.74	Yellow
East L. A.	Hollydale Park	I-710S	4700	11.57	Green
Santa Fe Spring	Norwalk	I-605S	3400	2.03	Purple
West Athems	Hollydale Park	I-105E	3680	8.00	Dark blue
Hollydale Park	Norwalk	I-105E	4000	5.58	Red

Table 4.4: Simulation parameters

Para.	Value	Para.	Value
$t^L_{(\mathrm{k,l})}$	$1.05t^0_{(\mathrm{k,l})}$	$t^U_{(\mathrm{k,l})}$	$1.15t^0_{(\mathrm{k,l})}$
$\rho_{\mathrm{i,h}}$	0.009	$\rho_{\mathrm{j,h}}$	0.018
$L_{\mathrm{av.}}$	30kWh	$\Delta E_{\mathrm{av.}}$	10kWh
P^C_{i}	120kW	P^C_{j}	90kW
C_{R_1}	3MWh	C_{R_2}	2.4MWh
$C^L_{\mathrm{Q}_1}$	450kWh	$C^L_{\mathrm{Q}_2}$	360kWh
a_1	0.34	b_1	7.81
a_2	0.18	b_2	8.44
κ_1	1	κ_2	50
$p_{\mathrm{Q_j,h}}$	0.885		

Figure 4.5: Station deployment within Los Angeles area.

Q_{i} at time h - $\rho_{\mathrm{j,h}}$ can be obtained. The average PEV charging energy is 30kWh, which is estimated based on a popular PEV model of Nissan Leaf. Meanwhile, LMESs with a similar vehicle model is considered to deliver on-average 10kWh.

For the RCSs that have sufficient power supply, they charge PEVs at a fast speed of 120kW using SAE CCS level 3 standard [21]. We consider that RCS R_1 at L.A. has a feeder capacity of 3MWh and RCS R_2 at East L.A. has a feeder capacity of 2.4MWh [7]. For the LCSs, their charging power is slower at 90kWh using SAE CCS level 2 standard [21]. We consider that LCS Q_1 at Hollydale Park has a feeder capacity of 450kWh and LCS Q_2 at Norwalk has the capacity of 360kWh. The LCSs are required to fulfill 87%-90% incoming PEV charging tasks to guarantee good customer satisfaction, which can be used to calculate the demanding energy of LMESs.

Although RCS loading pressure is an abstract concept, we want to measure it with real-life parameters so that it can be comparable with another scheduling objective. In

this work, we map different levels of loading pressures with price costs, which are extracted from the Southern California Edison pricing [130]. The mapping function is denoted as follow:

$$\begin{cases} \Gamma(\gamma_{\mathrm{R}_1,2} = 0.5) = 17 \\ \Gamma(\gamma_{\mathrm{R}_1,14} = 1) = 850 \end{cases} \quad \begin{cases} \Gamma(\gamma_{\mathrm{R}_2,2} = 0.5) = 12 \\ \Gamma(\gamma_{\mathrm{R}_2,14} = 0.95) = 540, \end{cases} \tag{4.30}$$

by calculating equation (4.30), a_{i} and b_{i} are calculated and shown in Table 4.4. For the dynamic pricing scheme, κ_1 is set to 1 and κ_2 is set is 50.

4.5.2 Simulation Results

We now validate the effectiveness of the proposed scheme from different perspectives. First, the effects of overload mitigation at LCSs and loading pressure optimization at RCSs are presented. Then, the time-efficiency of the proposed navigation scheme and pricing scheme is validated. Finally, we present the impact of objective weights on the scheduling results and discuss the trade-off between scheduling cost minimization and LMES following profile maximization.

Overload Mitigation at $\mathcal{Q}$

The power supply distribution at LCSs Q_1 and Q_2 are shown in Fig.4.6(a) and (b) respectively, where red histograms denote power supplied by the LMESs and blue histograms denote power supplied by local power feeders. It can be seen that during the time periods of 12 a.m.to 5 a.m., the power is fully supplied by local feeders as the PEV charging demands are within LCS feeder capacities. However, during daytime from 6 a.m.to 11 p.m., as on-road traffic flow increases, the PEV charging demand also increases at CSs. Correspondingly, to guarantee the pre-determined station availability, the LMES delivered energy increases. Hence, during these peak hours, without the help of LMESs, LCS local feeders would be heavily overloaded, while with the LMES delivered energy, LCS feeders only need to provide power at their capacities (i.e., 450kWh at Q_1 and 360kWh at Q_2). Therefore, the overload mitigation impact of LMESs is effective during peak traffic hours.

Loading Optimization at $\mathcal{R}$

By characterizing the loading pressure with South California electricity price, the comparison of loading pressure costs under the random-assigned case and the proposed loading-optimized scheme is shown in Fig.4.7. As LCSs only demand LMES delivered energy

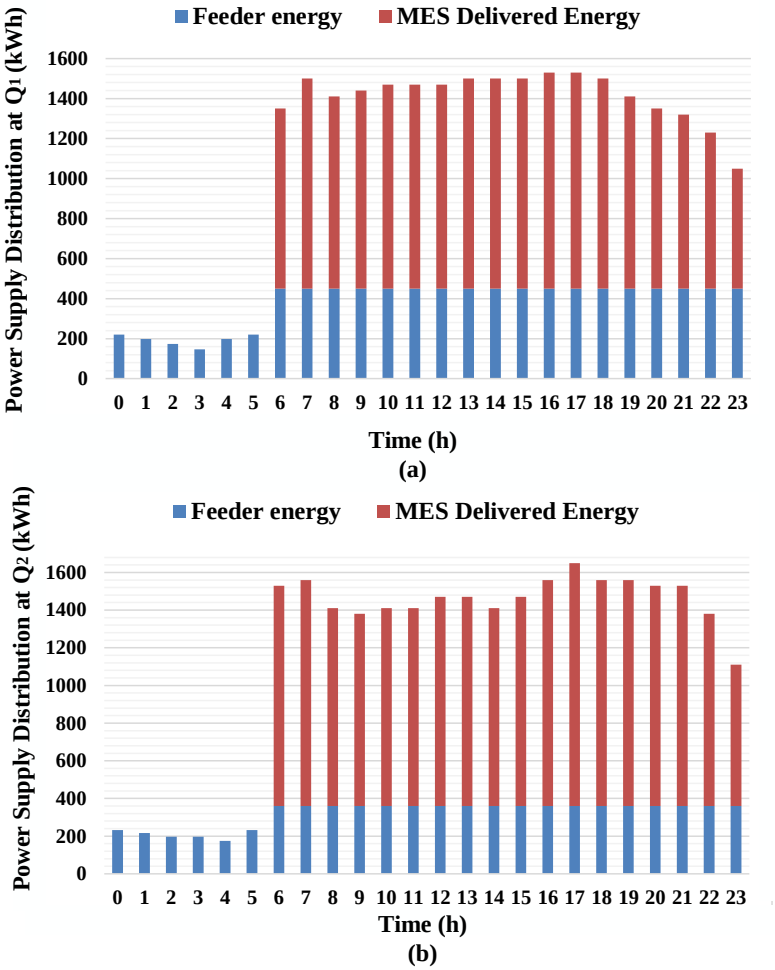

Figure 4.6: Power supply distribution at LCSs.

during peak hours (i.e., 6 a.m.-11 p.m.), RCS loading will be optimized during these peak hours. It can be seen that the loading-optimized scheme has a lower averaged loading ratio at all time compared with the randomly assigned case in which as long as the station has available power, LMESs can be allocated there. With the green line chart denoting the overall regular loads at RCSs, we can see that even during the RCS peak loading hours (e.g., 12 p.m.-7 p.m.), the loading-optimized scheme can keep the loading pressure costs at a lower level.

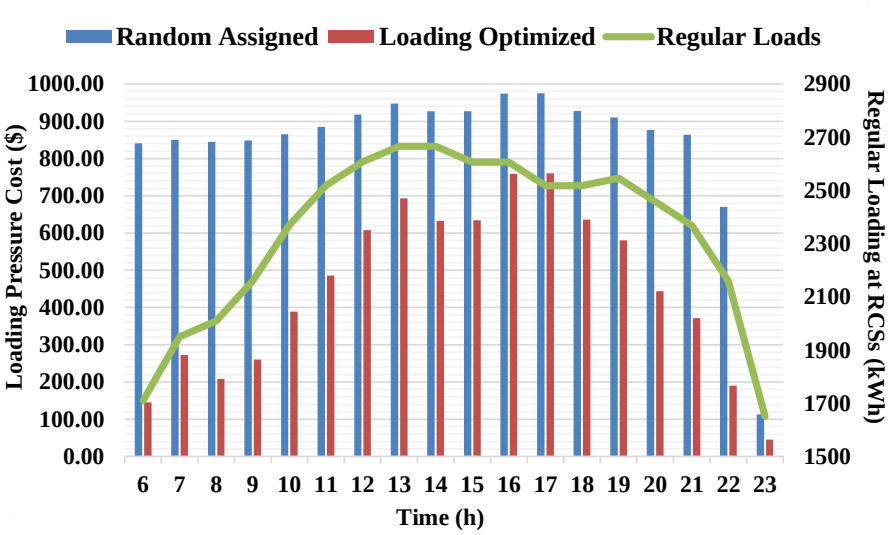

Figure 4.7: Loading pressure costs at RCSs.

Time Effectiveness of the Navigation Scheme

The comparison of averaged LMES energy delivery time under the optimal case, the pricing-based case and the fastest route search case is shown in Table 4.5. It can be seen that the optimal case has the shortest LMES energy delivery time (i.e., best case) and the fastest route search has the worst result. This is due to the route navigation difference on the saturated road. As shown in Fig.4.8, to deliver energy from RCS R_1 to LCSs, the shortest path is through $L_{(1,4)} - L_{(4,5)}$. During the time period from 6 a.m.to 11 p.m., the regular traffic flow on the link $L_{(1,4)}$ is around its link capacity. Unknowing the traffic capacity-related information and seeing the regular shortest route at its regular operation, LMES drivers would choose to go along $L_{(1,4)} - L_{(4,5)}$ as in the fastest route search case. Meanwhile, with a big picture of the transportation network, the optimal case considers the potential link congestion incurred by injected LMES traffic, and thus chooses another longer but less saturated route $(L_{(1,2)} - L_{(2,3)})$. When LMESs are provided with price-incentive, some LMESs will follow the directed routes while others will still choose the empirically fastest route due to limited price-incentive. Hence, LMES travelling time of the pricing-based case is in-between the optimal case and fastest route search case.

Table 4.5: Averaged LMES energy delivery time

Time/min	6	7	8	9	10	11	12	13	14	15	16	17	18	19	20	21	22	23
Optimal	9.51	9.98	10.01	9.93	10.20	10.81	10.84	11.05	11.06	10.93	10.87	10.99	11.04	10.81	10.66	10.44	10.18	8.88
Pricing	10.14	10.63	10.59	10.49	10.77	11.18	11.41	11.58	11.54	11.40	11.37	11.37	11.36	11.35	11.10	10.92	10.61	9.57
Fastest	10.79	11.63	11.58	11.34	11.74	12.10	12.70	12.81	12.79	12.54	12.46	12.29	12.30	12.46	12.04	11.76	11.12	10.00

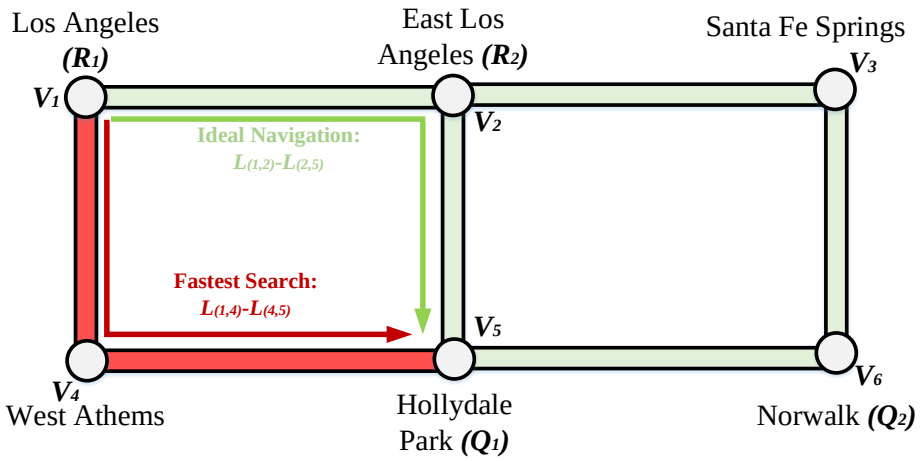

Figure 4.8: Route illustration from R_1 to Q_1.

κ_2/κ_1 v.s. Travelling Time

As κ_1 and κ_2 denote the objective weights of cost minimization and profile tracking maximization respectively, the ratio of κ_2/κ_1 has a non-negligible impact on the LMES travelling time, which is discussed as follow.

The comparisons of overall LMES travelling time under the scheduling of different κ_2/κ_1 ratios is shown in Fig. 4.9. It can be seen that the optimal navigation has the shortest travelling time and the fastest route search is the slowest case. The LMES travelling time of pricing-based navigations is in the range between the optimal scheduling case and fastest route navigation. It can be seen that as the objective ratio increases, the LMES travelling time decreases. The increasing κ_2/κ_1 ratio denotes the objective tendency towards the LMES profile tracking maximization that aims to mitigate the percentage gap between the optimal navigation and pricing-based navigation.

To encourage more LMESs following the optimal navigation demands a higher price for incentive, which also increases the overall navigation cost. Thus, an increasing naviga-

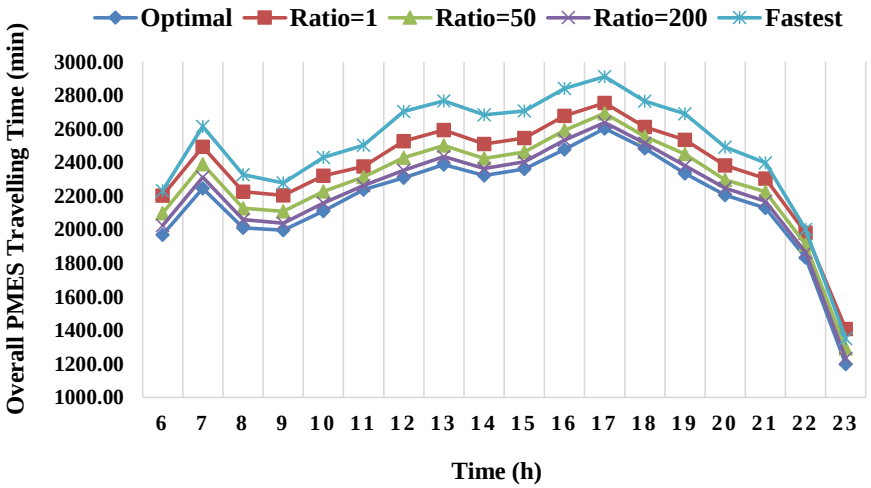

Figure 4.9: Overall LMES travelling time with different κ_2/κ_1 ratios.

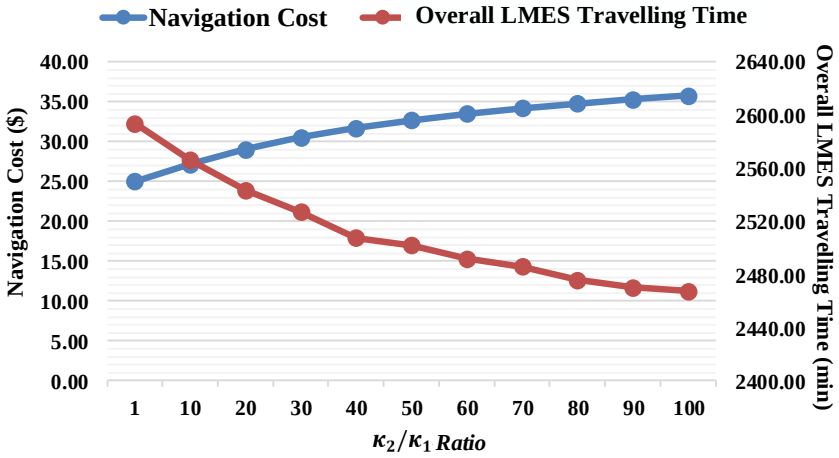

Figure 4.10: Trade-off between navigation cost and LMES travelling time.

tion cost leads to a decreasing LMES travelling time until all LMESs follow the optimal navigation, forming a trade-off between navigation cost and LMES travelling time. The trade-off condition at time $h = 13$ is shown in Fig.4.10.

4.6 Summary

In this chapter, we present the work of scheduling LMESs among a GCS to mitigate the LCS overload issue while considering their potential impact on the transportation network. A dynamic pricing-based scheduling scheme has been proposed with a two-stage operation. First, a loading-optimized navigation scheme has been proposed to calculate the LMES navigation route in the transportation network. Then, a dynamic pricing scheme has been proposed to encourage LMESs following the optimal navigation result to enable a fast energy delivery process. The formulated problems have been solved by the network simple algorithm and convex optimization. Performance evaluation has validated the effectiveness of the proposed scheme on both power overload mitigation and time-efficiency of energy delivery. Further, the impact of different scheduling objectives on the navigation results has been discussed. It is concluded that aligning the pricing-based navigation results with the optimal navigation result leads to an increasing navigation cost. Thus, in terms of the local power and traffic conditions, the UO needs to balance between the navigation cost and transportation time increment incurred by LMESs. The proposed scheduling scheme can be operated by the local power utility company when scheduling a large number of MESs for energy compensation tasks and avoiding interference with the transportation operation.

Chapter 5

Energy Scheduling of PMESs: a Stackelberg Game Approach

5.1 Introduction

As the electric battery technology advances and PEV commercialization proceeds, it is foreseen that PEVs will be prevalent and become a regular transportation option in every household [1]. In this case, the large fleet size of on-road private PEVs makes them ideal MES candidates with high flexibility [50]. In the power operation market, LCS operation considers the day-ahead market and real-time market. Regarding the LCS day-ahead operation planning, we propose to use UMESs to mitigate the LCS predictable and foreseeable large amount of energy shortage. For the real-time LCS operation, LMESs are utilized in Chapter 4 as an assistant fleet for LCS short-term overload issues. LMESs scheduling and navigation have been proven to be effective for the energy compensation tasks when PEV commercialization is still in process. When the PEV reaches its desired market share level and becomes prevalent, on-road PMESs will be the cost-efficient and ideal MES option for mitigating the LCS short-term overload issue. When schedule on-road PMESs, the impact of additional traffic on the transportation network does not exist as PMESs account for a portion of on-road traffic. To utilize on-road PMESs, the UO considers scheduling PMESs to CSs that are along their planned route as travelling to destination place is PMES primary objective. Thus, the energy compensation service will be conducted in a more efficient manner using the on-road resource. In addition, performing energy compensation tasks requires frequent charge/discharge cycle from PMESs. For some PMES owners, the service time and battery degradation could impede them from accepting mutually beneficial tasks. Therefore, incentive-based scheduling is essential for

PMES energy compensation tasks.

In literature, there have been extensive studies on price-incentive scheme for PEV scheduling [98, 103–110]. In the works [98, 103], the utility operator assumes homogeneous PEV objective and uses pricing to achieve the social optimum. The works in [104–106] consider the heterogeneity in PEV objectives and preferences, and use hierarchical pricing scheme. In addition, Stackelberg game has been utilized in many works [107–110] as a multi-layer architecture to characterize the interaction between utility operators, CSs, and PEVs. While incentive strategies have been extensively explored in PEV charging and occasionally PEV discharging, on-road PMES scheduling needs to consider two key factors collaboratively: MES service process and hierarchical pricing. To accomplish PMES energy compensation tasks, UO needs to schedule a three-step process: MES charging, discharging, and on-road travelling. Second, how to stimulate PMESs with different preferences while considering the battery degradation and service time compensation incurred by the energy compensation service is a challenging issue.

To effectively stimulate PMESs and address two key challenges collaboratively, our objective in this work is to design an effectively pricing-incentive strategy to stimulate on-road PMESs participating in the service by considering the heterogeneity in their objectives and preferences. The main contribution of this work is twofold. First, an incentive strategy is proposed to encourage PMESs participating in the service by improving their utilities that consider the service revenue, battery degradation, and service time costs. The proposed scheme also enables cost-efficient overload mitigation at the UO side. Second, corresponding to the proposed scheme, a Stackelberg game is formulated to characterize the price-service interaction between UO and PMESs, where the UO acts as the game leader and PMESs act as followers. The existence and uniqueness of the Stackelberg equilibrium are proved, and we design an efficient algorithm to find the equilibrium.

The remainder of the chapter is organized as follows. The system model of a GCS is introduced in Section II. The incentive strategy and the corresponding game formulation are presented in Section III. Performance evaluation of the proposed strategy is presented in Section IV. Finally, Section V summarizes this chapter.

5.2 System Model

The system model is shown in Fig.5.1, which consists of a GCS, on-road PMESs, UO, and communication infrastructure. The status of the GCS is analyzed on a regular basis by partitioning one day into H time slots with equal interval of Δt. Consider the PMES energy compensation service is fulfilled within Δt, the MES scheduling is regularly conducted at

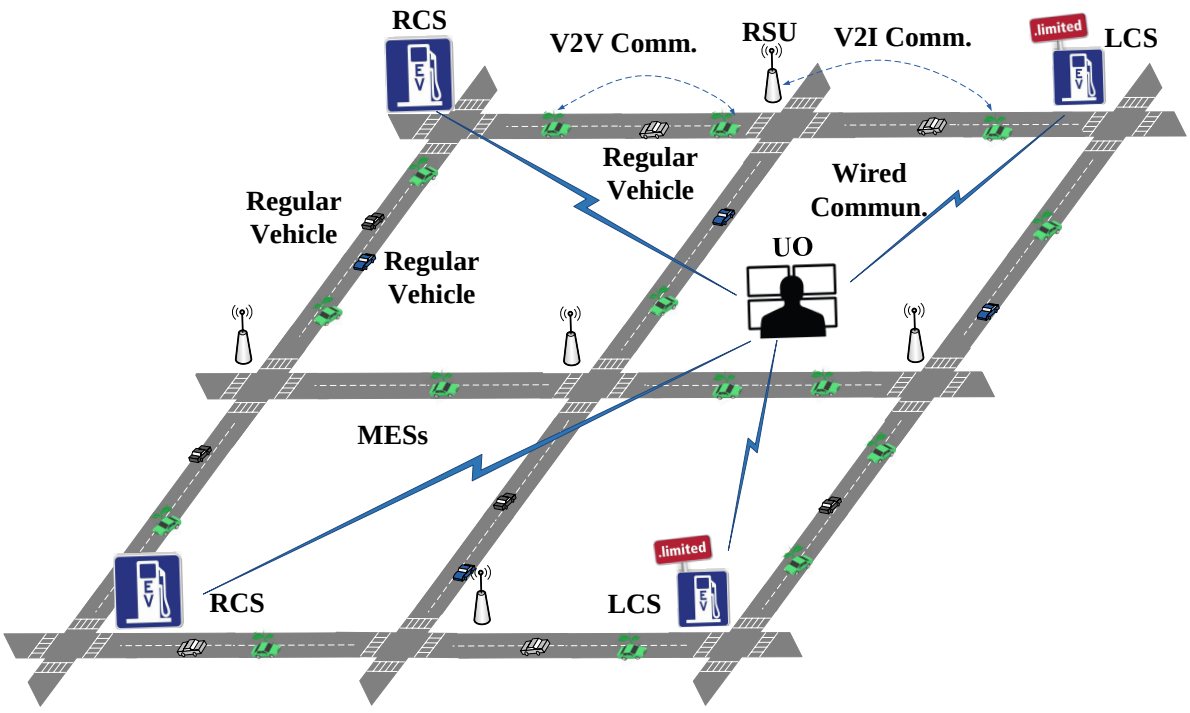

Figure 5.1: System model.

each time slot $h \in \mathcal{H}$. A summary of the notations used in this chapter is shown in Table 5.1.

5.2.1 On-road PMESs

To mitigate the LCS overloads without additional infrastructure upgrade, a set of on-road PMESs, denoted as $\mathcal{K} = \{1, \dots k, \dots K\}$, are stimulated by the UO to accomplish energy compensation tasks. Upon departure, PMESs send information about their planned travel routes and service capacities to the UO so that the UO can estimate the service capacity of each RCS-LCS pair.

Table 5.1: Notations for Chapter 5

Symbol	Description
$\mathcal{H}$	The set of time slots
$\mathcal{K}$	The set of PMESs
$\mathcal{L}$	The set of LCSs
$\mathcal{R}$	The set of RCSs
$\alpha_{\mathrm{k}}^T/\alpha_{\mathrm{k}}^D$	The weight of service time/battery degradation cost for k-th PMES
α_{L}	The weight of total LCS loading revenue
α_1/α_2	The depth-of-discharge weights of PMES
$\beta_1/\beta_2/\beta_3/\beta_4$	The weights of discharging power degradation of PMES
$a_{\mathrm{j}}/b_{\mathrm{j}}/c_{\mathrm{j}}$	The weights of loading revenue of LCS L_{j}
B_{k}	The battery capacity of k-th PMES, kWh
C_{k}^T	The service time of k-th PMES, *hour*
C_{k}^D	The battery degradation cost of k-th PMES, \$
$D_{\mathrm{j,h}}^L/D_{\mathrm{j,h}}^U$	Minimal/Maximal demanding energy of LCS L_{j} at time h, kWh
e_{k}	The energy service amount of k-th PMES, kWh
e_{k}^I	The initial energy status of k-th PMES, kWh
$E_{\mathrm{i,h}}$	The surplus energy at RCS R_{i} at time h, kWh
N_{ij}	The number of PMESs that deliver energy from R_{i} to LCS L_{j}, vehicles
p	The posted service price by UO, \$
P_{i}	The charging power at RCS R_{i}, kW
P_{j}	The discharging power at LCS L_{j}, kW

5.2.2 GCS

GCS itself presents a hierarchical architecture between the UO and the CSs deployed within the control area. In this work, we consider that UO is in full charge of balancing the GCS energy status.

RCSs and LCSs

As shown in Fig.5.1, the GCS is composed of RCSs and LCSs that are both geographically reachable by vehicles. RCSs, a set of CSs denoted by $\mathcal{R} = \{R_1, R_2 \dots R_\mathrm{i}\}$, are normally deployed at urban areas with sufficient power supplies. The RCS power not only can charge the incoming PEVs with charging demands, but its excess part can be stored by PMESs and delivered to LCSs. LCSs, a set of CSs denoted by $\mathcal{L} = \{L_1, L_2 \dots L_\mathrm{j}\}$, are usually deployed at rural areas with limited power capacities and thus could encounter overload issues at peak hours. To monitor the CS energy status, CSs regularly send their real-time energy status information to the operator. At time h, RCS R_i sends its real-time surplus energy $E_{\mathrm{i,h}}$ and LCS L_j sends its demanding energy range between the minimal energy $D^L_{\mathrm{j,h}}$ and maximal energy $D^U_{\mathrm{j,h}}$ to the operator.

UO

The UO regularly receives the energy status of monitored CSs, PMES service capacity, and planned routes. Upon receiving the information, the UO first estimates the on-road PMES service capacity between each RCS-LCS pair. For example, if the planned route of a PMES overlaps with the energy delivery route from RCS R_i to LCS L_j, the PMES is counted as an energy compensation server for $R_\mathrm{i} - L_\mathrm{j}$ pair. Notably, every on-road PMES will only be assigned to one RCS-LCS pair. By the end, the UO knows the number of PMESs N_{ij} for energy delivery along the route of R_i-L_j pair and their average service capacity. The operator then analyzes the energy status information of GCS and posts the service price to PMESs to stimulate them providing energy compensation service.

5.2.3 Communication Infrastructure

For the introduced system model, data/command communication occurs between the UO and CSs, the UO and PMESs, CSs and PMESs.

- ▷ **UO-CSs:** UO, usually the local utility company, are stationary, as are the CSs. To regularly monitor the CS operation status, wired communication technologies such as power line communication and fiber optics are their prior options [131, 132]. Due to the prevalent deployment of cellular networks, they are also a common option for UO-CSs communication;
- ▷ **UO-PMESs:** Since only on-road PMESs participate in energy compensation tasks, mobile-support communication technology is demanded to enable a smooth data transfer. Latest developed cellular networks are good communication candidates [133]. Moreover, VANETs can be used to transmit the vehicle information to the operator through V2V and V2I communication [134].
- ▷ **CSs-PMESs:** Upon connecting to the CSs for energy charging/discharging, CSs and PMESs will be exchanging the battery information and assigned service capacity. Moreover, PMES drivers can also monitor the task process by communicating with CSs via short-distance wireless communication technology such as WiFi [135] and ZigBee [136].

5.3 Incentive Strategy for On-road PMESs

At time h, UO posts the service price to PMESs to stimulate them actively undertaking the service tasks. In response to the price, PMESs choose how many battery capacities they will be used for the service (ranging from zero to all remaining battery capacity). The sequential operation can be precisely characterized by a sequential game model such as a Stackelberg game. Therefore, in this work, the interaction between the UO and MESs is formulated as a dynamic Stackelberg game at h-th time slot. As the MES scheduling is conducted at each time slot, the notation h is omitted.

5.3.1 Stackelberg Game Process

We define the game in its strategic form: $G = \{\{\mathcal{K} \cup \{PSO\}\}, \{p\}, \{e_{\mathrm{k}}\}_{\mathrm{k}\in\mathcal{K}}, \{U_{\mathrm{P}}\}, \{U_{\mathrm{k}}\}_{\mathrm{k}\in\mathcal{K}}\}$, where $\{e_{\mathrm{k}}\}_{\mathrm{k}\in\mathcal{K}}$ denotes the set of PMES strategies, $\{p\}$ denotes the UO strategy (i.e., pricing), $\{U_{\mathrm{P}}\}$ and $\{U_{\mathrm{k}}\}_{\mathrm{k}\in\mathcal{K}}$ represent utility functions of operator and PMESs, respectively. For a service price p posted by the operator, the PMES layer interaction is characterized as a non-cooperative game as follows:

- ▷ Players: a set of PMESs $\mathcal{K}$.

▷ Strategies: for the PMES $k \in \mathcal{K}$, chooses an energy service amount e_{k}.

▷ Payoffs: the k-th PMES receives revenue $U_{\mathrm{k}}(e_{\mathrm{k}}, p)$.

To find the Nash equilibrium, we need to find the best response function $e^{\star}_{\mathrm{k}}(p)$ of k-th MES under the service price p. The set of best response functions $\{e^{\star}_{\mathrm{k}}(p)\}_{\mathrm{k}\in\mathcal{K}}$ are sent to the UO. The operator then optimizes its service price $p^{\star}$ to maximize its utility function $U_{\mathrm{P}}(p, \{e^{\star}_{\mathrm{k}}(p)\}_{\mathrm{k}\in\mathcal{K}})$.

5.3.2 Game Formulation

As a hierarchical game model, the Stackelberg game formulation is presented first at PMES level, and then the PMES best response function will be used in the UO pricing decision.

PMES Model

For MES $k \in \mathcal{K}$, its utility function is defined as:

$$U_{\mathrm{k}}(e_{\mathrm{k}}, p) = pe_{\mathrm{k}} + p(e_{\mathrm{k}} - \bar{e}) - \alpha^{T}_{\mathrm{k}} C^{T}_{\mathrm{k}} - \alpha^{D}_{\mathrm{k}} C^{D}_{\mathrm{k}}, \tag{5.1}$$

The first term in the utility function is the service reward calculated by multiplying the MES served energy amount with the service price. The second term is the motivation reward that motivates MES providing energy more than the expected average service amount of $\bar{e}$. $\bar{e}$ is the average energy that on-road PMESs need to provide for LCSs to meet their minimal demands, which is calculated as $\bar{e} = (\sum_{L_{\mathrm{j}}\in\mathcal{L}} D^{L}_{\mathrm{j}})/(\sum_{R_{\mathrm{i}}\in\mathrm{R}} \sum_{L_{\mathrm{j}}\in\mathcal{L}} N_{\mathrm{ij}})$. When MES provides less energy than $\bar{e}$, the motivation reward is negative, meaning that PMESs will receive less reward than their originally should if the PMES does not meet the expected serving amount. On the contrary, when a PMES provides more service energy than $\bar{e}$, it will be rewarded more than service reward. The third terms in equation (5.1) is the weighted service time cost that is the product of the service time weight α^{T}_{k} of k-th PMES and its service time C^{T}_{k}. The service time consists of MES charging time at its passing RCS R_{i} and discharging time at its destined LCS L_{j}, which is calculated as:

$$C^{T}_{\mathrm{k}} = \frac{e_{\mathrm{k}}}{P_{\mathrm{i}}} + \frac{e_{\mathrm{k}}}{P_{\mathrm{j}}}, \tag{5.2}$$

where P_{i} and P_{j} denote average charging/discharging power of R_{i} and L_{j} respectively. The travelling time is excluded from the service time cost as R_{i} and L_{j} are on the MES

planned travel route. The weight of service time cost α_{k}^{T} ($\alpha_{\mathrm{k}}^{T} > 0$) indicates the MES driver preference towards service time. A high α_{k}^{T} indicates that MES driver is unwilling to spend too much time in-station, and more rewards are needed for them. The forth term of the function is the weighted battery degradation cost of MES discharging at LCS. It is calculated as the product of the battery degradation weight α_{k}^{D} of k-th PMES and the battery degradation cost C_{k}^{D} of k-th PMES. The battery degradation cost refers to a modified model as in work [137]:

$$C_{\mathrm{k}}^{D} = (\beta_1 P_{\mathrm{j}}^3 + \beta_2 P_{\mathrm{j}}^2 + \beta_3 P_{\mathrm{j}} + \beta_4)(\alpha_1 \frac{e_{\mathrm{k}}^2}{B_{\mathrm{k}}^2} + \alpha_2 \frac{e_{\mathrm{k}}}{B_{\mathrm{k}}}). \tag{5.3}$$

The term of discharging power degradation, $\beta_1 P_{\mathrm{j}}^3 + \beta_2 P_{\mathrm{j}}^2 + \beta_3 P_{\mathrm{j}} + \beta_4$, is a cubic function with coefficients β_1, β_2, β_3, and β_4. It is positively related to discharging power P_{j} at the MES destined LCS L_{j}. The term of depth-of-discharge (DoD) degradation, $\alpha_1 \frac{e_{\mathrm{k}}^2}{B_{\mathrm{k}}^2} + \alpha_2 \frac{e_{\mathrm{k}}}{B_{\mathrm{k}}}$, is a quadratic function that is positively related to the battery DoD $\frac{e_{\mathrm{k}}}{B_{\mathrm{k}}}$, and thus coefficient $\alpha_1 > 0$. Similar to α_{k}^{T}, a high degradation weight α_{k}^{D} denotes a high unwillingness to discharge and to countermeasure this issue, a higher service price is needed. To simplify the equation, we denote $D_{\mathrm{k}} = \beta_1 P_{\mathrm{j}}^3 + \beta_2 P_{\mathrm{j}}^2 + \beta_3 P_{\mathrm{j}} + \beta_4 > 0$.

Meanwhile, the MES service energy should be within its feasible range in terms of its current battery status:

$$0 \leq e_{\mathrm{k}} \leq B_{\mathrm{k}} - e_{\mathrm{k}}^{I}, \tag{5.4}$$

where B_{k} denotes the k-th MES battery capacity and e_{k}^{I} denotes the initial state-of-charge (SoC) of MES k. Meanwhile, MESs will not participate in the service when they cannot obtain any profit, thus the utility function should be positive, denoted as:

$$U_{\mathrm{k}}(e_{\mathrm{k}}, p) > 0. \tag{5.5}$$

Thus, given the posted price p, the MES decision making process is formulated as an optimization problem by choosing the service amount to maximize its utility function, which is denoted as:

$$\begin{aligned} \max_{e_{\mathrm{k}}} \quad & U_{\mathrm{k}}(e_{\mathrm{k}}, p) \\ \text{s.t.} \quad & (5.4), (5.5), \quad \forall k \in \mathcal{K}. \end{aligned} \tag{5.6}$$

UO Model

As the operator of GCS, the UO aims to adjust the posted price to maximize its utility function, which is denoted as:

$$U_{\mathrm{P}}(p, e_{\mathrm{k}}) = \alpha_{\mathrm{L}} \sum_{L_{\mathrm{j}} \in \mathcal{L}} (-(a_{\mathrm{j}} \sum_{k \in \Lambda_{\mathrm{j}}} e_{\mathrm{k}} - b_{\mathrm{j}})^2 + c_{\mathrm{j}}) - (\sum_{k \in \mathcal{K}} p e_{\mathrm{k}} + \sum_{k \in \mathcal{K}} p(e_{\mathrm{k}} - \bar{e})), \tag{5.7}$$

The first term is the weighted loading revenue that is the product of loading weight α_{L} and the summation of LCS loading revenues. Denote a set of PMESs whose destined LCS is L_{j} as Λ_{j}. Then, the LCS received delivered energy is the summation of the energy delivered by PMESs belong to the set Λ_{j}: $\sum_{k \in \Lambda_{\mathrm{j}}} e_{\mathrm{k}}$.

For LCS L_{j}, the loading revenue increases as more energy delivered to the station and reaches the peak revenue at the maximal demanding load D_{j}^U. Therefore, the loading revenue of LCS L_{j} is characterized as a quadratic function that reaches the peak revenue at the maximal demanding load of D_{j}^U. We set $a_{\mathrm{j}} = 5 \times 10^{-4} D_{\mathrm{j}}^U, b_{\mathrm{j}} = a_{\mathrm{j}} D_{\mathrm{j}}^U, c_{\mathrm{j}} = b_{\mathrm{j}}^2$. The second term of the function is the summation of all MES service costs and motivation costs, as introduced in the last subsection.

For LCS L_{j}, the MES delivered energy $\sum_{k \in \Lambda_{\mathrm{j}}} e_{\mathrm{k}}$ should be within its demanding energy range $[D_{\mathrm{j}}^L, D_{\mathrm{j}}^U]$, which is denoted as:

$$D_{\mathrm{j}}^L \leq \sum_{k \in \Lambda_{\mathrm{j}}} e_{\mathrm{k}} \leq D_{\mathrm{j}}^U, \forall L_{\mathrm{j}} \in \mathcal{L}. \tag{5.8}$$

On the energy supplier side, the energy stored by MESs should not exceed the maximal surplus energy capacities at RCSs. Denote a set of MESs whose departure station is R_{i} as Ω_{i}. Then, the RCS energy constraint is denoted as:

$$\sum_{k \in \Omega_{\mathrm{i}}} e_{\mathrm{k}} \leq E_{\mathrm{i}}, \forall R_{\mathrm{i}} \in \mathcal{R}. \tag{5.9}$$

Therefore, the price decision process of UO is formulated as an optimization problem as:

$$\begin{aligned} \max_{p} \quad & U_{\mathrm{P}}(e_{\mathrm{k}}, p) \\ \text{s.t.} \quad & (5.8), (5.9). \end{aligned} \tag{5.10}$$

5.3.3 Game Analysis

Existences and Uniqueness of Stackelberg Game

Given the posted service price p, we can solve problem (5.6) and obtain the best-response strategy of MES k, denoted as $e_{\mathrm{k}}^{\star}(p)$. When the game reaches Nash equilibrium, all followers are choosing their best-response strategies and the strategy set is denoted as $\{e_{\mathrm{k}}^{\star}(p)\}_{\mathrm{k}\in\mathcal{K}} = \{e_1^{\star}(p), \ldots, e_{\mathrm{K}}^{\star}(p)\}$. Given MES best-response strategy profile, the optimal price $p^{\star}$ can be obtained by solving problem (5.10). Therefore, the profile of $(p^{\star}, \{e_{\mathrm{k}}^{\star}(p)\}_{\mathrm{k}\in\mathcal{K}})$ is the Stackelberg equilibrium for the proposed game, which is calculated as:

$$\begin{aligned}(p^{\star}, \{e_{\mathrm{k}}^{\star}(p)\}_{\mathrm{k}\in\mathcal{K}}) =& \underset{P}{arg max} U_{\mathrm{p}}(p, \{e_{\mathrm{k}}^{\star}(p)\}_{\mathrm{k}\in\mathcal{K}}) \\ &\text{s.t.} \quad e_{\mathrm{k}}^{\star}(p) = arg\, max U_{\mathrm{k}}(e_{\mathrm{k}}, p), \quad k \in \mathcal{K}.\end{aligned} \tag{5.11}$$

We first analyze the follower-level game by computing MES best-response strategy using the following lemma.

Lemma 1 *PMES k has a unique best-response strategy $e_{\mathrm{k}}^{\star}(p)$ for a given service price p, denoted as:*

$$e_{\mathrm{k}}^{\star}(p) = \begin{cases} 0, & p \le p_{\mathrm{k}}^{L} \\ \frac{2p - \alpha_{\mathrm{k}}^{T} \frac{P_{\mathrm{i}}+P_{\mathrm{j}}}{P_{\mathrm{i}}P_{\mathrm{j}}} - \alpha_{\mathrm{k}}^{D}\alpha_2 D_{\mathrm{k}}/B_{\mathrm{k}}}{2\alpha_1 \alpha_{\mathrm{k}}^{D} D_{\mathrm{k}}/B_{\mathrm{k}}^2}, & p_{\mathrm{k}}^{L} < p < p_{\mathrm{k}}^{U} \\ B_{\mathrm{k}} - e_{\mathrm{k}}^{I}, & p \ge p_{\mathrm{k}}^{U} \end{cases} \tag{5.12}$$

where p_{k}^{L} is the rejection price, below which the PMES will not provide service. p_{k}^{U} is the saturated price at which PMES k provides its maximal service capacity. p_{k}^{L} and p_{k}^{U} are denoted as:

$$\begin{cases} p_{\mathrm{k}}^{L} = 0.5(\alpha_{\mathrm{k}}^{T} \frac{P_{\mathrm{i}}+P_{\mathrm{j}}}{P_{\mathrm{i}}P_{\mathrm{j}}} + \alpha_{\mathrm{k}}^{D}\alpha_2 D_{\mathrm{k}}/B_{\mathrm{k}}) \\ p_{\mathrm{k}}^{U} = p_{\mathrm{k}}^{L} + \alpha_1 \alpha_{\mathrm{k}}^{D} D_{\mathrm{k}}(B_{\mathrm{k}} - e_{\mathrm{k}}^{I})/B_{\mathrm{k}}^2 \end{cases} \tag{5.13}$$

Proof 4 *For MES k, the strategy set is denoted as $\{e_{\mathrm{k}} | e_{\mathrm{k}} \in R, 0 \le e_{\mathrm{k}} \le B_{\mathrm{k}} - e_{\mathrm{k}}^{I}\}$, which is the intersection of two halfspace. Thus, the MES strategy set is non-empty and convex. To find the best-response strategy of k-th MES, we solve the optimization problem (5.6). First,*

we analyze the property of the objective function $U_{\mathrm{k}}(e_{\mathrm{k}}, p)$ by calculating the second-order derivative of the objective function:

$$\frac{\partial^2 U_{\mathrm{k}}(e_{\mathrm{k}}, p)}{\partial e_{\mathrm{k}}^2} = -2\alpha_{\mathrm{k}}^D \alpha_1 D_{\mathrm{k}}. \tag{5.14}$$

As $\alpha_{\mathrm{k}}^D, \alpha_1, D_{\mathrm{k}} > 0$, the value of equation (5.14) is always negative. Thus, problem (5.6) is proven to be a convex optimization problem, and the best response strategy for MES k is global optimum. By applying Lagrangian function and Karush-Kuhn-Tucker (KKT) conditions to problem (5.6), we can obtain the best response strategy of MES k. The detailed calculation is omitted.

Based on MES best-response strategy, we define the feasible range of service price p. The UO adjusts its price within the range between the minimal and maximal value of $p_{\mathrm{range}} \triangleq [p_1^L \dots p_{\mathrm{K}}^L, p_1^U \dots p_{\mathrm{K}}^U]$. $\min\{p_{\mathrm{range}}\}$ is the overall rejection price, under which all PMESs will not participate in energy compensation service. On the other hand, when the price is at $\max\{p_{\mathrm{range}}\}$ (i.e., overall saturated price), all PMESs use up their battery space for the service and no higher price is needed. By calculating p_{k}^L and p_{k}^U for MES k using equation (5.13), and sorting all p_{k}^L and p_{k}^U in an ascending order, we have the feasible set of the price. The price set is a M-element vector γ, where $\gamma_1 \le \gamma_2 \le \dots \le \gamma_{\mathrm{m}} \le \gamma_{\mathrm{m+1}} \dots \gamma_{\mathrm{M}}$. Further, define $\Gamma_{\mathrm{m}} \triangleq [\gamma_{\mathrm{m}}, \gamma_{\mathrm{m+1}}]$ for $m = 1, 2, \dots M-1$, we can divide the price p range into $M-1$ intervals.

To find the optimal price for UO, we decompose problem (5.10) into $M-1$ sub-problems where the m-th sub-problem aims to finding the optimal price within the range Γ_{m}, similar to works in [138, 139].

Lemma 2 *In the sub-domain of $\Gamma_{\mathrm{m}}, \forall m$, problem (5.10) is a convex optimization problem.*

Proof 5 *As the price is continuous within Γ_{m}, the price set is convex. By substituting the MES best-response strategy into problem (5.10), the objective function is calculated as:*

$$\begin{aligned} U_{\mathrm{P}}(p, \Gamma_{\mathrm{m}}) = \alpha_{\mathrm{L}} \sum_{L_{\mathrm{j}} \in \mathcal{L}} (-(a_{\mathrm{j}}(\sum_{k \in \Lambda_{\mathrm{j}} \cap \phi_1} (y_{\mathrm{k}} p - z_{\mathrm{k}}) + \sum_{k \in \Lambda_{\mathrm{j}} \cap \phi_2} (B_{\mathrm{k}} - e_{\mathrm{k}}^I)) - b_{\mathrm{j}})^2 + c_{\mathrm{j}}) \\ - 2p(\sum_{k \in \phi_1} (y_{\mathrm{k}} p - z_{\mathrm{k}}) + \sum_{k \in \phi_2} (B_{\mathrm{k}} - e_{\mathrm{k}}^I)) + \sum_{k \in \mathcal{K}} p\bar{e}, \end{aligned} \tag{5.15}$$

where $y_{\mathrm{k}}p - z_{\mathrm{k}}$ *is the simplied function of* $e_{\mathrm{k}}^{\star}$ *for* $p_{\mathrm{k}}^{L} < p < p_{\mathrm{k}}^{U}$*, and* y_{k}*,* z_{k} *are denoted as:*

$$\begin{cases} y_{\mathrm{k}} = \frac{2}{2\alpha_1 \alpha_{\mathrm{k}}^{D} D_{\mathrm{k}}/B_{\mathrm{k}}^{2}}, \\ z_{\mathrm{k}} = \frac{\alpha_{\mathrm{k}}^{D}\alpha_2 D_{\mathrm{k}}/B_{\mathrm{k}}}{2\alpha_1 \alpha_{\mathrm{k}}^{D} D_{\mathrm{k}}/B_{\mathrm{k}}^{2}}, \end{cases} \tag{5.16}$$

For MESs with non-zero best-response value within Γ_{m}*, they are divided into two sets:* ϕ_1 *and* ϕ_2*, where* $\phi_1 = \{k | y_{\mathrm{k}}p - z_{\mathrm{k}} < B_{\mathrm{k}} - e_{\mathrm{k}}^{I}\}$ *and* $\phi_2 = \{k | y_{\mathrm{k}}p - z_{\mathrm{k}} \geq B_{\mathrm{k}} - e_{\mathrm{k}}^{I}\}$*. As* p_{k}^{L} *and* p_{k}^{U} *are deterministic and irrelevant to* p*,* ϕ_1 *and* ϕ_2 *are deterministic and fixed. The second derivative of the utility function is calculated as:*

$$\frac{\partial^2 U_{\mathrm{P}}(p, \Gamma_{\mathrm{m}})}{\partial p^2} = -2\alpha_{\mathrm{L}} \sum_{L_{\mathrm{j}} \in \mathcal{L}} a_{\mathrm{j}}^{2} \sum_{k \in \Lambda_{\mathrm{i}} \cap \phi_1} y_{\mathrm{k}}^{2} - 4 \sum_{k \in \phi_1} y_{\mathrm{k}}, \tag{5.17}$$

where $\alpha_{\mathrm{L}}, a_{\mathrm{j}}, y_{\mathrm{k}} > 0$*. Thus,* $\partial^2 U_{\mathrm{P}}(p, \Gamma_{\mathrm{m}})/\partial p^2 < 0$*, making the utility function concave and differential. Moreover, by substituting equation (5.13) to constraints (5.8), (5.9), both constraints are convex (half-space). Therefore, problem (5.10) within the sub-domain* Γ_{m} *is a convex optimization problem.*

Lemma 3 *The utility function of UO has a globally optimal price, given the best-response strategies of MESs.*

Proof 6 *By decomposing problem (5.10) into* $M - 1$ *sub-problems as defined in Lemma 2, the original problem can be rewritten as:*

$$\begin{aligned} \max_{m} \max_{p \in \Gamma_{\mathrm{m}}} \quad & U_{\mathrm{P}}(p, \Gamma_{\mathrm{m}}) \\ s.t. \quad & (5.8), (5.9). \end{aligned} \tag{5.18}$$

By obtaining the optimal result $p_{\mathrm{m}}^{\star}$ *of the convex sub-problem follow Lemma 2, we can find the globally optimal price* $p^{\star}$ *by searching the maximum utility value from* $[p_1^{\star}, \ldots, p_{\mathrm{m}}^{\star}, \ldots, p_{\mathrm{M}-1}^{\star}]$*:*

$$\begin{aligned} p^{\star} = \underset{p \in [p_1^{\star}, \ldots, p_{\mathrm{m}}^{\star}, \ldots, p_{\mathrm{M}-1}^{\star}]}{argmax} \quad & U_{\mathrm{P}}(p, \Gamma_{\mathrm{m}}) \\ s.t. \quad & (5.8), (5.9). \end{aligned} \tag{5.19}$$

Thus, the existences and uniqueness of the Stackelberg equilibrium can be proved in the following proposition.

Proposition 3 *For the formulated game, a unique Stackelberg equilibrium exists.*

Proof 7 *As shown in Lemma 1, each MES has a unique best-response strategy $e_{\mathrm{k}}^{\star}(p)$ given as a posted price p. Then, by substituting $e_{\mathrm{k}}^{\star}(p)$ to problem (5.10), we prove that the global optimum of PSO strategy exists as in Lemma 2 and Lemma 3. As PSO achieves its global optimum and each MES has a unique best-response strategy, the unique Stackelberg equilibrium is obtained.*

Stackelberg Game Algorithm

During each scheduling time period Δt, the UO scheduling price can be obtained as in Algorithm 4 by first calculating the PMES best response function and substituting the set of functions to problem (5.10) and iteratively solve the problem within Γ_{m}. The optimal result can be obtained as the maximal solution of the iterated problem.

Algorithm 4: Stackelberg game solution.

for *k=1 to K* **do**
  Calculate p_{k}^{L} and p_{k}^{L} according to equation (5.13) ;
Sorting p_{k}^{L} and p_{k}^{L} in an ascending order to form vectors γ and Γ
for *m=1 to M-1* **do**
  Find $p_{\mathrm{m}}^{\star}$ by solving problem (5.10) within $[\Gamma_{\mathrm{m}}, \Gamma_{\mathrm{m+1}}]$;
Find the optimal $p^{\star}$ with the maximal utility value according to equation (5.19).

The proposed algorithm does not require iterations to analyze the Stackelberg game. As the number of MESs increases, the algorithm complexity increases polynomially. Thus, the proposed algorithm can be applied to schedule a large number of MESs.

5.4 Performance Evaluation

To validate the effectiveness of the proposed scheme, we present the simulation results in this section. First, the optimality of the proposed scheme is validated. Then, we discuss the scheduling results under different operating scenarios.

Table 5.2: Simulation parameters

Para.	Value	Para.	Value
E_1	1.6MWh	E_2	900kWh
D_1^L	100kWh	D_1^U	200kWh
D_2^L	150kWh	D_2^U	300kWh
$P_{\mathrm{R_1/R_2}}$	90kW	$P_{\mathrm{L_1/L_2}}$	60kW
N_{11}	6	N_{12}	8
N_{21}	7	N_{22}	4
$\mathrm{E}(e_\mathrm{k})$	14kWh	$\sigma(e_\mathrm{k})$	5kWh
$\mathrm{E}(B_\mathrm{k})$	80kWh	$\sigma(B_\mathrm{k})$	10kWh
α_k^T	30	α_k^D	10^5
D_k	5.08×10^{-4}	α_1	1
α_2	-0.222	α_L	0.5

5.4.1 Simulation Setup

The parameter setting is shown in Table 5.2. RCSs are considered with a large amount of excess energy, where R_1 has 1.6MWh and R_2 has 900kWh surplus energy. LCS L_1 demands 100-200kWh energy to be delivered while L_2 demands energy between 150-300kWh. RCSs adopt SAE CCS level 2 charging standard at 90kW and LCSs adopt SAE CCS charging standard at 60kW [21]. The number of MESs N_{ij} along each R_i-L_j pair is also included in Table 5.2. The MES service capacities are considered as random variables that follow a normal distribution with a mean value of 14 and a standard deviation of 5 (kWh). Similarly, the MES battery capacities also follow a normal distribution with an 80kWh mean and a standard deviation of 10kWh. The battery degradation parameters D_k, α_1, α_2, α_3 are calculated according to data in work [140]. While the MES battery degradation cost is relatively low (e.g., 4×10^{-4}) per cycle, it is still a great concern for MES drivers. Thus, α_k^D is set to 10^5 and α_k^T is set to 30 to make them comparable with service reward and motivation reward. The loading cost weight α_L is set to 0.5.

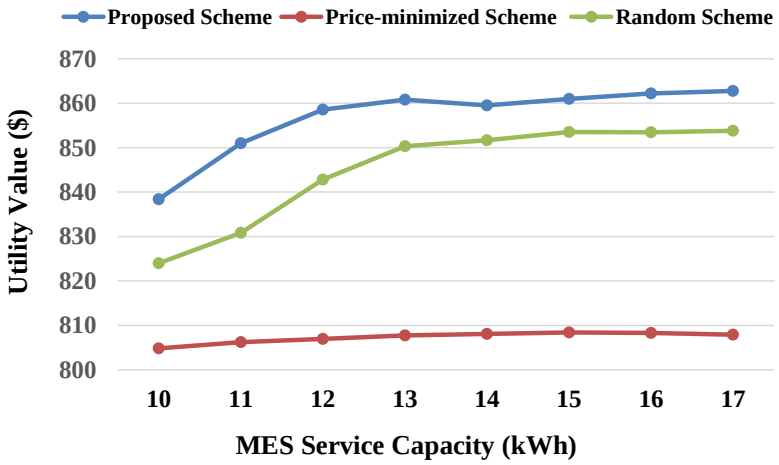

Figure 5.2: Optimal utility revenue with different MES service capacities.

5.4.2 Simulation Results

Scheme Optimality

We simulate the proposed scheme and compare its performance with the price-minimized scheme and random scheme, as shown in Fig. 5.2. In the price-minimized scheme, the PSO aims to minimize its service price. In the random scheme, the PSO randomly adjusts the service price to meet LCS energy demands. It can be seen that the proposed scheme has the highest utility revenue compared with both price-minimized and random schemes as the price-minimized scheme only tries to minimize the price, but ignores the loading revenue impact on the utility function. Compared to the price-minimized scheme, random scheme schedules more MESs and can achieve higher revenue as it does not put strict constraints to achieve minimal loading demands. Moreover, as MES service capacities increase, revenues of both proposed and random schemes increase. As for now, there are more on-road service capacities to meet the LCS energy demand, and a lower service price can be provided for incentive. For the price-minimized scheme, the revenue increment is smaller as its loading revenue stay almost the same.

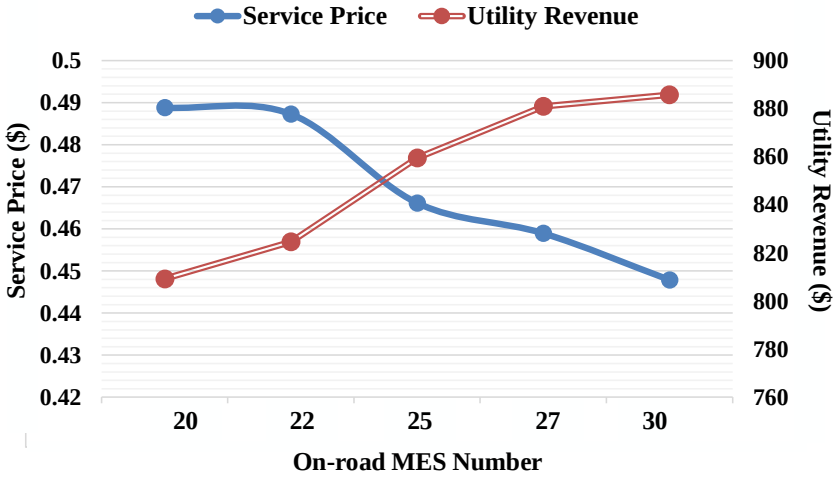

Figure 5.3: Impact of on-road MES number on energy scheduling.

Impact of MES Number

We also discuss the energy scheduling scheme under different operation scenarios. The impact of on-road MES number on scheduling result is shown in Fig.5.3. It can be seen that as the on-road MES number increases, the service price decreases since the operator has more potential energy servers, and less price-incentive is required. Correspondingly, the UO utility revenue increases. Moreover, with more MESs participating in the service, more energy can be delivered to LCSs, which increases the loading revenue part of the utility.

Impact of Loading Weight

Depending on the GCS operation goal, the objective of MES scheduling could lean towards operation cost minimization or loading revenue maximization. By adjusting the loading weight α_{L}, the operation objectives vary and the scheduling result also changes, as shown in Fig.5.4. It can be seen that as the loading weight increases, the MES scheduling mainly focuses on loading revenue maximization. To encourage MESs delivering more energy, the service price increases until α_{L} reaches 0.6. We can observe from the figure that when $\alpha_{\mathrm{L}} = 0.6$, the loading at L_1 reaches its maximal demanding load D_1^U. Therefore, a higher loading weight will result in the same loading results as limited by the loading constraints and the service price will remain the same.

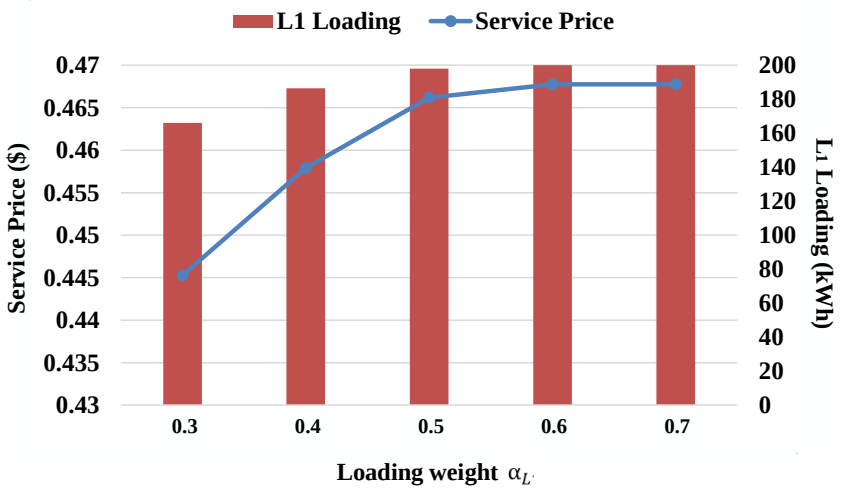

Figure 5.4: Impact of the loading weight on energy scheduling.

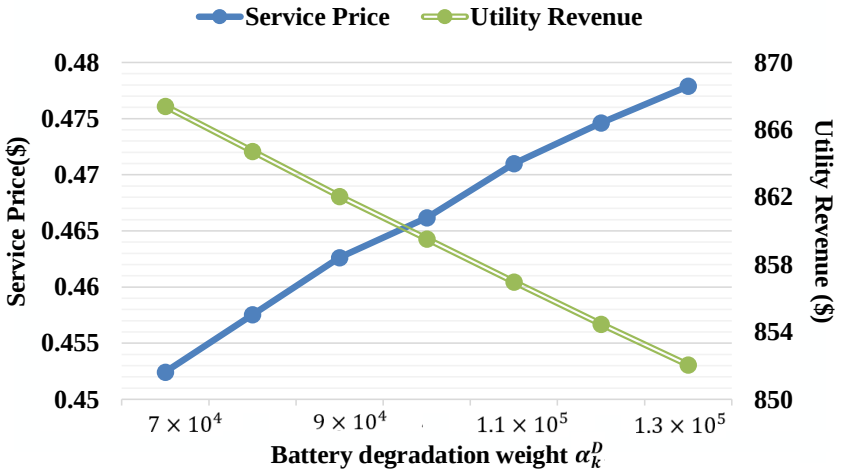

Figure 5.5: Impact of the battery degradation weight on energy scheduling.

Impact of Battery Degradation Weight

As the battery technology advances, the MES driver's preference towards energy discharging also changes. Therefore, we discuss the battery degradation weight impact on schedul-

ing results, as shown in Fig.5.5. As the weight α_{k}^{D} increases, MES drivers are more reluctant to discharge energy and the price range p_{range} becomes wider. Therefore, for the same energy compensation tasks, to stimulate MESs actively fulfilling the tasks, the UO needs to post a higher service price. As a result, the operation cost increases and the operator utility revenue decreases accordingly.

5.5 Summary

To fully utilize the on-road energy storage resource, a price-incentive scheme that stimulates on-road PMESs fulfilling energy compensation tasks has been proposed to mitigate overload issues at LCSs. The sequential decision-making process has been formulated as a Stackelberg game to characterize the interaction between the UO and PMESs. The existence and uniqueness of Stackelberg equilibrium have been proven, and an algorithm has been designed to find the equilibrium. Performance evaluation has validated the effectiveness of the proposed scheme under different operation scenarios. The proposed scheduling scheme can be applied by the local power utility company to balance the GCS energy with on-road energy resource in a cost-efficient manner.

Chapter 6

Conclusions and Future Work

In this chapter, we summarize the main contributions and impacts of the presented works and highlight future research directions.

6.1 Main Research Contributions

In this thesis, we aim to explore the potentials of PEVs serving as MESs in the smart grid. At different PEV commercialization stages, the MES ownerships, battery-capacities, and fleet sizes vary correspondingly. Therefore, we propose three scheduling schemes for MESs to mitigate the overload issues in the smart grid under three different scenarios: UMESs when PEVs are at their early developing stage, LMESs when PEV commercialization is promoted by the legislation, and PMESs when PEVs have been prevalent in the automobile market and become a regular transportation option for every household. The proposed MES scheduling schemes can be applied by the local power utility company to fully utilize on-road energy storages to mitigate the local overload issues without spending excessive expenditure on infrastructure upgrade. The main research contributions are summarized as follows:

1. First, we study the scenario when PEVs are at their early development stage, and UMESs are large capacity electric vehicles solely used to mitigate the overload issues among a GCS. To accurately characterize the CS operation dynamics, a two-dimensional Markov Chain model is developed to estimate the surplus energy of RCSs and demanding energy of LCSs. Then, a two-tier energy compensation framework is introduced to effectively use UMESs as energy porters at peak hours. To minimize

the scheduling cost, a convex optimization problem is formulated and solved through DCP of CVX. Through simulation, we validate that the introduced framework can effectively mitigate the GCS overload issues using UMESs in a cost-efficient and timely manner. We can also conclude from the simulation that as battery technology develops, the increasing UMES energy transmission efficiency contributes to wider transmission coverage and more flexible scheduling. Further, strict station availability requirement can result in a drastic increment of scheduling cost, leading to a trade-off between the station availability and scheduling costs.

2. Second, as we foresee the legislation promotion and commercialization of PEVs, LMESs will enter the MES market. Under this scenario, we consider the impact of additional MES traffic on the transportation networks when schedule the energy compensation tasks. Therefore, the proposed scheduling strategy has two objectives: balancing energy among a GCS and achieving a stable and uncongested transportation operation. To measure the LMES travelling capacity on-road, an energy-capacitated transportation network model is developed. Based on the model, LMES scheduling is conducted in two steps: first, a loading-optimized navigation scheme is proposed to calculate the optimal navigation routes for LMESs, followed by a dynamic pricing scheme to stimulate LMESs following the navigation results. Solving the formulated problem by the network simplex algorithm and convex optimization, the effectiveness of the proposed scheme on overload mitigation and time-efficiency of energy delivery can be validated. Further, the simulation results also present the impact of different scheduling objectives on the navigation results. It is concluded that aligning the pricing-based navigation result with the optimal navigation result leads to an increasing navigation cost. Thus, in terms of the local power and traffic conditions, the UO needs to balance between the navigation cost and transportation time increment incurred by LMESs.

3. Third, when PEVs are prevalent in the automobile marker and therefore, private PEVs become the most convenient and cost-efficient MES option, a price-incentive scheme is in demand to stimulate them fulfilling the assigned tasks aside from travelling to their destined places. The sequential decision-making process of the UO and PMESs is formulated as a Stackelberg game to characterize the price-service interaction between these two entities. Through the game analysis, the existence and uniqueness of Stackelberg equilibrium are proven, and an algorithm is designed to find the equilibrium efficiently. Simulation results validate the optimality of the proposed scheme while also discuss the results under different operating scenarios. It can be concluded that PEV prevalence and battery technology advancement can effectively reduce MES operation costs.

6.2 Future Work

In this thesis, we exploit the PEVs' potentials as MESs and their functionality as a solution to the overload issues in the smart grid. The challenges of MES scheduling are identified and three scheduling schemes are proposed for MES utilization during different PEV commercialization stages. Although several critical issues have been addressed in our previous, there are still many open research issues:

1. **Facilitate the renewable energy integration:** As more renewable energy generations are integrated into the smart grid, their fluctuating electricity generation may not match the energy demand in the grid, and therefore lead to either electricity waste or energy imbalance. To flatten the renewable energy generation profile, MESs can be used as energy buffers to store surplus energy of renewable generation and deliver the energy to energy-demanding areas. The electricity generation of renewable energy plants can be characterized as a Markov Chain model, in which the MES charging rate depends on the weather condition and MES chargers.

2. **Robust MES scheduling on-road:** While the CS dynamic has been modelled and predicted by stochastic analysis, in real life, there are still unpredictable factors that could lead to energy imbalance among a GCS, e.g., human factors, unexpected PEV charging demands, uncertain MES discharging, and so on. Therefore, robust design of the MES energy scheduling is required by including the unpredicted errors during the scheduling process so that the scheduling scheme is guaranteed to achieve the minimal CS operation requirements [107]. Factors such as environmental uncertainty can be considered during the problem formulation and stochastic programming can be an effective optimization tool to solve this problem.

3. **Cooperative LMES scheduling:** In addition to their fleet size and battery capacity, LMESs have a unique feature compared to UMESs and PMESs: the LMESs that belong to the same company have the same service objective: to maximize the company's overall revenue of energy compensation service. Therefore, to achieve the overall service revenue maximization, the interaction between these LMESs is not competitive, but rather cooperative. If LMESs from the same company cooperate together to bargain with the GCS, a better overall service revenue could be achieved since a group of LMESs are considered as a larger service capacity MES and have more leverage. Therefore, a cooperative game can be an effective mathematical model to characterize the interaction among LMES service.

References

[1] "World energy outlook," International Energy Agency, Tech. Rep., November 2018.

[2] H. Liang, A. K. Tamang, W. Zhuang, and X. Shen, "Stochastic information management in smart grid," *IEEE Communications Surveys and Tutorials*, vol. 16, no. 3, pp. 1746–1770, Feburary 2014.

[3] R. H. Byrne, T. A. Nguyen, D. A. Copp, B. R. Chalamala, and I. Gyuk, "Energy management and optimization methods for grid energy storage systems," *IEEE Access*, vol. 6, pp. 13 231–13 260, 2018.

[4] K. Lindquist and M. Wendt, "Electric vehicle policies, fleet, and infrastructure: Synthesis," Washington State Department of Transportation, Tacoma, WA,, Tech. Rep., 2011.

[5] M. Wang, H. Liang, R. Zhang, R. Deng, and X. Shen, "Mobility-aware coordinated charging for electric vehicles in VANET-enhanced smart grid," *IEEE Journal on Selected Areas in Communications*, vol. 32, no. 7, pp. 1344–1360, July 2014.

[6] W. Su, H. Eichi, W. Zeng, and M. Chow, "A survey on the electrification of transportation in a smart grid environment," *IEEE Transactions on Industrial Informatics*, vol. 8, no. 1, pp. 1–10, Feburary 2012.

[7] N. Chen, J. Ma, M. Wang, and X. Shen, "Two-tier energy compensation framework based on mobile vehicular electric storage," *IEEE Transactions on Vehicular Technology*, vol. 67, no. 12, pp. 11 719–11 732, December 2018.

[8] *Guide for smart grid interoperability of energy technology and information technology operation with the electric power system (EPS), and end-use applications and loads*, IEEE 2030-2011 Std., 2011.

[9] X. S. Shen, "Empowering the smart grid with wireless technologies [editor's note]," *IEEE Network*, vol. 26, no. 3, pp. 2–3, May 2012.

[10] K. Zheng, Q. Zheng, P. Chatzimisios, W. Xiang, and Y. Zhou, "Heterogeneous vehicular networking: A survey on architecture, challenges, and solutions," *IEEE Communications Surveys Tutorials*, vol. 17, no. 4, pp. 2377–2396, Fourthquarter 2015.

[11] Z. He, J. Cao, and X. Liu, "SDVN: enabling rapid network innovation for heterogeneous vehicular communication," *IEEE Network*, vol. 30, no. 4, pp. 10–15, July 2016.

[12] Y. Huo, G. Prasad, L. Lampe, and V. C. M. Leung, "Efficient access control for broadband power line communications in home area networks," *IEEE Transactions on Communications*, vol. 66, no. 4, pp. 1649–1660, April 2018.

[13] G. P. Agrawal, *Fiber-optic Communication Systems*. John Wiley & Sons, 2012, vol. 222.

[14] H. Al Haj Hassan, A. Pelov, and L. Nuaymi, "Integrating cellular networks, smart grid, and renewable energy: Analysis, architecture, and challenges," *IEEE Access*, vol. 3, pp. 2755–2770, 2015.

[15] R. Molina-Masegosa and J. Gozalvez, "LTE-V for sidelink 5G V2X vehicular communications: A new 5G technology for short-range vehicle-to-everything communications," *IEEE Vehicular Technology Magazine*, vol. 12, no. 4, pp. 30–39, December 2017.

[16] A. Laha, B. Yin, Y. Cheng, and L. X. Cai, "A location aware game theoretic approach for charging plug-in hybrid electric vehicles," in *Proc. IEEE GLOBECOM*, 2016, pp. 1–6.

[17] D. B. Sandalow, *Plug-In Electric Vehicles: What Role for Washington?* Brookings Institution Press, 2009.

[18] (2019) Nissan leaf 2019. [Online]. Available: https://www.nissan.ca/en/electric-cars/leaf/versions-specs

[19] (2019) Tesla model S. [Online]. Available: http://www.teslamotors.com/models

[20] S. Chen, J. Hu, Y. Shi, and L. Zhao, "LTE-V: A TD-LTE-based V2X solution for future vehicular network," *IEEE Internet of Things Journal*, vol. 3, no. 6, pp. 997–1005, December 2016.

[21] *SAE Electric Vehicle and Plug in Hybrid Electric Vehicle Conductive Charge Coupler*, SAE Std., 2017.

[22] *IEEE Standard Technical Specifications of a DC Quick Charger for Use with Electric Vehicles*, IEEE Std 2030.1.1-2015 Std., 2016.

[23] "Global electric vehicle market outlook report 2019-2025," Research and Markets, Tech. Rep., April 2019.

[24] (2019, March) Tesla launches faster third generation supercharger. [Online]. Available: https://www.theverge.com/2019/3/6/18253618/tesla-supercharger-250kw-v3-specs-location

[25] (2018, July) Porsche connects its first ultra-fast 800-volt charging station to the grid ahead of the taycan. [Online]. Available: https://electrek.co/2018/07/11/porsche-taycan-connects-first-ultra-fast-800-volt-charging-station-grid/

[26] K. Clement-Nyns, E. Haesen, and J. Driesen, "The impact of charging plug-in hybrid electric vehicles on a residential distribution grid," *IEEE Transactions on Power Systems*, vol. 25, no. 1, pp. 371–380, Feburary 2010.

[27] Z. Jiang, L. Shalalfeh, and M. J.Beshir, "Impact of electric vehicle infrastructure on the city of Chatsworth distribution system," in *Proc. IEEE IEVC*, 2014, pp. 1–5.

[28] M. F. Shaaban, M. Ismail, E. F. El-Saadany, and W. Zhuang, "Real-time PEV charging/discharging coordination in smart distribution systems," *IEEE Transactions on Smart Grid*, vol. 5, no. 4, pp. 1797–1807, July 2014.

[29] H. Chen, Z. Hu, H. Luo, J. Qin, R. Rajagopal, and H. Zhang, "Design and planning of a multiple-charger multiple-port charging system for PEV charging station," *IEEE Transactions on Smart Grid*, vol. 10, no. 1, pp. 173–183, January 2019.

[30] L. Zhu, M. Li, Z. Zhang, X. Du, and M. Guizani, "Big data mining of users' energy consumption patterns in the wireless smart grid," *IEEE Wireless Commununications*, vol. 25, no. 1, pp. 84–89, Feburary 2018.

[31] K. Wang, Y. Wang, X. Hu, Y. Sun, D. J. Deng, A. Vinel, and Y. Zhang, "Wireless big data computing in smart grid," *IEEE Wireless Commununications*, vol. 24, no. 2, pp. 58–64, April 2017.

[32] S. Bae and A. Kwasinski, "Spatial and temporal model of electric vehicle charging demand," *IEEE Transactions on Smart Grid*, vol. 3, no. 1, pp. 394–403, July 2012.

[33] X. Dong, Y. Mu, H. Jia, J. Wu, and X. Yu, "Planning of fast EV charging stations on a round freeway," *IEEE Transactions on Sustainable Energy*, vol. 7, no. 4, pp. 1452–1461, October 2016.

[34] M. Wang, M. Ismail, X. Shen, E. Serpedin, and K. Qaraqe, "Spatial and temporal online charging/discharging coordination for mobile PEVs," *IEEE Wireless Communications*, vol. 22, no. 1, pp. 112–121, Feburary 2015.

[35] N. Akhtar, S. C. Ergen, and O. Ozkasap, "Vehicle mobility and communication channel models for realistic and efficient highway VANET simulation," *IEEE Transactions on Vehicular Technology*, vol. 64, no. 1, pp. 248–262, January 2015.

[36] G. Li and X.-P. Zhang, "Modeling of plug-in hybrid electric vehicle charging demand in probabilistic power flow calculations," *IEEE Transactions on Smart Grid*, vol. 3, no. 1, pp. 492–499, March 2012.

[37] W. Alharbi and K. Bhattacharya, "Electric vehicle charging facility as a smart energy microhub," *IEEE Transactions on Sustainable Energy*, vol. 8, no. 2, pp. 616–628, April 2017.

[38] A. Y. S. Lam, K. Leung, and V. O. K. Li, "Capacity estimation for vehicle-to-grid frequency regulation services with smart charging mechanism," *IEEE Transactions on Smart Grid*, vol. 7, no. 1, pp. 156–166, January 2016.

[39] C. Kong, R. Jovanovic, I. S. Bayram, and M. Devetsikiotis, "A hierarchical optimization model for a network of electric vehicle charging stations," *Energies*, vol. 10, no. 5, pp. 675–694, May 2017.

[40] H. Zhang, Z. Hu, Z. Xu, and Y. Song, "An integrated planning framework for different types of PEV charging facilities in urban area," *IEEE Transactions on Smart Grid*, vol. 7, no. 5, pp. 2273–2284, September 2016.

[41] G. Wang, Z. Xu, F. Wen, and K. P. Wong, "Traffic-constrained multiobjective planning of electric-vehicle charging stations," *IEEE Transactions on Power Delivery*, vol. 28, no. 4, pp. 2363–2372, July 2013.

[42] S. Chung and C. Kwon, "Multi-period planning for electric car charging station locations: A case of Korean expressways," *Enrupean Journal of Operation Research*, vol. 242, no. 2, pp. 677–687, April 2015.

[43] L. Gan, U. Topcu, and S. H. Low, "Optimal decentralized protocol for electric vehicle charging," *IEEE Transactions on Power Systems*, vol. 28, no. 2, pp. 940–951, May 2013.

[44] K. Zhang, L. Xu, M. Ouyang, H. Wang, L. Lu, J. Li, and Z. Li, "Optimal decentralized valley-filling charging strategy for electric vehicles," *Energy Conversion and Management*, vol. 78, pp. 537–550, Feburary 2014.

[45] R. Wang, P. Wang, and G. Xiao, "Two-stage mechanism for massive electric vehicle charging involving renewable energy," *IEEE Transactions on Vehicular Technology*, vol. 65, no. 6, pp. 4159–4171, June 2016.

[46] J. de Hoog, T. Alpcan, M. Brazil, D. A. Thomas, and I. Mareels, "Optimal charging of electric vehicles taking distribution network constraints into account," *IEEE Transactions on Power Systems*, vol. 30, no. 1, pp. 365–375, January 2015.

[47] S. Vazquez, S. M. Lukic, E. Galvan, L. G. Franquelo, and J. M. Carrasco, "Energy storage systems for transport and grid applications," *IEEE Transactions on Industrial Electronics*, vol. 57, no. 12, pp. 3881–3895, December 2010.

[48] Y. Wang, W. Saad, Z. Han, H. V. Poor, and T. Baar, "A game-theoretic approach to energy trading in the smart grid," *IEEE Transactions on Smart Grid*, vol. 5, no. 3, pp. 1439–1450, May 2014.

[49] C. Jin, J. Tang, and P. Ghosh, "Optimizing electric vehicle charging with energy storage in the electricity market," *IEEE Transactions on Smart Grid*, vol. 4, no. 1, pp. 311–320, March 2013.

[50] N. Chen, J. Ma, M. Li, M. Wang, and X. Shen, "Energy management framework for mobile vehicular electric storage," *IEEE Network*, to appear.

[51] L. Lu, X. Han, J. Li, J. Hua, and M. Ouyang, "A review on the key issues for lithium-ion battery management in electric vehicles," *Journal of Power Sources*, vol. 226, pp. 272–288, March 2013.

[52] (2019) Electric vehicle battery life and warranties. [Online]. Available: https://www.energysage.com/electric-vehicles/buyers-guide/battery-life-for-top-evs/

[53] (2018) Electric vehicle battery: Materials, cost, lifespan. [Online]. Available: https://www.ucsusa.org/clean-vehicles/electric-vehicles/electric-cars-battery-life-materials-cost

[54] (2018) Hydrogen fuel cell and battery electric vehicles - technology rundown. [Online]. Available: https://cleantechnica.com/2018/08/11/hydrogen-fuel-cell-battery-electric-vehicles-technology-rundown/

[55] P. Siglinda and C. Gabriele, *Emerging Materials for Energy Conversion and Storage*. Elsevier, 2018, vol. 9.

[56] L. Grande and X. He, "Advanced li-ion and beyond li-ion batteries 2018-2028," IDTechEx, Tech. Rep., 2018.

[57] P. Kurzweil and J. Garche, *Lead-Acid Batteries for Future Automobiles*. Elsevier, 2017.

[58] (2019, Feburary) BU-808: How to prolong lithium-based batteries. [Online]. Available: https://batteryuniversity.com/learn/article/how_to_prolong_lithium_based_batteries

[59] X. Han, M. Ouyang, L. Lu, and J. Li, "A comparative study of commercial lithium ion battery cycle life in electric vehicle: Capacity loss estimation," *Journal of Power Sources*, vol. 268, pp. 658–669, 2014.

[60] K. Uddin, T. Jackson, W. D. Widanage, G. Chouchelamane, P. A. Jennings, and J. Marco, "On the possibility of extending the lifetime of lithium-ion batteries through optimal V2G facilitated by an integrated vehicle and smart-grid system," *Energy*, vol. 133, pp. 710–722, August 2017.

[61] K. Uddin, M. Dubarry, and M. B. Glick, "The viability of vehicle-to-grid operations from a battery technology and policy perspective," *Energy Policy*, vol. 113, pp. 342–347, Feburary 2018.

[62] C. Zhu, F. Lu, H. Zhang, and C. C. Mi, "Robust predictive battery thermal management strategy for connected and automated hybrid electric vehicles based on thermoelectric parameter uncertainty," *IEEE Journal of Emerging and Selected Topics in Power Electronics*, vol. 6, no. 4, pp. 1796–1805, December 2018.

[63] Y. Song, P. Li, Y. Zhao, and S. Lu, "Design and integration of the bi-directional electric vehicle charger into the microgrid as emergency power supply," in *Proc. IEEE ECCE Asia*, 2018, pp. 3698–3704.

[64] P. Singh Tomar, M. Srivastava, and A. Kumar Verma, "An efficient bi-directional DC/DC charger for electric vehicle battery charging," in *Proc. IEEE ICEPE*, June 2018, pp. 1–9.

[65] C. Shin and J. Lee, "An electrolytic capacitor-less bi-directional EV on-board charger using harmonic modulation technique," *IEEE Transactions on Power Electronics*, vol. 29, no. 10, pp. 5195–5203, October 2014.

[66] K. Gupta, C. Da Silva, M. Nasr, A. Assadi, H. Matsumoto, O. Trescases, and C. H. Amon, "Thermal management strategies for a high-frequency, bi-directional, on-board electric vehicle charger," in *Proc. IEEE ITherm*, May 2018, pp. 935–943.

[67] (2019, January) CharIN: CCS combo standard to offer V2G by 2025. [Online]. Available: https://insideevs.com/news/342354/charin-ccs-combo-standard-to-offer-v2g-by-2025/

[68] (2018, November) Nissan launches 'nissan energy' to commercialize vehicle-to-home/building with the leaf. [Online]. Available: https://electrek.co/2018/11/28/nissan-energy-leaf-vehicle-to-home-building/

[69] (2019, April) IT giant cisco launches UK vehicle-to-grid demonstrator project. [Online]. Available: https://www.energy-storage.news/news/it-giant-cisco-launches-uk-vehicle-to-grid-demonstrator-project

[70] P. Yi, Y. Tang, Y. Hong, Y. Shen, T. Zhu, Q. Zhang, and M. M. Begovic, "Renewable energy transmission through multiple routes in a mobile electrical grid," in *Proc. IEEE ISGT*, 2014, pp. 1–5.

[71] (2019, May) Tesla semi. [Online]. Available: https://www.tesla.com/en_CA/semi?redirect=no

[72] (2019, May) Vehicle incentive (plug in BC). [Online]. Available: https://pluginbc.ca/incentives/vehicle-incentives/

[73] (2019, May) Plug n' drive: Electric vehicle incentives. [Online]. Available: https://www.plugndrive.ca/electric-vehicle-incentives/

[74] N. Chen, M. Li, M. Wang, and X. Shen, "A dynamic pricing based scheduling scheme for electric vehicles as mobile energy storages," *IEEE Transaction on Intelligent Transportation System*, under review.

[75] N. Chen, M. Li, M. Wang, J. Ma, and X. Shen, "Compensation of charging station overload via on-road mobile energy storage scheduling," in *Proc. IEEE GLOBECOM*, to appear.

[76] R. Leou, C. Su, and C. Lu, "Stochastic analyses of electric vehicle charging impacts on distribution network," *IEEE Transactions on Power Systems*, vol. 29, no. 3, pp. 1055–1063, May 2014.

[77] J. A. P. Lopes, F. J. Soares, and P. M. R. Almeida, "Integration of electric vehicles in the electric power system," *Proceedings of the IEEE*, vol. 99, no. 1, pp. 168–183, January 2011.

[78] K. Clement-Nyns, E. Haesen, and J. Driesen, "The impact of charging plug-in hybrid electric vehicles on a residential distribution grid," *IEEE Transactions on Power Systems*, vol. 25, no. 1, pp. 371–380, Feburary 2010.

[79] M. Wang, M. Ismail, R. Zhang, X. Shen, E. Serpedin, and K. Qaraqe, "Spatio-temporal coordinated V2V energy swapping strategy for mobile PEVs," *IEEE Transactions on Smart Grid*, vol. 9, no. 3, pp. 1566–1579, May 2018.

[80] W. Kempton and J. Tomic, "Vehicle-to-grid power fundamentals: Calculating capacity and net revenue," *Journal of Power Sources*, vol. 144, no. 1, pp. 268–279, June 2005.

[81] T. Sousa, H. Morais, J. ao Soares, and Z. Vale, "Day-ahead resource scheduling in smart grids considering vehicle-to-grid and network constraints," *Applied Energy*, vol. 96, pp. 183–193, August 2012.

[82] S. Shafiq and A. T. Al-Awami, "Reliability and economic assessment of renewable micro-grid with v2g electric vehicles coordination," in *Proc. IEEE AEECT*, Novermber 2015, pp. 1–6.

[83] R. Wang, Y. Li, P. Wang, and D. Niyato, "Design of a V2G aggregator to optimize PHEV charging and frequency regulation control," in *Proc. IEEE SmartGridComm*, October 2013, pp. 127–132.

[84] J. J. Escudero-Garzas, A. Garcia-Armada, and G. Seco-Granados, "Fair design of plug-in electric vehicles aggregator for V2G regulation," *IEEE Transactions on Vehicular Technology*, vol. 61, no. 8, pp. 3406–3419, October 2012.

[85] A. Mohamed, V. Salehi, T. Ma, and O. Mohammed, "Real-time energy management algorithm for plug-in hybrid electric vehicle charging parks involving sustainable energy," *IEEE Transactions on Sustainable Energy*, vol. 5, no. 2, pp. 577–586, April 2014.

[86] M. Zeng, S. Leng, Y. Zhang, and J. He, "QoE-aware power management in vehicle-to-grid networks: A matching-theoretic approach," *IEEE Transactions on Smart Grid*, vol. 9, no. 4, pp. 2468–2477, July 2018.

[87] F. Rassaei, W. Soh, and K. Chua, "Demand response for residential electric vehicles with random usage patterns in smart grids," *IEEE Transactions on Sustainable Energy*, vol. 6, no. 4, pp. 1367–1376, October 2015.

[88] M. S. Ahmad and S. Sivasubramani, "Optimal number of electric vehicles for existing networks considering economic and emission dispatch," *IEEE Transactions on Industrial Informatics*, vol. 15, no. 4, pp. 1926–1935, April 2019.

[89] N. Z. Xu and C. Y. Chung, "Reliability evaluation of distribution systems including vehicle-to-home and vehicle-to-grid," *IEEE Transactions on Power Systems*, vol. 31, no. 1, pp. 759–768, January 2016.

[90] V. N. Coelho, I. M. Coelho, B. N. Coelho, M. W. Cohen, A. J. R. Reis, S. M. Silva, M. J. F. Souza, P. J. Fleming, and F. G. G. aes, "Multiobjective energy storage power dispatching using plug-in vehicles in a smart-microgrid," *Renewable Energy*, vol. 89, pp. 730–742, April 2016.

[91] P. Yi, Y. Tang, Y. Hong, Y. Shen, T. Zhu, Q. Zhang, and M. M. Begovic, "Renewable energy transmission through multiple routes in a mobile electrical grid," in *Proc. IEEE ISGT*, Feburary 2014, pp. 1–5.

[92] H. Ko, S. Pack, and V. C. M. Leung, "Vehicle-to-Grid control algorithm in microgrids," *IEEE Transactions on Intelligent Transportation Systems*, vol. 19, no. 7, pp. 2165–2174, July 2018.

[93] R. Yu, W. Zhong, S. Xie, C. Yuen, S. Gjessing, and Y. Zhang, "Balancing power demand through EV mobility in vehicle-to-grid mobile energy networks," *IEEE Transactions on Industrial Informatics*, vol. 12, no. 1, pp. 79–90, Feburary 2016.

[94] W. Zhong, R. Yu, S. Xie, Y. Zhang, and D. K. Y. Yau, "On stability and robustness of demand response in V2G mobile energy networks," *IEEE Transactions on Smart Grid*, vol. 9, no. 4, pp. 3203–3212, July 2018.

[95] A. Y. S. Lam, K. Leung, and V. O. K. Li, "Vehicular energy network," *IEEE Transactions on Transportation Electrification*, vol. 3, no. 2, pp. 392–404, June 2017.

[96] K. Hou, X. Xu, H. Jia, X. Yu, T. Jiang, K. Zhang, and B. Shu, "A reliability assessment approach for integrated transportation and electrical power systems incorporating electric vehicles," *IEEE Transactions on Smart Grid*, vol. 9, no. 1, pp. 88–100, January 2018.

[97] J. Xiong, K. Zhang, Y. Guo, and W. Su, "Investigate the impacts of PEV charging facilities on integrated electric distribution system and electrified transportation system," *IEEE Transactions on Transportation Electrification*, vol. 1, no. 2, pp. 178–187, August 2015.

[98] M. Alizadeh, H. Wai, M. Chowdhury, A. Goldsmith, A. Scaglione, and T. Javidi, "Optimal pricing to manage electric vehicles in coupled power and transportation networks," *IEEE Transactions on Control of Network Systems*, vol. 4, no. 4, pp. 863–875, December 2017.

[99] W. Wei, S. Mei, L. Wu, J. Wang, and Y. Fang, "Robust operation of distribution networks coupled with urban transportation infrastructures," *IEEE Transactions on Power Systems*, vol. 32, no. 3, pp. 2118–2130, May 2017.

[100] S. Pourazarm and C. G. Cassandras, "Optimal routing of energy-aware vehicles in transportation networks with inhomogeneous charging nodes," *IEEE Transactions on Intelligent Transportation Systems*, vol. 19, no. 8, pp. 2515–2527, Auguest 2018.

[101] M. M. de Weerdt, S. Stein, E. H. Gerding, V. Robu, and N. R. Jennings, "Intention-aware routing of electric vehicles," *IEEE Transactions on Intelligent Transportation Systems*, vol. 17, no. 5, pp. 1472–1482, May 2016.

[102] Z. Yi and P. H. Bauer, "Optimal stochastic eco-routing solutions for electric vehicles," *IEEE Transactions on Intelligent Transportation Systems*, vol. 19, no. 12, pp. 3807–3817, December 2018.

[103] Z. Moghaddam, I. Ahmad, D. Habibi, and M. A. S. Masoum, "A coordinated dynamic pricing model for electric vehicle charging stations," *IEEE Transactions on Transportation Electrification*, vol. 5, no. 1, pp. 226–238, March 2019.

[104] S. Misra, S. Bera, and T. Ojha, "D2P: Distributed dynamic pricing policyin smart grid for PHEVs management," *IEEE Transactions on Parallel and Distributed Systems*, vol. 26, no. 3, pp. 702–712, March 2015.

[105] A. Ghosh and V. Aggarwal, "Menu-based pricing for charging of electric vehicles with vehicle-to-grid service," *IEEE Transactions on Vehicular Technology*, vol. 67, no. 11, pp. 10 268–10 280, Novermber 2018.

[106] D. A. Chekired, L. Khoukhi, and H. T. Mouftah, "Decentralized cloud-SDN architecture in smart grid: A dynamic pricing model," *IEEE Transactions on Industrial Informatics*, vol. 14, no. 3, pp. 1220–1231, March 2018.

[107] H. Yang, X. Xie, and A. V. Vasilakos, "Noncooperative and cooperative optimization of electric vehicle charging under demand uncertainty: A robust stackelberg game," *IEEE Transactions on Vehicular Technology*, vol. 65, no. 3, pp. 1043–1058, March 2016.

[108] W. Yuan, J. Huang, and Y. J. A. Zhang, "Competitive charging station pricing for plug-in electric vehicles," *IEEE Transactions on Smart Grid*, vol. 8, no. 2, pp. 627–639, March 2017.

[109] I. S. Bayram, G. Michailidis, and M. Devetsikiotis, "Unsplittable load balancing in a network of charging stations under QoS guarantees," *IEEE Transactions on Smart Grid*, vol. 6, no. 3, pp. 1292–1302, May 2015.

[110] X. Chen and K. Leung, "A game theoretic approach to vehicle-to-grid scheduling," in *Proc. IEEE GLOBECOM*, 2018, pp. 1–6.

[111] H. Ko, S. Pack, and V. C. M. Leung, "Mobility-aware vehicle-to-grid control algorithm in microgrids," *IEEE Transactions on Intelligent Transportation Systems*, vol. 19, no. 7, pp. 2165–2174, July 2018.

[112] S. Han, S. Han, and K. Sezaki, "Estimation of achievable power capacity from plug-in electric vehicles for V2G frequency regulation: Case studies for market participation," *IEEE Transactions on Smart Grid*, vol. 2, no. 4, pp. 632–641, December 2011.

[113] L. P. Fernandez, T. G. S. Roman, R. Cossent, C. M. Domingo, and P. Frias, "Assessment of the impact of plug-in electric vehicles on distribution networks," *IEEE Transactions on Power Systems*, vol. 26, no. 1, pp. 206–213, Feburary 2011.

[114] E. Sortomme, M. M. Hindi, S. D. J. MacPherson, and S. S. Venkata, "Coordinated charging of plug-in hybrid electric vehicles to minimize distribution system losses," *IEEE Transactions on Smart Grid*, vol. 2, no. 1, pp. 198–205, March 2011.

[115] N. Wisitpongphan, F. Bai, P. Mudalige, V. Sadekar, and O. Tonguz, "Routing in sparse vehicular ad hoc wireless networks," *IEEE Journal on Selected Areas in Communications*, vol. 25, no. 8, pp. 1538–1556, October 2007.

[116] A. Santos, N. McGuckin, H. Y. Nakamoto, D. Gary, and S. Liss, "Summary of travel trends: 2009 national household travel survey," U. S. Department of Transportation, Washington, D.C., Tech. Rep., June 2011.

[117] H. M. Taylor and S. Karlin, *An introduction to stochastic modeling*. Academic Press, 2014.

[118] I. CVX Research. (2011) CVX: Matlab software for disciplined convex programming, version 2.0. [Online]. Available: http://cvxr.com/cvx

[119] (2017) Caltrans PeMS. [Online]. Available: http://pems.dot.ca.gov

[120] H. Xiao, Y. Huimei, W. Chen, and L. Hongjun, "A survey of influence of electrics vehicle charging on power grid," in *Proc. IEEE ICIEA*, 2014, pp. 121–126.

[121] (2017) Electric vehicle rate plans. [Online]. Available: https://www.pge.com

[122] R. Alvaro-Hermana, J. Fraile-Ardanuy, P. J. Zufiria, L. Knapen, and D. Janssens, "Peer to peer energy trading with electric vehicles," *IEEE Intelligent Transportation Systems Magazine*, vol. 8, no. 3, pp. 33–44, Fall 2016.

[123] (2017) Google map. [Online]. Available: https://www.google.ca/maps

[124] (2018) CHAdeMO chargers. [Online]. Available: https://www.chademo.com/products/chargers/

[125] B. Lee, J. Kim, S. Kim, and J. Lee, "An isolated/bidirectional PWM resonant converter for V2G(H) EV on-board charger," *IEEE Transactions on Vehicular Technology*, vol. 66, no. 9, pp. 7741–7750, September 2017.

[126] H. N. de Melo, J. P. F. Trovão, P. G. Pereirinha, H. M. Jorge, and C. H. Antunes, "A controllable bidirectional battery charger for electric vehicles with vehicle-to-grid capability," *IEEE Transactions on Vehicular Technology*, vol. 67, no. 1, pp. 114–123, January 2018.

[127] (2014) Appendix b - traffic level of service calculation methods. [Online]. Available: http://ccag.ca.gov

[128] K. Zhou and L. Cai, "Randomized PHEV charging under distribution grid constraints," *IEEE Transactions on Smart Grid*, vol. 5, no. 2, pp. 879–887, March 2014.

[129] D. Pacciarelli, A. Agnetis, and M. Pranzo. (2018) Min-cost flow problems and network simplex algorithm. [Online]. Available: http://www.dii.unisi.it/agnetis/simpretENG.pdf

[130] (2018) Time-of-use rate plan. [Online]. Available: https://www.sce.com/wps/portal/home/residential/rates

[131] F. Chiti, R. Fantacci, D. Marabissi, and A. Tani, "Performance evaluation of an efficient and reliable multicast power line communication system," *IEEE Journal on Selected Areas in Communications*, vol. 34, no. 7, pp. 1953–1964, July 2016.

[132] R. Nakao, N. Naganuma, S. Takano, and H. Otsuka, "Performance analysis of fiber-optic inband relaying against both self- and inter-cell interference," in *Proc. IEEE VTC-Fall*, 2017, pp. 1–5.

[133] A. Gupta and R. K. Jha, "A survey of 5G network: Architecture and emerging technologies," *IEEE Access*, vol. 3, pp. 1206–1232, 2015.

[134] G. Luo, Q. Yuan, H. Zhou, N. Cheng, Z. Liu, F. Yang, and X. S. Shen, "Cooperative vehicular content distribution in edge computing assisted 5G-VANET," *China Communications*, vol. 15, no. 7, pp. 1–17, July 2018.

[135] W. Xu, H. A. Omar, W. Zhuang, and X. S. Shen, "Delay analysis of in-vehicle internet access via on-road WiFi access points," *IEEE Access*, vol. 5, pp. 2736–2746, 2017.

[136] V. Kounev and D. Tipper, "Advanced metering and demand response communication performance in Zigbee based HANs," in *Proc. IEEE INFOCOM WKSHPS*, 2013, pp. 31–36.

[137] A. Ahmadian, M. Sedghi, B. Mohammadi-ivatloo, A. Elkamel, M. Aliakbar Golkar, and M. Fowler, "Cost-benefit analysis of V2G implementation in distribution networks considering PEVs battery degradation," *IEEE Transactions on Sustainable Energy*, vol. 9, no. 2, pp. 961–970, April 2018.

[138] M. Li, J. Gao, L. Zhao, and X. Shen, "Task time allocation and reward scheme for PEV charging station advertising," in *Proc. IEEE ICC*, 2019.

[139] Q. Cao, H. V. Zhao, and Y. Jing, "Power allocation and pricing in multiuser relay networks using stackelberg and bargaining games," *IEEE Transactions on Vehicular Technology*, vol. 61, no. 7, pp. 3177–3190, September 2012.

[140] C. Guenther, B. Schott, W. Hennings, P. Waldowski, and M. A. Danzer, "Model-based investigation of electric vehicle battery aging by means of vehicle-to-grid scenario simulations," *Journal of Power Sources*, vol. 239, no. 1, pp. 604–610, October 2013.

[141] I. Bayram, G. Michailidis, M. Devetsikiptis, and F. Granelli, "Electric power allocation in a network of fast charging stations," *IEEE Journal on Selected Areas in Communications*, vol. 31, no. 7, pp. 1235–1246, July 2013.

[142] (2016, Feburary) PEV incentive program. [Online]. Available: http://www.mto.gov.on.ca/english/vehicles/electric/index.shtml

List of Publications

Journal Papers

1. **N. Chen**, J. Ma, M. Li, M. Wang, and X. Shen, "Energy Management Framework for Mobile Vehicular Electric Storage", *IEEE Network*, to appear.

2. **N. Chen**, J. Ma, M. Wang, and X. Shen, "Two-Tier Energy Compensation Framework Based on Mobile Vehicular Electric Storage", *IEEE Transactions on Vehicular Technology*, vol. 67, no.12, pp.11719-11732, Dec. 2018.

3. **N. Chen**, M. Wang, N. Zhang, and X. Shen, "Energy and Information Management of Electric Vehicular Network: A Survey", *IEEE Communication Surveys and Tutorials*, under revision.

4. **N. Chen**, M. Li, M. Wang, and X. Shen, "A Dynamic Pricing Based Scheduling Scheme for Electric Vehicles as Mobile Energy Storages", *IEEE Transactions on Intelligent Transportation System*, under review.

Conference Papers

1. **N. Chen**, M. Li, M. Wang, J. Ma, and X. Shen, "Compensation of Charging Station Overload via On-road Mobile Energy Storage Scheduling", *Proc. IEEE Globecom'19*, to appear.